UNIVERSITÁ DEGLI STUDI DI PADOVA
DIPARTIMENTO DI SCIENZE CHIMICHE
CORSO DI LAUREA MAGISTRALE IN CHIMICA

TESI DI LAUREA MAGISTRALE

Synthesis and characterisation of novel tris(2-pyridilmethyl) amine complexes for reductive catalysis applications

Relatore: Prof. Cristiano Zonta

Controrelatore: Prof. Paolo Centomo

Laureando: Alessandro Baghin

ANNO ACCADEMICO: 2021/2022

TABLE OF CONTENTS

1 INTRODUCTION

1.1 LIGANDS IN COORDINATION CHEMISTRY

In coordination chemistry, ligands are used to control the environment of metal centers modulating their electronic and steric properties. One of the main challenges for scientists is to design new molecular structures inspired by nature. Many efforts have been spent on the synthesis of novel molecules that are able to reproduce the catalytic activity of enzymes. In this context, synthetic transition metal complexes represent a large category of catalysts where ligands modulate the electronic and steric properties, and the metal characteristic governed the activity of the catalyst.[1]

Beside the catalytic activity, metal complexes have also found several applications in supramolecular chemistry as building block for synthesis of supramolecular architectures due to their thermodynamic stability and the possibly to exploit also molecular recognition.[2] Among many different ligands, polypyridines are one of the widest groups of polydentate ligands reported in literature.

1.2 TRIS(2-PYRIDILMETHYL)AMINE (TPMA) LIGANDS

Multidentate ligands containing two or more pyridine donor units play an important role in modern coordination chemistry. While polypyridines have extensively used since the early age of supramolecular chemistry, more recently a significant class of ligands is represented by tripodal ligands having three pyridyl system linked to a central nitrogen atom (Figure 1). The most common ligands among this class are tris(2-pyridilmethyl)amine (**TPMA**) where the position of the nitrogen atoms on the aromatic rings allows the formation of four coordination bonds with a central ions. Steric and electronic characteristics of the tripodal ligand can be changed by modifying the substituents of the pyridyl units.[3,4]

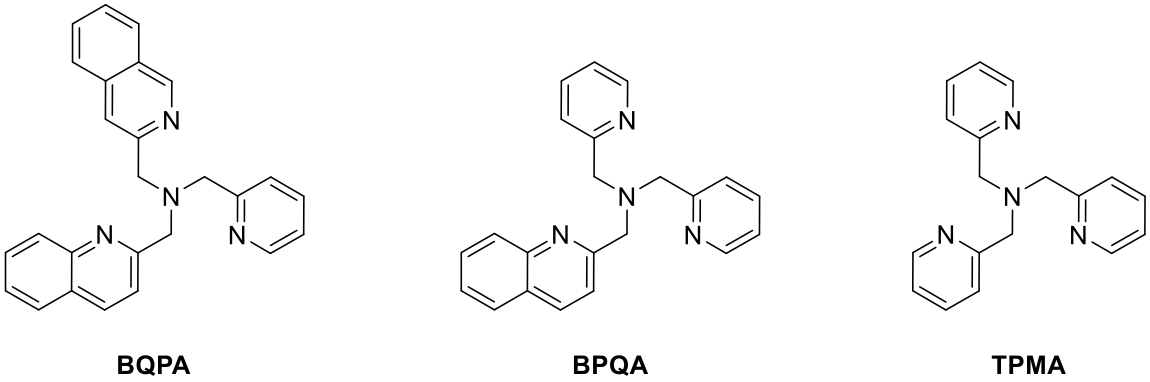

Figure 1: Structure of bis(2-quinolylmethyl)2-pyridylmethylamine **BQPA**, bis(2-pyridylmethyl)-2-quinolyamine **BPQA**, tris(2-pyridilmethyl)amine **TPMA** ligands.

1.2.1 Tris(2-pyridilmethyl)amine (TPMA) synthesis

The first synthesis of tris(2-pyridilmethyl)amine date back to a study of Andregg and Wenk in 1967[5,6]. The ligand was obtained by alkylation of primary (2-pyridyl)methylamine **1** with two equivalents of (chloromethyl)pyridine **2** in NaOH aqueous solution (Scheme 1). A brown solid was obtained after recrystallization from water (90 % yield).

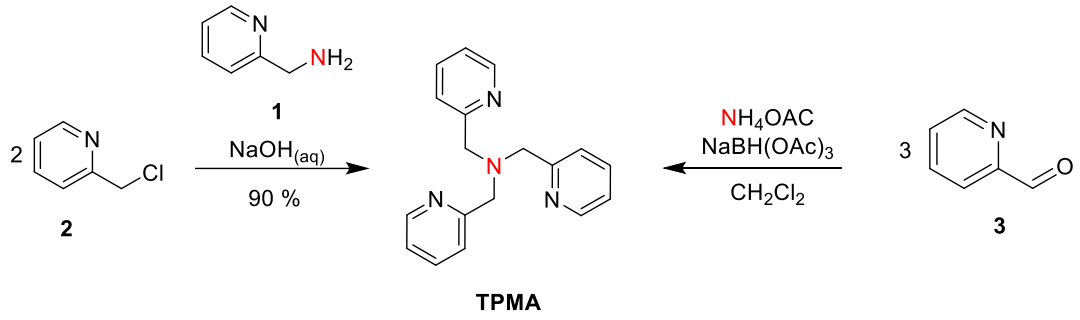

Scheme 1: Main strategies adopted for **TPMA** synthesis: alkylation and reductive amination.

While along the years alkylation has remained the most studied method, in recent years reductive amination has shown to represent a valuable alternative in the presence of sensitive groups. In this case, the reaction between an aldehyde precursor **3** with the ammonium acetate as nitrogen source and sodium triacetoxyborohydride as reducing agent.

1.2.2 TPMA metal complexes and geometries

Soon after the synthesis, in 1969, the first TPMA metal complex was reported with iron.[7] While iron remains the most studied metal within these type of structure, other metals such as cobalt, copper, zinc, nickel, ruthenium, and manganese have been reported (Figure 2).

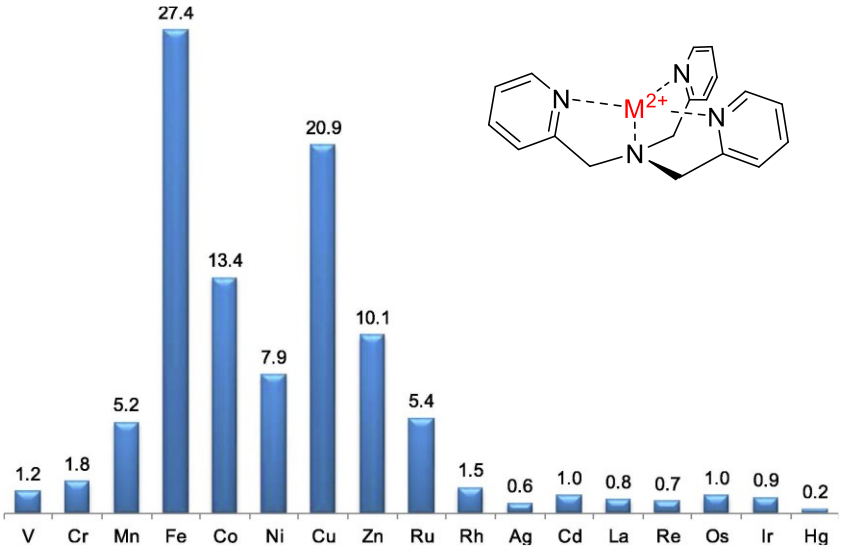

Figure 2: Metal distribution in crystallographic structures based on TPMA ligands. (Cambridge Crystallographic Data Centre, 2019)

In general, a 1:1 stoichiometry metal to **TPMA** is observed, but there are exceptions with ions owning ionic radii greater than 0.9 Å such as Calcium (II) and Lanthanides, in these cases a 1:2 stoichiometry is observed.[8,9] The most common geometry of metal based **TPMA** complex is trigonal bipyramidal where one apical position is occupied by the amine type nitrogen and three equatorial positions are occupied by pyridine nitrogen of **TPMA** ligand. The other apical position is usually occupied by a monodentate ligand or by a solvent molecule. Other geometries are less common, octahedral complexes are obtained preferentially with Iron or Nickel and tetrahedral coordination is scarcely observed because bite angle of the **TPMA** is not wide enough.[7,10,11] The d^8 metals ions such as Platinum (II) or Palladium (II) are an important exception because they tend to adopt a square planar geometry where **TPMA** is forced to behave as tridentate ligand binding the metal with amine nitrogen and two pyridine arms and the third pyridine arm remains uncoordinated.[12] Hypodentate coordination is also observed in some Copper (I) complexes where tetrahedral geometry is preferred, and an arm is replaced by a much more mobile solvent molecule or anion (Figure 3).[13]

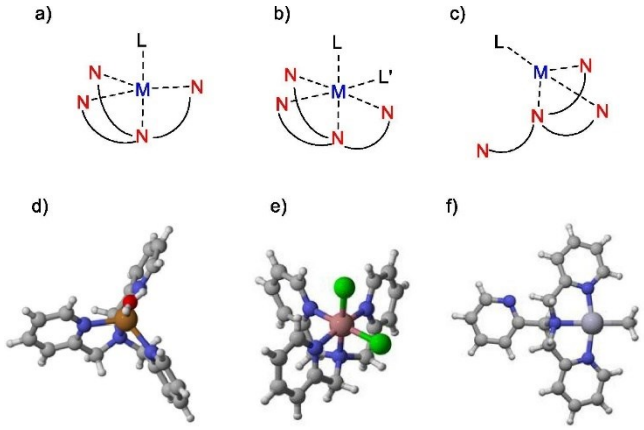

Figure 3: Common geometries in metal complexes based on **TPMA** ligands and the respective examples: **a)** Trigonal bipyramidal, **b)** Octahedral, **c)** Tridentate, **d)** Copper (II),[14] **e)** Cobalt (III),[15] **f)** Platinum (II)[16] complexes.

1.3 USES OF TPMA AS LIGAND AND COMPLEXES

TPMA metal complexes have a wide range of catalytic applications from hydrogen production with Cobalt, Iron or Nickel complexes,[17,18] atom transfer radical addition and polymerization with Copper complexes[19], carbon dioxide reduction with Cobalt complexes.[20,21] In the group where this thesis has been carried out, TPMA-based systems have been extensively studied over the years and they have found applications in different areas such as the determination of enantiomeric excess of a wide range of substrates[22,23] and the reductive catalysis[17,18,20,21] (Figure 4). The work of this thesis is focused on the latter purpose which will be deepened in the next chapter.

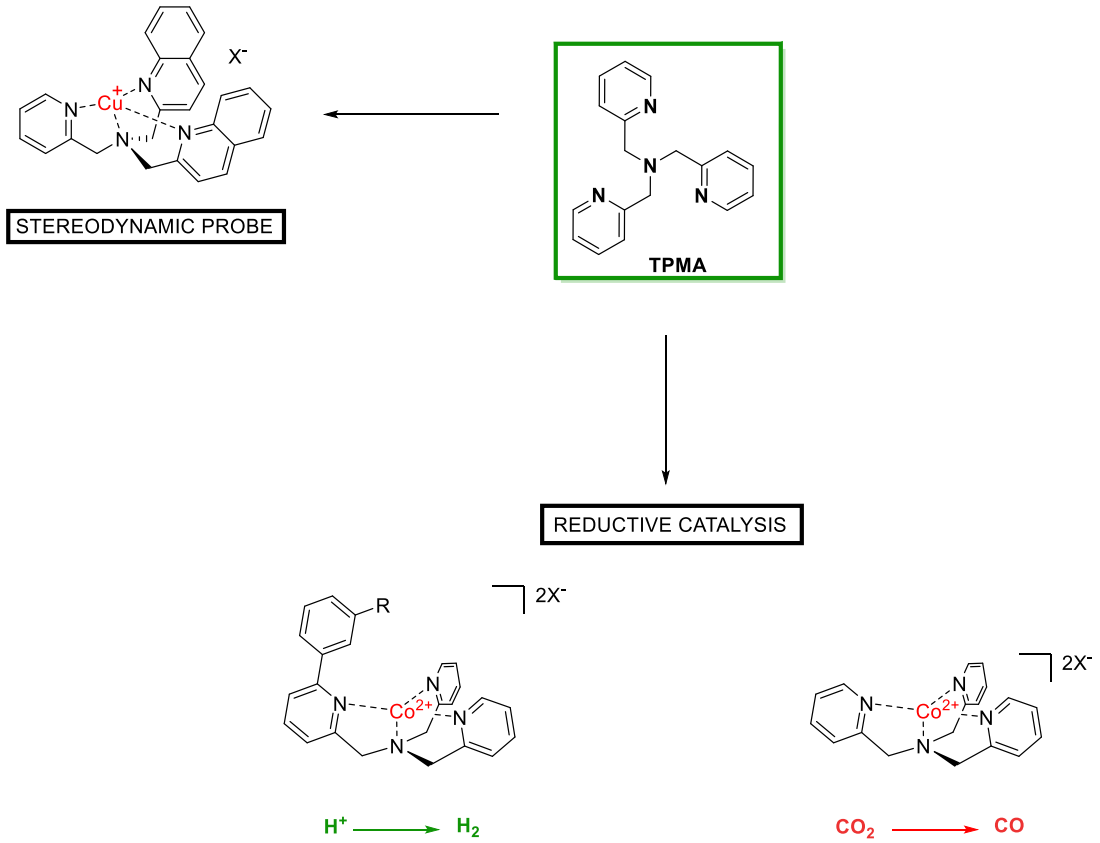

Figure 4: Uses of TPMA as stereodynamic probe for determination of enantiomeric excess, formation of supramolecular cage, catalyst in reduction reaction.

1.3.1 Determination of enantiomeric excess

Determination of the enantiomeric purity of chiral compounds is performed routinely in synthetic organic chemistry. Several **TPMA**-based systems have been developed over the years to be used in the determination of the enantiomeric excess of molecules such as carboxylic acids, which are one of the most used functional groups in pharmaceutical chemistry and are often intermediates in the synthesis of complex natural products. A sensor is defined as a receptor (host) that interacts with an analyte (guest) producing a detectable change in a generic signal. **TPMA** complexes belong to the class of stereodynamic probes which are characterized by the presence of an interconverting stereogenic element. The addition of a chiral analyte, which contains at least one stereogenic unit, shifts this balance towards the formation of a preferred diasteroisomer (Figure 5).

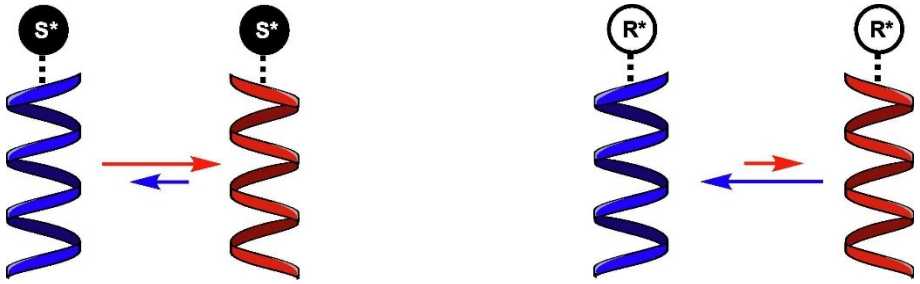

Figure 5: General working principle of a stereodynamic probe represented by the helix. The formation of the preferred diasteroisomer is induced by the attachment of a chiral molecule to the probe.

This equilibrium can be studied through the technique of circular dichroism (CD) where the presence of a chromophore is required, in this case the pyridine systems of the **TPMA**. This system is advantageous because common techniques such as HPLC or GC, while being accurate, fail to keep up with the number of samples that are created when several hundred reactions are performed in parallel. Anslyn *et al.* worked on systems based on metals and **TPMA** for the detection of the enantiomeric excess of carboxylic acids and alcohols were proposed systems based on copper[22] and **TPMA** (**5**) and zinc[23] and **TPMA** (**6**) respectively (Figure 6). The association between the achiral copper (II), host, and the chiral carboxylic acid, guests, (**5**) or between the zinc (II) and the secondary chiral alcohols (**6**) has been studied and thanks to the different CD recording signals in which the difference in magnitude and shape of the signal allows us to recognize the identity of the guest successfully.[22] In detail, a particular form of circular dichroism called exciton-coupled circular dichroism (ECCD) has been used for a non-empirical determination of the absolute configuration of chiral amines, β-aminoalcohols or epoxy alcohols. In the case of zinc **TPMA** (**6**) complex the presence of chiral alkoxy group in benzylic position create a hemiaminal which give similar ECCD signals and allows to determine the *ee* of unknow samples of three chiral secondary alcohols and another advantages and another advantage is related to the fact that no elaborate preparation is required to prepare the chiral host.[23]

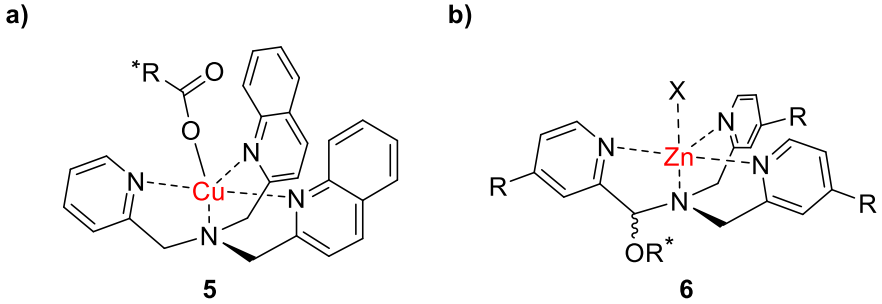

5 6

Figure 6: TPMA complexes used to determine the enantiomeric excess of a) carboxylic acid and b) secondary alcohol.[23]

1.4 TPMA COMPLEX IN REDUCTION CATALYSIS

1.4.1 Hydrogen evolution reaction (HER)

The continuous consumption of fossil fuels linked to the growing demand of energy is a serious problem that prevents sustainable development.[24] Within this context, hydrogen is a promising alternative and its direct production from water (protons) has a complex mechanism and requires the use of a catalyst capable of combining two protons and two electrons for the formation of H-H bonds with a sufficiently high speed (eqn. (1)).

$$2H^{+}+2e^{-} \longrightarrow H_2 \qquad (1)$$

In recent years, molecular catalysts have been developed, inspired by natural hydrogenases,[25] for the Hydrogen Evolution Reaction (HER) based on abundant metals on the earth's crust. Depending on the specific application, molecular catalysts show a high degree of tunability by synthetic modification with many possibilities for optimization. Among the transition metals of the first series, cobalt complexes have so far played a prominent role as catalysts for both electrochemical and light-driven conditions. The main advantages in using cobalt polypyridine complexes in HER are the ability to develop hydrogen in a purely aqueous environment with better stability due to the presence of reductively stable ligands and the absence of decomposition products, like the heterogeneous cobalt nanoparticles. The photosynthetic evolution of hydrogen performed under homogeneous conditions is conducted using a standard multi-component photochemical system composed of a light collection sensitizer ($Ru(bpy_3)$), a sacrificial electron donor (Ascorbate) and the cobalt polypyridine complex (Figure 7). In particular, the choice to use the Ru/ascorbate couple derives from the ability to work in the greenest solvent available, pure water and $Ru(bpy)_3^{2+}$ is chosen as photosensitiser because it combines several key properties.[26] Firstly, it has a strong absorption in the visible region with a long duration excited state that allows it to participate effectively in bimolecular reactions. Secondly, it has suitable reduction and oxidation potentials in the excited state (0,86 and +0,84 V vs. SCE in aqueous solution) to effectively promote the photoinduced electron transfer processes, both by oxidative and reductive means. Finally, it has suitable ground state reduction and oxidation potentials (1.28 and +1.26 V vs. SCE) to promote catalyst activation or donor oxidation. In combination with $Ru(bpy)_3^{2+}$ ascorbate is often used as a sacrificial agent

since it is soluble in water and can be used in high concentrations, it is possible to work at acidic pH levels (pH = 4-6) optimal for HER photochemically and it can also be used both as a sacrificial donor and buffer (pKa $_{\text{ascorbic acid}}$ = 4,1, in water).

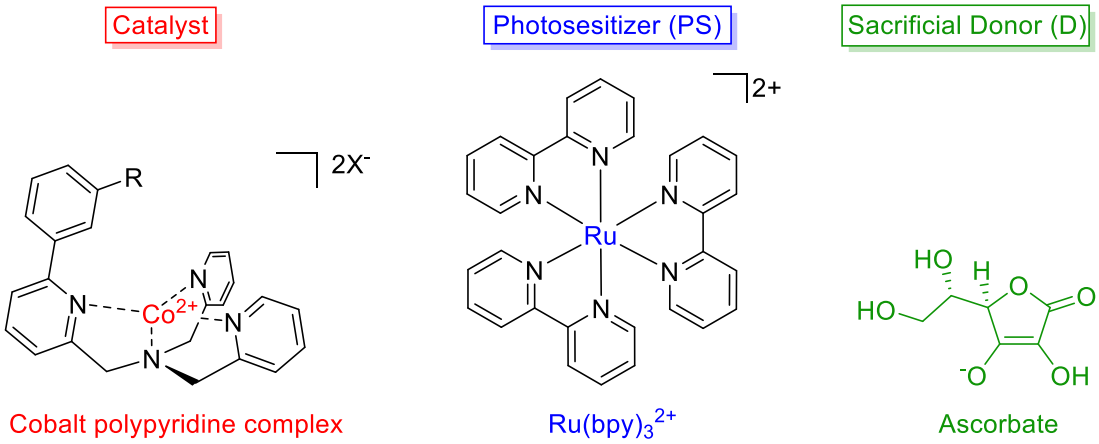

Figure 7: Standard photochemical system for HER involving a catalyst based on cobalt polypyridine complex, a phosesitizer based on $Ru(bpy)_3^{2+}$and ascorbate as sacrificial donor.

The reductive activation of the catalyst in the three-component system described so far, can be obtained following an oxidative or reductive pathway (scheme 3) where are involved bimolecular process in homogeneous photochemical conditions. In the first case, the species of $Ru(bpy)_3^{2+}$ is irradiated undergoing oxidative extinction by the catalyst that passes to a reduced form and an oxidized chromophore is obtained. This is then reduced again by reacting with the ascorbate (Scheme 2a, orange box). The photoinduced electron transfer observed in the oxidative process between the excited state of the photosesitizer and the catalyst usually occurs with a bimolecular rate constant of 10^9 $M^{-1}s^{-1}$.[17,27] In the second case, after the excitation of the photosensitizer follows the reductive quenching by the ascorbate, which leads to a reduction of the chromophore that eventually undergoes the transfer of electrons to the catalyst (Scheme 2b, purple box). In this case the rate constant for reductive electron transfer involving the ascorbate donor is 10^7 M^{-1} s^{-1} in aqueous solution. Based on this kinetic data, pseudo first order rate constants can be estimated in the range 10^3-10^5 s^{-1} by the oxidative pathway of $*Ru(bpy)_3^{2+}$ by the cobalt complex, while values of $>10^6$ s^{-1} are estimated by the reductive pathway of $*Ru(bpy)_3^{2+}$ from ascorbate. The rate of the reductive process is ten times higher than the oxidative one and this establishes that the light-driven evolution of hydrogen using the three-component system (Figure 9) follows a reductive quenching path (Scheme 3b). By repeating the same reaction sequence a second time, two electrons are stored on the catalyst platform that can

reduce two protons to one hydrogen molecule. The use of ascorbate as a sacrificial donor is also justified by the fact that the reaction is limited by paths of "short circuit" that involve a damaging recombination of charge, then a donor is used that undergoes a rapid and irreversible reaction to electron transfer.[28]

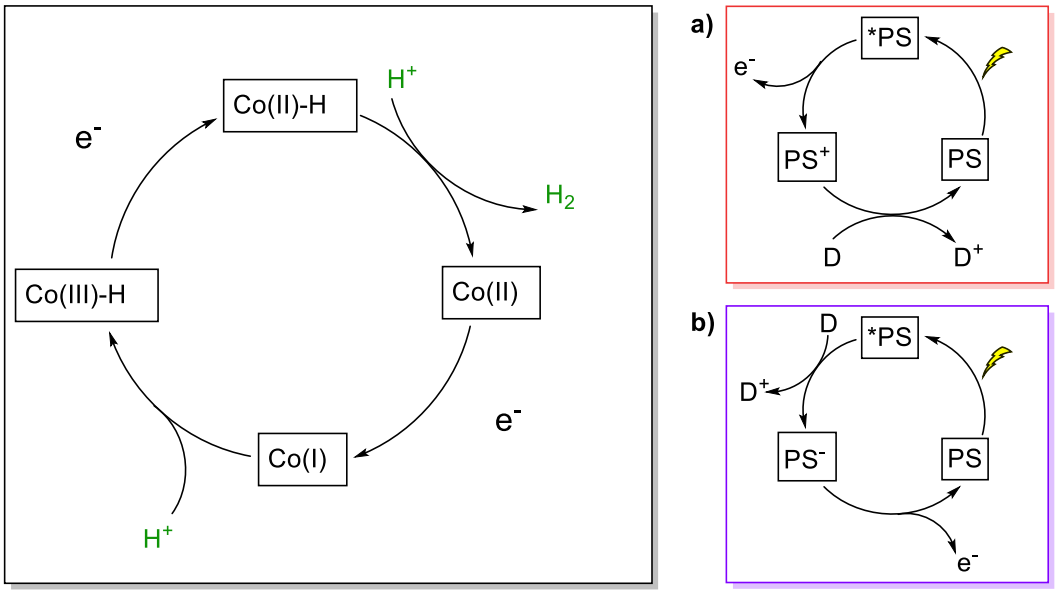

Scheme 2: Possible mechanism of photochemical HER with cobalt polypyridine complexes. **a)** Oxidative quenching pathway and **b)** reductive pathway.

Usually, photosynthetic activities are evaluated with parameters related to the photochemical process that can be obtained from the analysis of the amount of hydrogen produced (n, mol) *vs.* the irradiation time (s). From these data can be derived the initial rate of produced hydrogen (r, mol s^{-1}) (eqn. (2)), the value of turnover frequency (TOF) where n_{cat} are the moles of the catalyst in the solution subjected to irradiation (eqn. (3)), the turnover number (TON) (eqn. (3)), quantum yield of the evolution of hydrogen (Φ) where φ is the incident photon flow and LHE is the recovery efficiency of light (eqn. (5)). and the total amount of hydrogen produced (n_{max}, mol) (Figure 8).

$$\mathbf{r} = \Delta n/\Delta t \quad (2)$$

$$\mathbf{TOF} = r/n_{cat} \quad (3)$$

$$\mathbf{TON} = n_{max}/n_{cat} \quad (4)$$

$$\mathbf{\Phi} = 2r/\int \varphi \cdot \mathrm{LHE}\, d\lambda \quad (5)$$

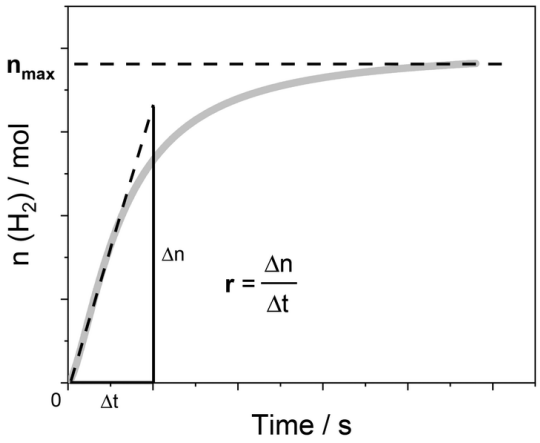

Figure 8: Example of the kinetic trace obtained from a typical photochemical experiment from r and n_{max} are identified (eqn. (3)-(5)).[29]

1.4.1.1 Cobalt polypyridine complexes for HER

In recent years, the use of cobalt complexes based on polypyridine ligands or amine-polypyridines ligands is increasing in reduction reactions such as Hydrogen Evolution Reaction (HER) under photochemical conditions (Figure 9). In 1981, Sutin *et al*. studied a cobalt-based polypyridine system which, working under photochemical conditions with $Ru(bpy)_3^{2+}$ as a photosensitizer and ascorbate as a sacrificial donor, catalysed the reduction of hydrogen to aqueous solution at pH = 5.[30,31]

In 2010 Chang *et al*. presented a new cobalt octahedral complex based on a polypyridine ligand (**9**) which had two free coordination sites to be used in reduction reactions. The complex is able to reduce hydrogen protons under electrochemical condition with a Faraday yield of 99% in acetonitrile solution, or 50% aqueous solutions, in the presence of trifluoroacetic acid (TFA) which triggers the appearance of a catalytic wave close to the catalytic pair Co^{II}/Co^{I} of **9**.[32]

In 2014, Thummel *et al*. introduced a new cobalt catalyst based on a planar polypyridine ligand (**10**) with two axial chlorides ligands that catalysed light-driven hydrogen reduction in an aqueous environment. Under irradiation with blue light, at pH = 4 and utilizing $Ru(bpy)_3^{2+}$ and ascorbate as sensing photo and sacrificial donor presents a TON = 333 and a TOF = 586 h^{-1} after 3 h.[33]

In 2016 Blackman *et al*., studied the influence of the apical ligand in a polypyridine complex of cobalt (**13**) used for the photochemical reduction of hydrogen in water solution using the same multicomponent system showed in Figure 9. Among the various anionic ligands studied (X = Cl^-, NO_3^-, $CF_3SO_3^-$, H_2O) the complex showing

the best catalytic activity is chlorine adduct (TON_{cat} = 13,5). In addition, by adding NaCl (0.3 M) the TON_{cat} increases by a factor of 2 for X = Cl^-, $CF_3SO_3^-$, and H_2O.[34]

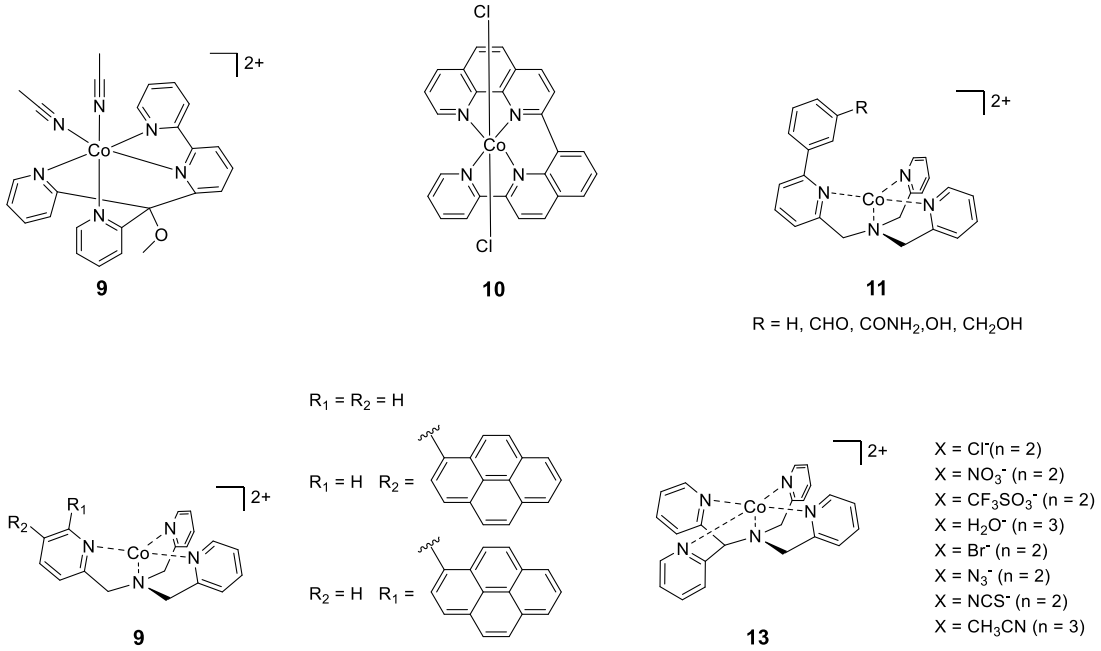

Figure 9: Cobalt complexes based on polypyridine or amino-polypyridines ligands for HER.

In the group where the thesis work was carried out, in 2016 a new cobalt complexes based on TPMA ligands (**11**), was developed to promote hydrogen production with a lower overpotential in aqueous solutions under photochemical condition. The presence of substituents with different hydrogen bond donor or acceptor abilities, in the second coordination sphere, stabilized the catalytic unit. Functionalization of the **TPMA** ligand is usually obtained by the introduction of a bromide in the skeleton, followed by a cross-coupling reaction for the insertion of the desired functional group (Scheme 3).[17]

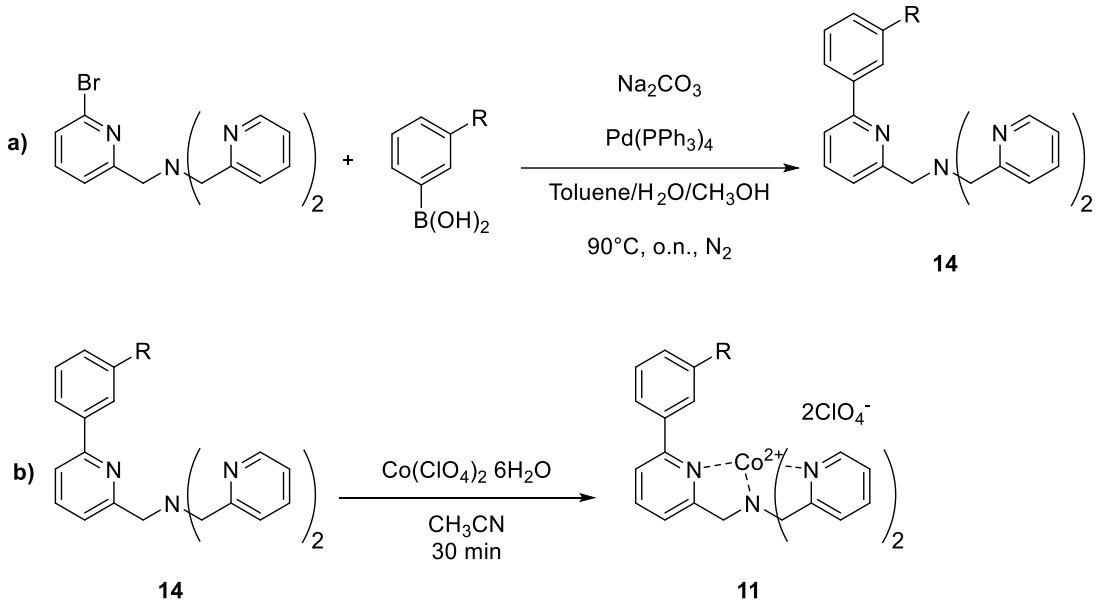

Scheme 3: General synthetic procedure for the synthesis of complex **11**.[17]

In 2021 the group where the thesis was carried out, proposed a new use of TPMA complexes **12** to produce hydrogen. Hybrid electrodes have been developed based on the combination of carbon nanotubes and new cobalt complexes based on TPMA functionalized with pyrenes to allow anchoring to the carbon nanotube. This system can work in neutral aqueous solution and are able to produce H_2 also under lighted assisted conditions.[18]

1.5 CARBON DIOXIDE REDUCTION

Carbon dioxide is a small and more inert molecule that required a relatively high overpotential to be reduced. A promising alternative to the use of hydrocarbon sources for petrochemical raw materials and chemicals is to obtain energy-dense compounds by converting CO_2 into methanol or ethanol, formate and CO through electrochemical methods in which the electricity used can be stored and reused for other purposes. [35–37]

In this approach, catalysis is of fundamental importance to find a new way to reuse carbon dioxide both photo and electrochemically. Different products can be obtained and further employed to produce fuels and chemicals. The electrochemical reduction to CO or photochemical reduction to ethylene are two of the most promising approaches for sustainable production of renewable fuels and chemicals. In the coming

years, other methods to reuse CO_2 will be improved and developed thanks to technological and scientific development such as polymerization, biohybrids and molecular machines (Figure 10).[38] In this thesis work, the synthesis of a series of TPMA-based cobalt complexes will be followed by their possible application in the electrochemical reduction of the CO_2.

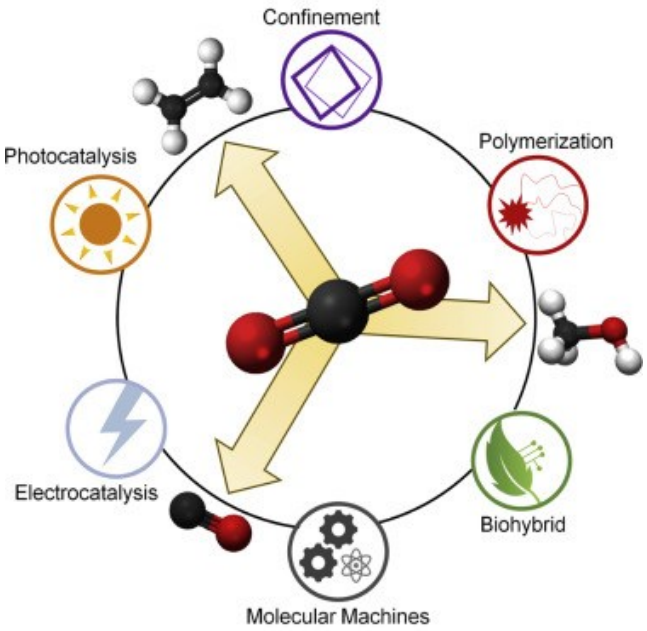

Figure 10: Methods for reusing CO_2: electrochemical or photochemical pathways, polymerizations, biohybrids and molecular machines.

A good catalyst suitable for practical applications must have a good thermodynamic and kinetic stability, robustness, and selectivity to have high turnover number (TON) and in the case of the electrocatalytic reduction of CO_2, also a good Faradaic yield (FY) defined as the selectivity of the catalyst to produce CO. In addition, the ideal catalyst should allow electrochemical reduction with a low potential in order not to have to apply large voltages. Catalytic activity is influenced by the environment around the metal centre and the modification of the catalysts is an alternative strategy to enhance it.

In the last years many catalysts were developed, and transition metal complexes supported by nitrogen donor ligands constitute an important class for our purpose (Figure 11).[39–43] The electrocatalytic performance of the catalyst are limited by their low stability and selectivity resulting in low TON and faradic yields (FY). For these complexes, where the chelating ligand is highly basic, the Co(I) species are nucleophilic enough to coordinate the CO_2 molecule. This is experimentally proved by measuring the anodic shift of the half-wave ($E_{1/2}$) of the reduce couple Co^{II}/Co^{I}

measured first under nitrogen and then under CO_2.[44–46] There are several mechanism hypotheses for the reduction of CO_2 to CO catalyzed by cobalt complexes and two proposed mechanisms are reported in Scheme 4.[47]

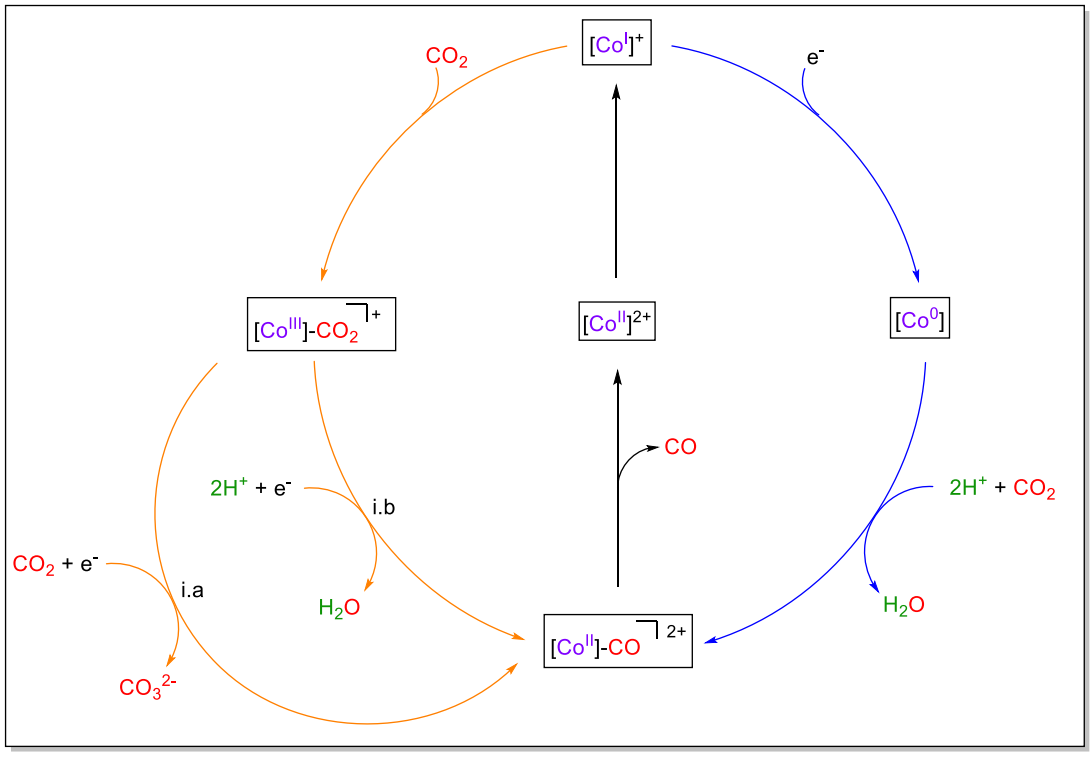

Scheme 4: Two proposed mechanism from electrocatalytic reduction of CO_2 to CO catalysed by cobalt complexes based on nitrogen donor ligands. Orange route is proposed for cobalt catalyst with nitrogen donor ligand while blue route is for catalyst with less basic nitrogen donor ligands.[47]

In the first route (Scheme 4, orange arrows) there are two critical steps for reducing CO_2 to CO both electrochemically and photochemically: i) the formation of adduct Co^{III}- CO_2 formed by the coordination of carbon dioxide with the Co^{I} species created *in situ* and, ii) the breakdown of the C-O bond which can be promoted by another CO_2 molecule by releasing a CO_3^{2-} anion (aprotic solvent ,Scheme 4 i.a) or by two hydrogen ions with the releasing of water molecule (protic solvent, Scheme 4 i.b). Another mechanistic way is proposed for cobalt complexes with less basic ligands for which it is necessary the formation of a Co^{0} species to bind the CO_2 and reduce it (Scheme 5, blue arrows).[47]

Once reduced CO_2 to CO, the release of CO from the Co^{II}-CO adduct is usually quick, also because it is very rare to see this intermediate directly during an electrochemical analysis.[48]

As reported above between the various families of CO_2 catalysts, cobalt complexes based on **15-19** polypyridine or amino pyridine ligands are the most versatile and are the most widely used to study the mechanism.

In 2013 Peters *et al* studied of a cobalt complex **15** based on a polynitrogen ligand with a high impact on catalyst selectivity in favour of CO rather than H_2 in the presence of water or weak acids. The complex can be selective in reducing CO_2 in acetonitrile and H_2O (10 M) solution despite being known to be also competent in reducing H^+.[39]

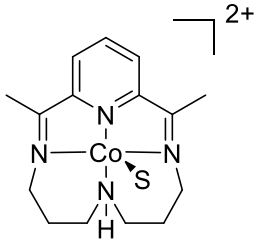

15
S = MeCN
-2.1 V, 45% FY_{CO}
4.1 TON_{CO}, 40 min

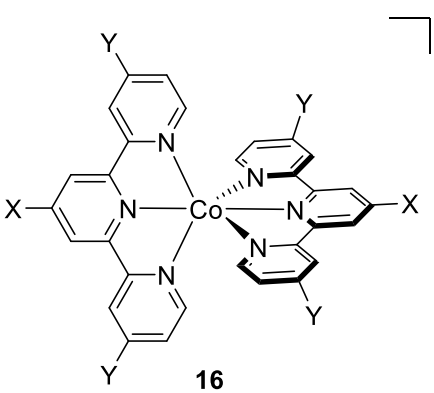

16
-2.0 V, 12% FY_{CO}
<1 TON_{CO}, 180 min
X = PhCl, PhMe, H, OMe, ^{t}Bu
Y = H, ^{t}Bu

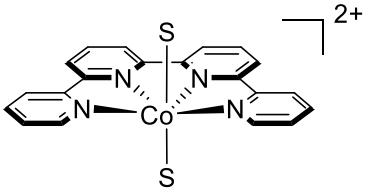

17
S = H_2O
-1.5 V, 94%FY_{CO}
17 TON_{CO}, 180 min

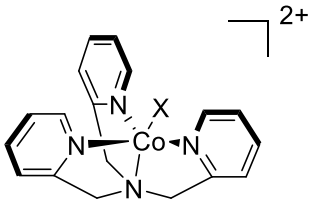

X = Cl
-1.9 V, 60%FY_{CO}
5.0 TON_{CO}, 300 min

18 = Cl
19 = Br
20 = I
21 = NCS

Figure 11: Cobalt catalyst supported by nitrogen donor ligand. Counterions are removed for clarity.

In 2015 Fontecave et al. proposed a new cobalt catalytic system based on two substituted terpyridine ligands **16** able to catalyse both HER and the electrochemical reduction of carbon dioxide from a mixture of H^+ and CO_2 resulting in products in modulated quantities. By acting on the applied potential and on the substituents of the pyridine rings in para position to minimize the perturbation of the steric properties of

the compounds around the cobalt atom it is possible to increase the selectivity towards one of the two products inhibiting the other. The electrochemical behaviour of these complexes was first tested under argon in DMF to see how it changes the reduction potential of the Co^{II}/Co^{I} species directly involved in coordinating CO_2. Terpyridines carrying electronwithdrawing substituents show a more positive reduction potential while with electrondonating substituents more negative reduction potentials result.[40]
Robert, Lau and coworkers proposed in 2018 a quaternary pyridine cobalt complexe which showed a high selectivity in CO production of 96% with TON = 17 in 3 h in acetonitrile solution.[41]
In the same year Wang et al. studied the behaviour of cobalt **TPMA** system **18** in carbon dioxide reduction in acetonitrile/water (4:1 v/v) solution. They not only used the previous complex but also tested BPQA and BQPA ligands reported in Figure 1. The overpotential to be applied to obtain the electrochemical reduction of CO_2 to CO decreases to 200 mV (the lowest reported) increasing the number of quinoline groups.[43] More cobalt complexes based on **TPMA** system are treated in the next paragraph.

1.5.1 Cobalt TPMA complex for electrochemically reduction of CO_2

Although the above complexes are not very efficient, the cobalt and **TPMA** complex based catalysts show good stability and TON potentials due to the strong chelating effect of the ligand. In 2015 Cheng et al reported a robust cobalt catalyst for carbon dioxide reduction based on **TPMA** ligands complexed with cobalt chloride **20**. The isolated complex had a trigonal bipyramidal geometry confirmed by X-ray crystallographic analysis (Figure 12a). The reduction potential of Co^{II}/Co^{I} results more negative compared with other cobalt complexes supported by similar ligand scaffolds, and this may be crucial for an effective carbon dioxide reduction. For a reasonable bond of CO_2 with metal complexes the peak of $Co^{II/I}$ reduction should be more negative than 1,65 V. The electrocatalytic current at the $Co^{II/I}$ reduction potential observed in the CO_2 atmosphere shows a marked increase indicating that the complex can be a good catalyst for reduction (Figure 12b). This can also be used as a pre-catalyst to be coupled to a kind of iridium for a photochemical reduction of carbon dioxide to carbon monoxide with good TON (CO) (> 900) and selectivity for CO (85%).[21]

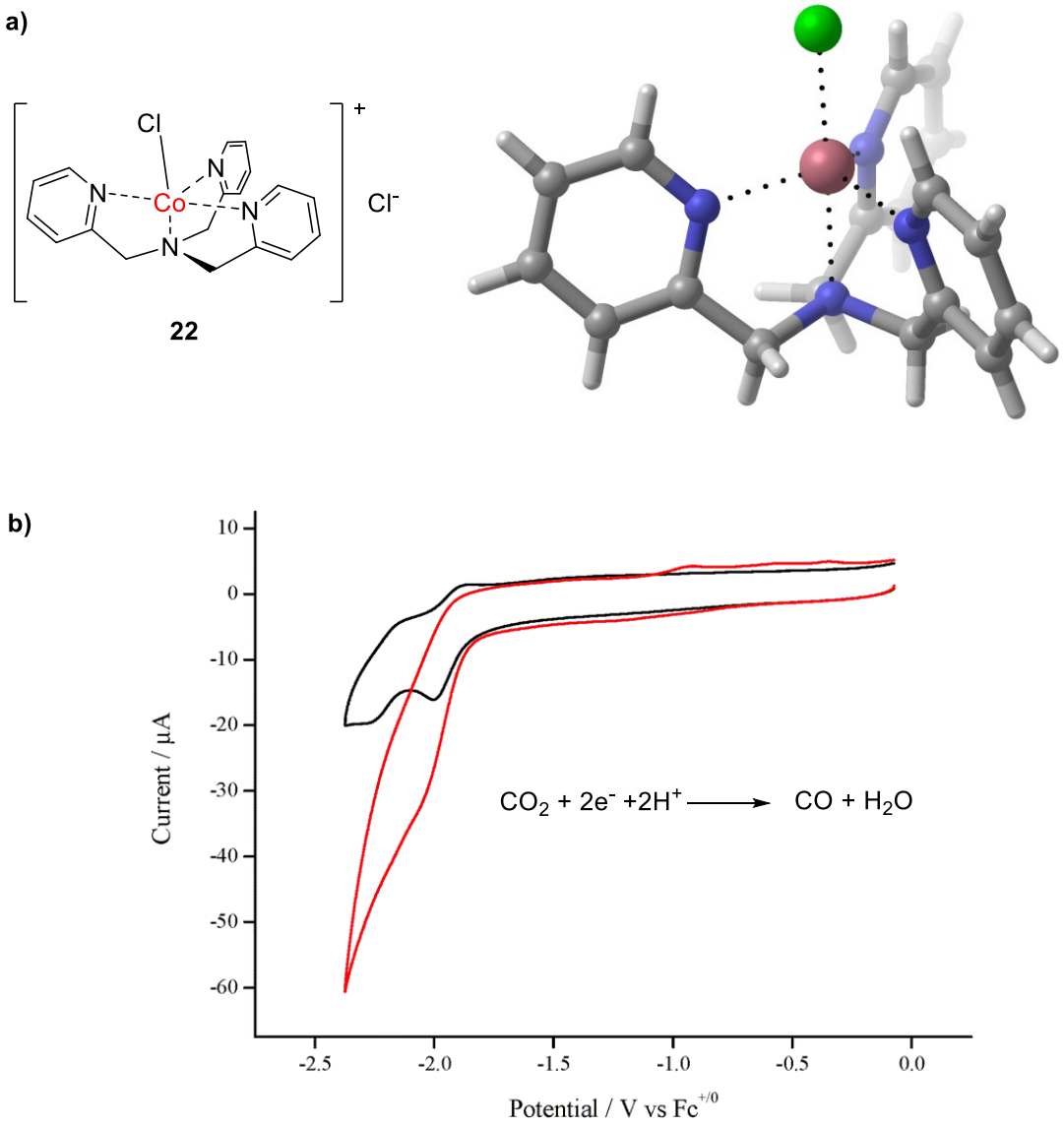

Figure 12: a) Cobalt **TPMA** complex structure and X-ray crystal. **b)** Cyclic voltammetry of Cheng's cobalt **TPMA** complex under argon (black) and carbon dioxide (red) using a glassy carbon disk electrode, scan rate = 100 mV s^{-1}.[21]

Another cobalt catalyst based on **TPMA** is reported by Zhu and others in 2016. In this case the skeleton of the **TPMA** is the same reported by Cheng (**18-21**) but the cobalt salt used is changed to evaluate the effect of the coordinate anion to cobalt. In particular, four cobalt salts were used and as a result four **TPMA** cobalt complexes, $[Co(\mathbf{TPMA})X]^+$ were studied where X = Cl^-, Br^-, I^-, NCS^- (Figure 13). The reduction peak of $Co^{II/I}$ is more negative with Cl^- as coordinated anion and with other this wave decreases in potential to -1.76 V. also in this case the adduct $[Co^{I}\text{-}CO_2]$ is form at first reduction peak of cobalt.

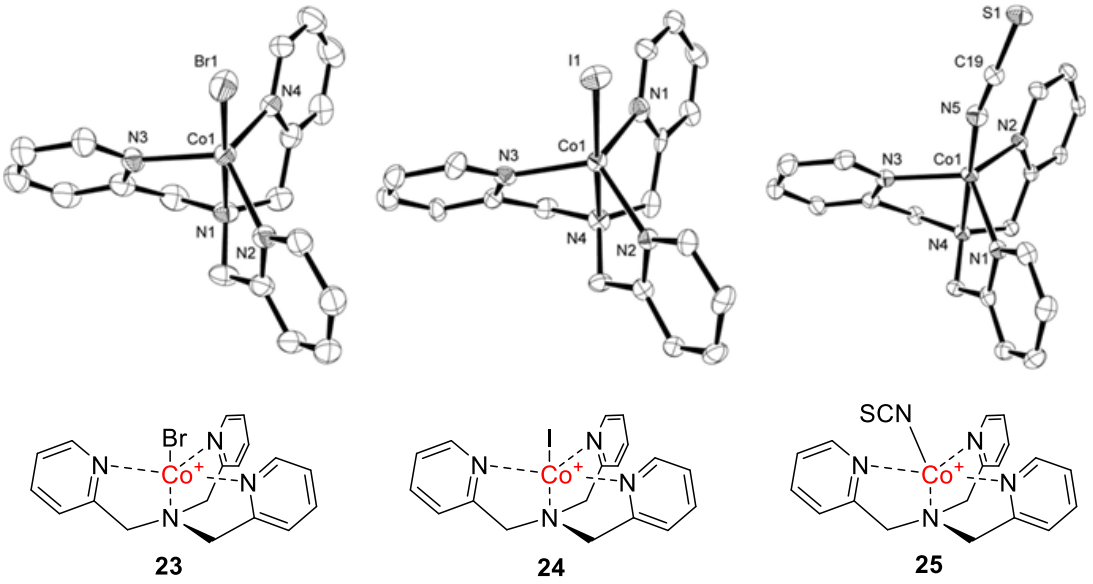

Figure 13: Structure of cobalt TPMA complex with different anion coordinated to cobalt: X = Br (**21**), I (**22**), NCS (**23**).[20] Counterions and solvents molecules have been removed for clarity.

These complexes are good electrocatalysts that can also be used for photocatalysis by always using a *fac*-Ir(ppy)$_3$ as a photosensitizer and the effect of different coordinated anion is reflected in the performance of the catalyst under irradiation. The bromide ion demonstrates the best performance with TON >100 0 and selectivity for CO >90%.[20]

2 AIM OF THE THESIS

The main aim of the thesis is the synthesis and characterization of new *para*-substituted **TPMA** based cobalt complexes and some preliminary studies of their electrochemistry. In particular, this thesis will offer the series of different complexes that in virtue of their different electronic properties of the pyridine ligands, can be use as mechanistic tools for the study of reductive reactivity.

More in detail the three main objectives of this thesis work will be *i)* the synthesis and the characterization of **TPMA**-based ligands replaced in *para*-position with different substituents i.e. NO_2, Cl, Br, OCH_3, Pyrrolidine one two or three times *ii)* complexation of the ligands with a cobalt salt to obtain a **Co-TPMA** complexes, *iii)* preliminary investigate the electrochemistry of these complexes.

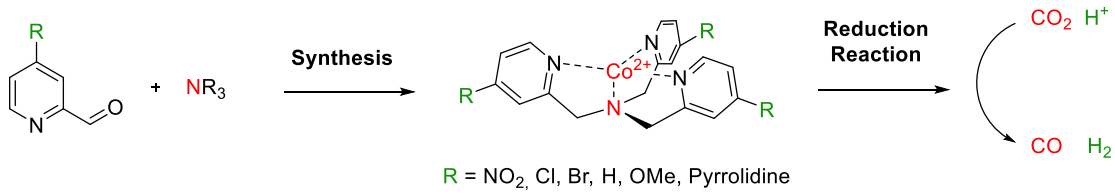

Figure 14: Schematic representation of aim of the thesis.

3 RESULTS AND DISCUSSION

3.1 SYNTHESIS OF *PARA*-SUBSTITUTED TRIS(2-PYRIDILMETHIL)AMINE

The first part of the work has been directed towards the synthesis of *para*-substituted **TPMA** ligands with one, two or three electron-donating or withdrawing substituents. In particular, six different substituents have been chosen: NO_2, Cl, Br, H, OCH_3, and pyrrolidine. While the direct introduction of a substituents position starting from a formed **TPMA** is difficult to achieve selectively, it is possible to obtain these types of products with a different design. The retrosynthetic approach is reported in Scheme 5 and it shows the synthetic strategy used for the synthesis of ligands through the reductive amino reaction starting from the respective substituted aldehyde and a source of nitrogen: bis(pyridin-2-ylmethyl)amine for *mono*-substituted **TPMA**, pyridin-2-ylmethanamine for *di*-substituted and ammonium acetate for *tri*-substituted **TPMA** (Scheme 5).

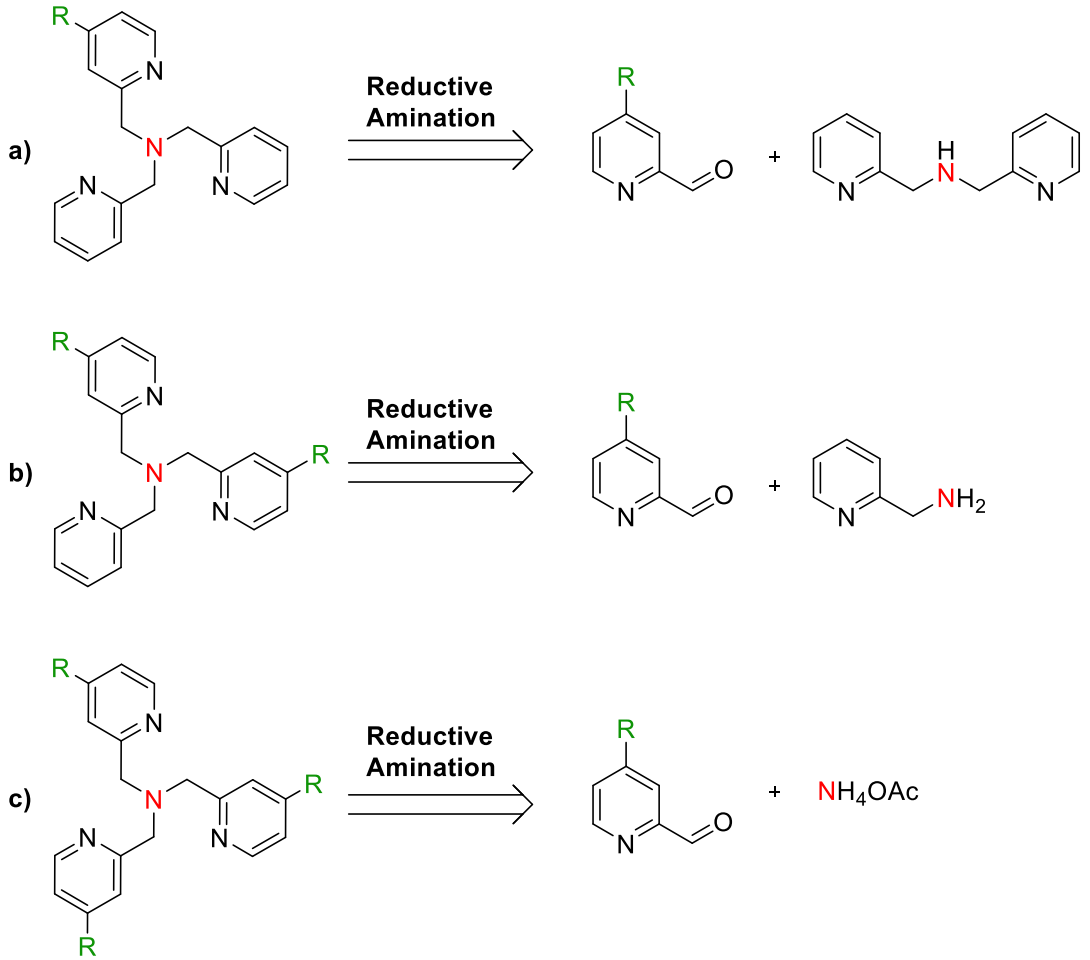

Scheme 5: Retrosynthesis approach adopted for the synthesis of **TPMA** with one (**a**), two (**b**) or three (**c**) substituent.

The reaction requires anhydrous conditions, under nitrogen and with dry DCM as the solvent using a mild reducing agent such as sodium triacetoxyborohydride.

The synthesis of the **TPMA** ligand bearing the pyrrolidine will follow a different approach recently reported in the literature.[49] The synthesis will be performed through a nucleophilic substitution reaction from the corresponding **TPMA** previously prepared with the chlorine substituents (Scheme 6).

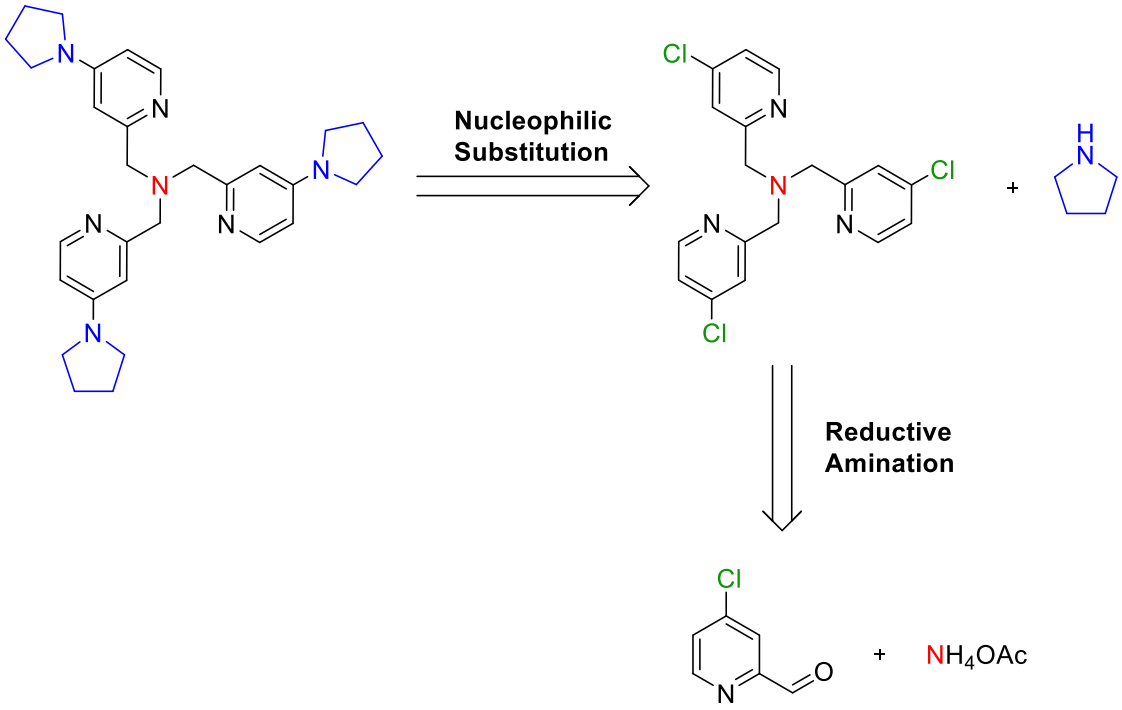

Scheme 6: Retrosynthesis approach for the synthesis of **TPMA** with pyrrolidine as substituent in *para*-position.

3.1.1 Nitro-substituted TPMA

Nitro group was the first substituent chosen for substitution of **TPMA.** The synthesis of ligands with one, two and three nitro groups followed the reductive amination reaction starting from the aldehyde replaced with the NO_2 group in the *para* position. This aldehyde is not commercially available, and it was previously synthesized in the group following a recent literature approach (Scheme 7).[50] Starting from N-Oxide **26,** it was first acetylated with trifluoroacetic anhydride under reflux and then hydrolysed to the alcohol **27** in a single synthetic step. The formation of compound **27** was confirmed by ^{1}H-NMR (Figure 15) that shows the two characteristic methyl protons at 4.94 ppm and the three aromatic protons of pyridine between 7.78 and 8.87 ppm.

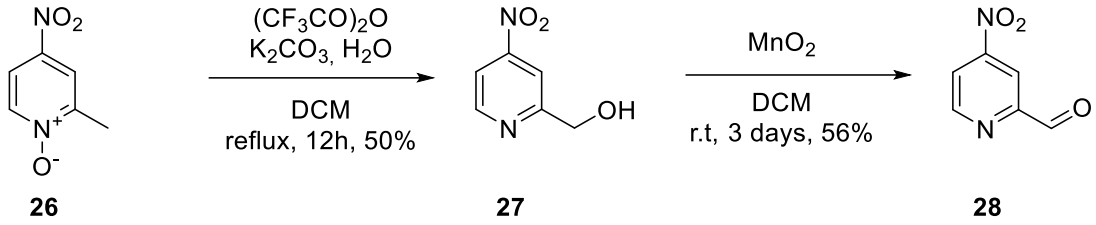

Scheme 7: Synthesis of 4-nitropicolinaldheyde (**28**) from 2-methyl-4-nitropyridine 1-oxide (**26**).

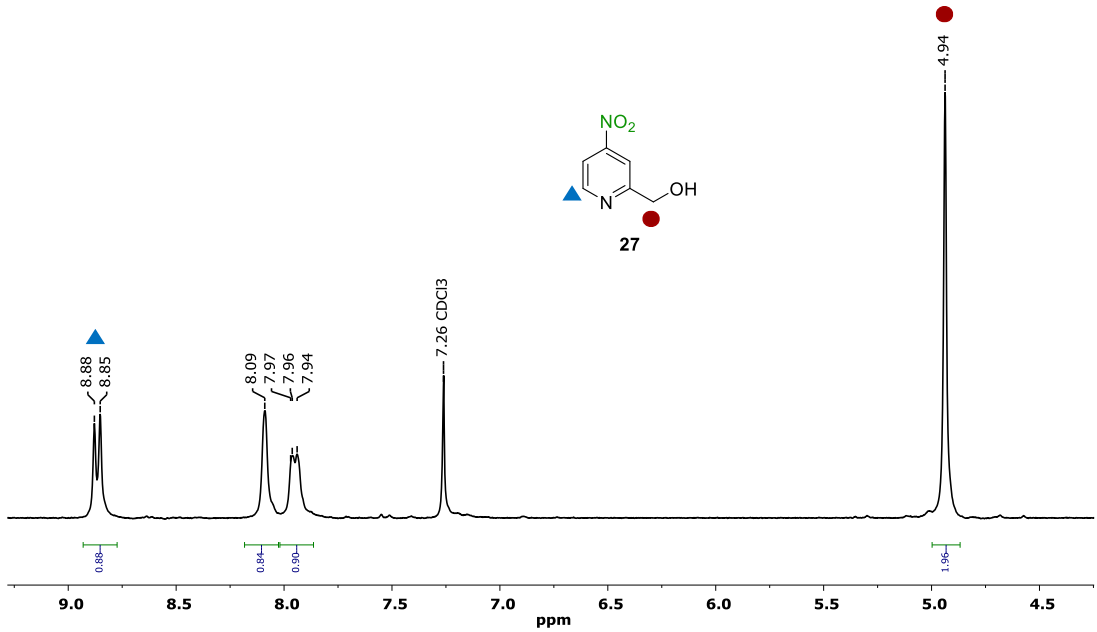

Figure 15: ^{1}H-NMR (300 MHz, $CDCl_3$) of alcohol **27**.

The alcohol obtained after the work-up was oxidized to the respective aldehyde **28** with manganese dioxide at room temperature for three days. The reaction was monitored by ^{1}H-NMR, observing the progressive disappearance of the reagent and the simultaneous increment of the desired aldehyde product. The manganese dioxide is a suitable oxidant for substrates such as pyridines, but the presence of a strong electron-withdrawing group decreased the reaction yield significantly. Even if reaction conditions, such as the temperature and the solvent, were changed trying to improve the reaction yields, a final yield of 50% was obtained. After purification on a chromatographic column, aldehyde **28** was used for the synthesis of **TPMA** replaced one and three times with nitro group (Scheme 8).

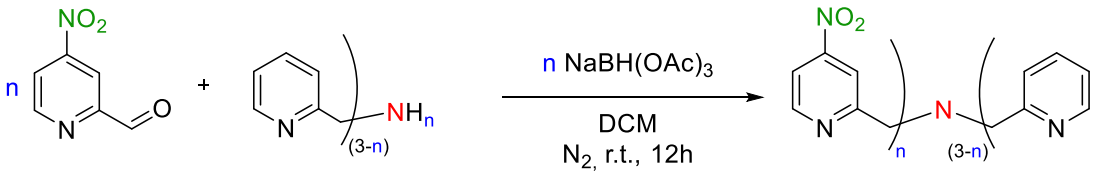

	Yield (%)	Name
n = 1	61	**NO_2-TPMA 29**
n = 2	/	**$(NO_2)_2$-TPMA 30**
n = 3*	86	**$(NO_2)_3$-TPMA 31**

Scheme 8: Synthesis of **TPMA** ligands with nitro groups as substituent through reductive amination reaction. *In the synthesis of **$(NO_2)_3$-TPMA 31** the nitrogen source is ammonium acetate (NH_4OAc).

For the *mono*-substituted **NO_2-TPMA 29** one equivalent of aldehyde **28** react with one equivalent of bis(pyridin-2-ylmethyl)amine in dichloromethane using sodium triacetoxyborohydride as reducing agent. The ligand **29** was purified though chromatography column in silica gel with a gradient elution (from DCM to DCM:MeOH 9:1) The product has been characterized through ^{1}H-NMR, ^{13}C-NMR and ESI-MS (Figure S3, S4, S5) which confirm the formation of the ligand. The ^{1}H-NMR shows the singlet of the 4 benzyl protons of the two unsubstituted arms of the **TPMA** not replaced with the substituent and the two benzyl protons of the other. It is worthy also to notice that the signals of the alpha protons of pyridine ring bearing the nitro substituent at 8.79 ppm and the unsubstituted ones at 8.55 ppm (Figure 16a).

For the synthesis of **$(NO_2)_3$-TPMA 31**, three equivalents of aldehyde **28** react with one equivalent of ammonium acetate and three equivalent of sodium triacetoxyborohydride in dichloromethane to give an orange oil after work up. A good yield of final product is obtained after purification using a alumina gel chromatography column with a gradient elution (from DCM to DCM:MeOH 9:1). The pure ligand is an orange solid and was confirmed using ^{1}H-NMR. The spectra displayed the characteristic signals of 6 benzylic protons at 4.17 ppm and the alpha pyridine protons at 8.88 ppm. (Figure 16b). The increase of nitro groups from one to three is responsible for a shift of the NMR signals of benzylic protons to higher ppm due to the strong deactivation given by the three NO_2 groups.

While the synthesis of **$(NO_2)_2$-TPMA** with two nitro groups **30** proceeded similarly to the other, the product was not present after the purification phase. In more detail, the analysis after work using ESI-MS analysis (Figure 17) confirmed the presence of the

desired ligand with the characteristic molecular ion at 381,1 m/z. However, after purification in the chromatographic column it was not possible to recover the ligand.

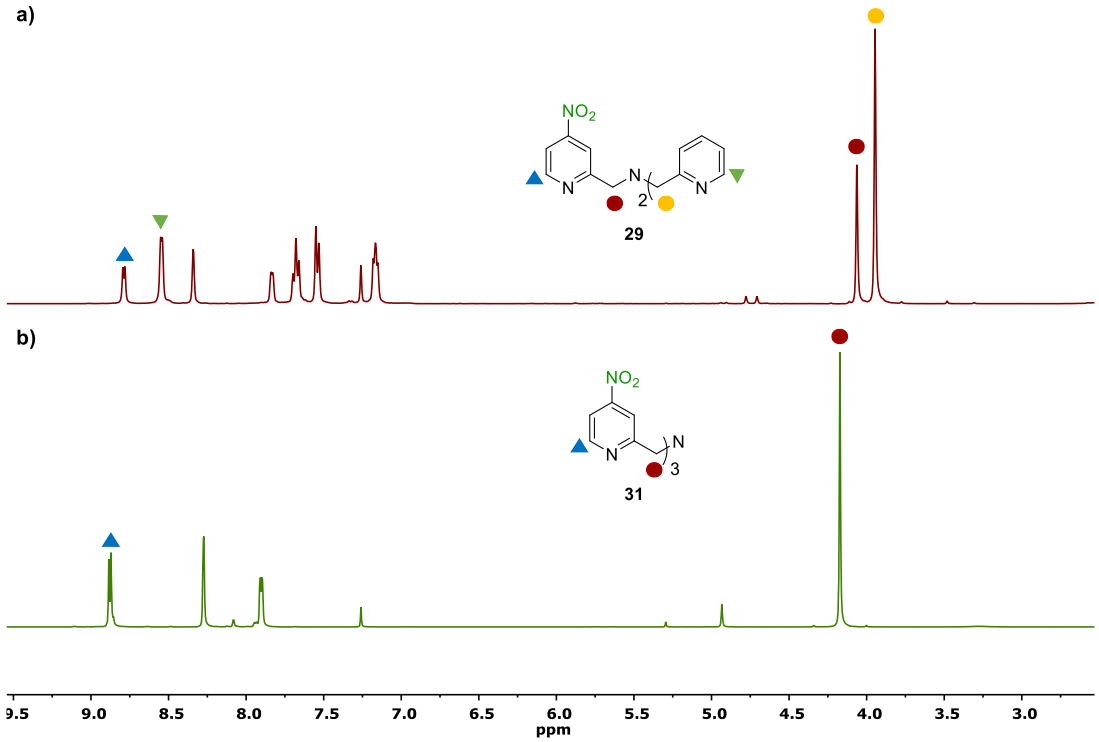

Figure 16: ^{1}H-NMR (400 MHz, $CDCl_3$) of **a) NO_2-TPMA29** and **b) $(NO_2)_3$-TPMA 31**.

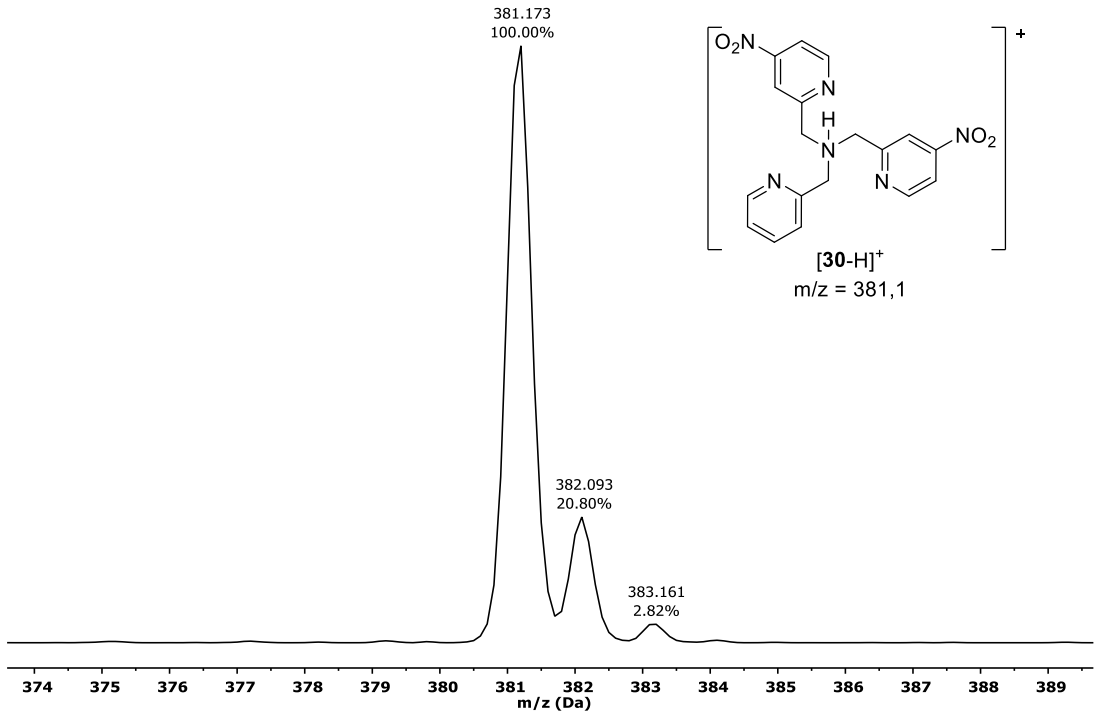

Figure 17: Experimental ESI-MS of protonated ligand [**$(NO_2)_2$-TPMA 30**-H]$^+$ in ACN/H$^+$ before the chromatography column purification.

3.1.2 Chloro-substituted TPMA

Chlorine has been the substituent chosen for the second series of synthesized **TPMA**s. These ligands are very versatile because in addition to the main purpose of being studied in reduction reaction after complexation with a cobalt salt, they have also been used for the synthesis of another class of **TPMA**, those replaced with pyrrolidine (Scheme 6).

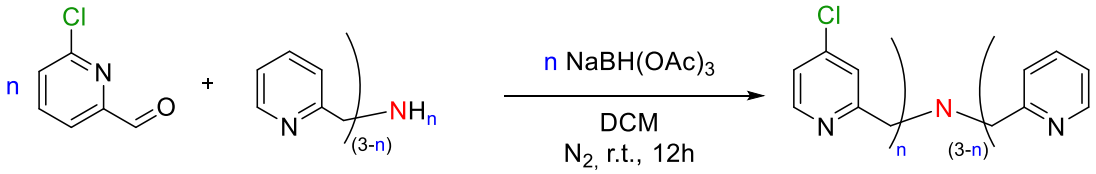

	Yield (%)	Name
n = 1	57	**Cl-TPMA 32**
n = 2	83	**Cl_2-TPMA 33**
n = 3*	32	**Cl_3-TPMA 34**

Scheme 9: Synthesis of **TPMA** ligands with chlorine as substituent through reductive amination reaction. *In the synthesis of **$(Cl)_3$-TPMA 34** the nitrogen source is ammonium acetate (NH_4OAc).

The chlorine substituted aldehyde used for the reductive amino reaction is commercial and the synthesis of *para* substituted **TPMA** occurred following reductive amino reaction (Scheme 9). After a simple work-up, it was necessary to purify the ligands with a chromatography column in all the three cases. The same eluent, gradient DCM:MeOH from 100:0 to 9:1, was used but different stationary phases were required: *mono*-substituted **Cl-TPMA 32** was purified in silica gel to give an orange oil, *di*-substituted **Cl_2-TPMA 33** in alumina gel to give a yellow oil in a good yield and *tri*-substituted **Cl_3-TPMA 34** with silica gel to give an orange solid in low yield. The ligands were characterized with ^{1}H-NMR, ^{13}C-NMR and ESI-MS (Figure S6-S8, S21-S23, S34-S36) which confirmed the identity of the products. ^{1}H-NMR spectrum revealed signals referred to the six benzylic protons at 3.86 ppm for the monosubstituted **Cl-TPMA 32**, at 3.89 ppm for the disubstituted **Cl_2-TPMA 33** and at 3.88 ppm for the trisubstituted **Cl_3-TPMA 34**. Also visible are the peaks related to the alpha protons of the pyridine between 8.51and 8.38 ppm for **32**, 8.55 and 8.42 ppm for **33** and at 8.41 ppm for **34** (Figure 18).

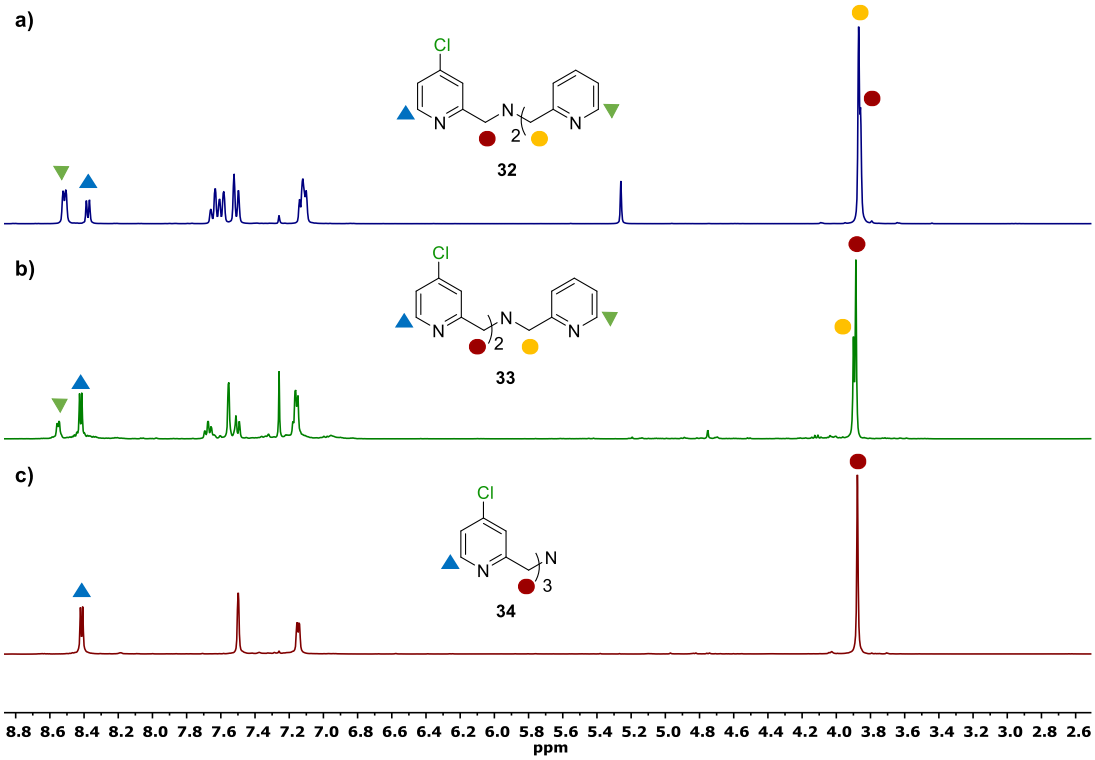

Figure 18: ^{1}H-NMR (400 MHz, $CDCl_3$) of **a) Cl-TPMA 32**, **b) Cl_2-TPMA 33,** and **c) Cl_3-TPMA 34**.

A difference in the chlorine and nitro substitution can be noticed between the *mono* nitro ligand **29** and *mono* chlorine **32** on the separation of benzyl proton peaks. The presence of a less electron-withdrawing group as chlorine, in comparison with nitro, results in a significantly lower separation of the benzylic protons.

The ESI-MS analysis shows the molecular ion of the desired products with the isotopic distribution typical of molecules that contains chlorine atoms.

3.1.3 Bromo-substituted TPMA

The synthesis of the bromine substituted **TPMA** ligands followed the synthetic strategies similarly to the previous substituted ligand (Scheme 10). The aldehyde bearing a bromine in position 4 of the pyridine ring is commercially available and had a good solubility in the reaction solvent (DCM).

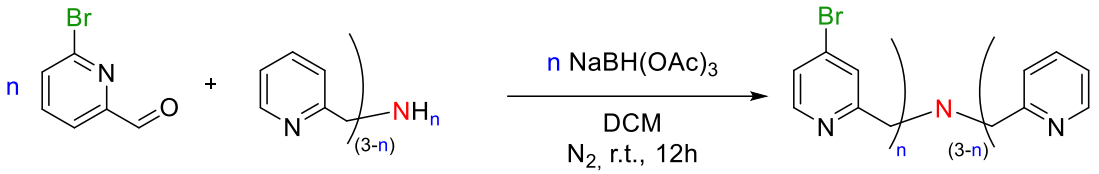

	Yield (%)	Name
n = 1	97	**Br-TPMA 35**
n = 2	91	**Br_2-TPMA 36**
n = 3*	74	**Br_3-TPMA 37**

Scheme 10: Synthesis of **TPMA** ligands with bromine as substituent through reductive amination reaction. *In the synthesis of **$(Br)_3$-TPMA 37** the nitrogen source is ammonium acetate (NH_4OAc).

The synthesis of the *mono*-substituted **Br-TPMA 35** was performed by the reaction between one equivalent of aldehyde and one equivalent of bis(pyridine-2-ylmethyl)amine in dichloromethane using sodium triacetoxyborohydride as reducing agent. After washing with KOH the product was an amber oil in high yield (^{1}H-NMR spectra, Figure 19 and ESI-MS spectra Figure S11). In the ESI-MS spectra is visible the molecular ion [**35**-H]$^+$ at 369.1 m/z with the characteristic isotopic pattern of bromide molecule.

For **Br_2-TPMA 36** the crude resulting from the work up was purified by chromatographic column with alumina gel and eluent gradient (from DCM to DCM:MeOH 9:1) to give also an amber oil.

The synthesis of *tri*-substituted **Br_3-TPMA 37** furnished a reaction crude with several impurities in comparison with the previous *mono* and *di* substituted **35** and **36**. However, purification on a chromatographic column using silica gel and the same eluent of **36** allow to purify the product which turned out to be an amber solid that crystallized after solvent evaporation. In ESI-MS spectra was observed the molecular ion [**37**-H]$^+$ at 369 m/z (Figure 20).

^{1}H-NMR analysis reveals the characteristic peaks of a **TPMA** substituted in *para* position with one, two or three substituents for the all the ligands **35**, **36**, **37**. The different number of bromine atoms on the **TPMA** skeleton causes a slight separation of the six benzylic proton peaks in a similar way to the chlorine substituent due to the similar electronic effect. (Figure 19).

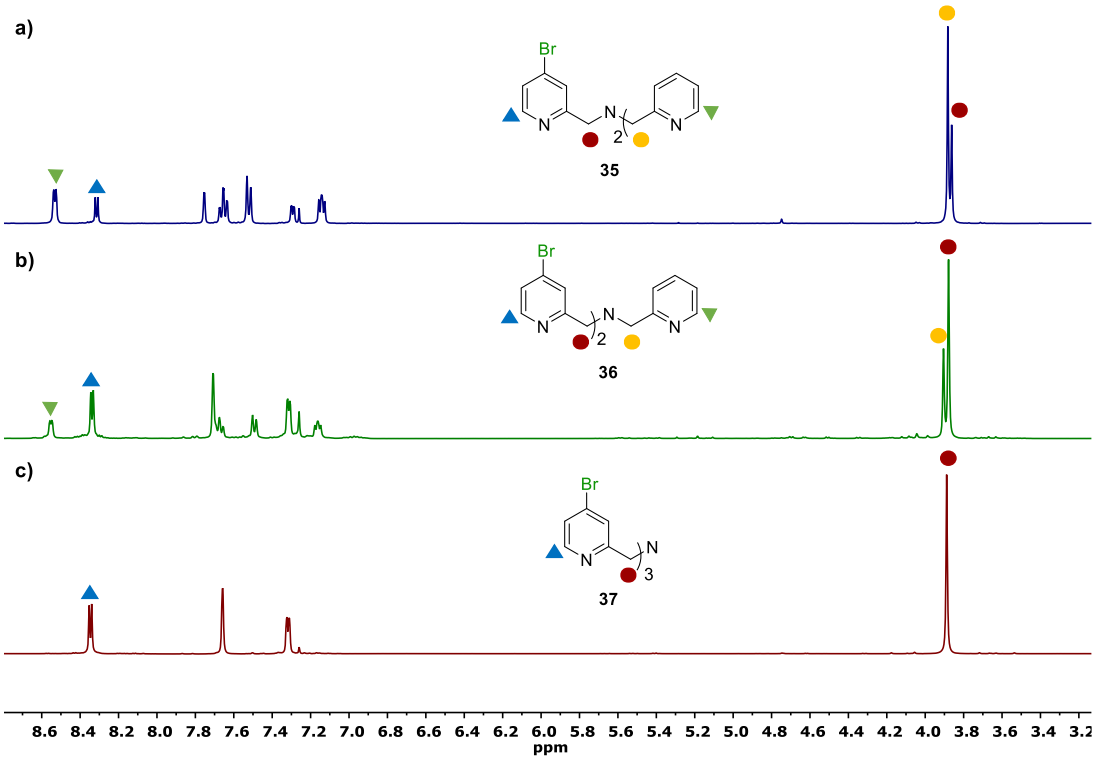

Figure 19: ^{1}H-NMR (400 MHz, $CDCl_3$) of **a) Br-TPMA 35**, **b) Br_2-TPMA 36,** and **c) Br_3-TPMA 37**.

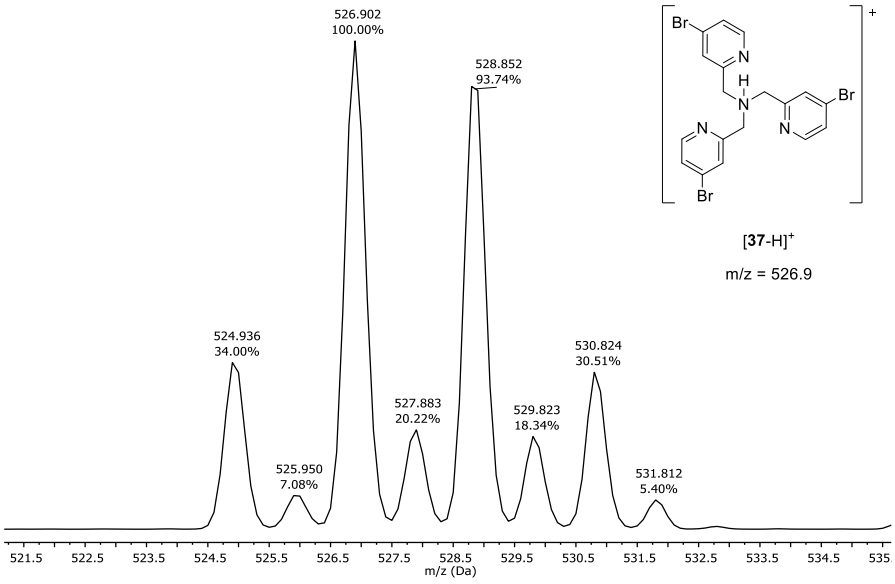

Figure 20: Experimental ESI-MS of protonated ligand [**37**-H]$^{+}$ at 526.9 m/z in ACN/H^{+}. The isotopic pattern is typical of molecule contains three bromine atoms.

3.1.4 Methoxy-substituted TPMA

The methoxide group is one of the two electrondonor groups of the series of substituents examined. The reductive amino reaction for ligand synthesis in this series

also starts from a commercial aldehyde which appears as a hygroscopic yellow solid (Scheme 11).

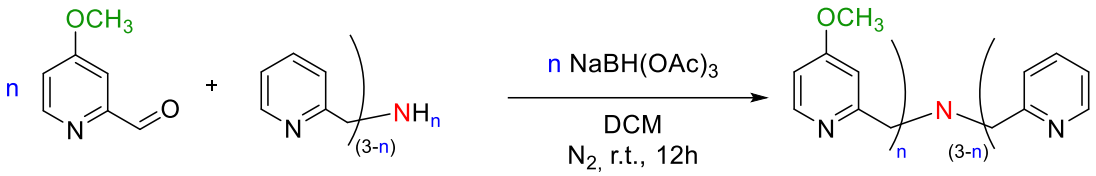

	Yield (%)	Name
n = 1	81	**OCH_3-TPMA 38**
n = 2	62	**$(OCH_3)_2$-TPMA 39**
n = 3*	58	**$(OCH_3)_3$-TPMA 40**

Scheme 11: Synthesis of **TPMA** ligands with methoxy group as substituent through reductive amination reaction. *In the synthesis of **$(OCH_3)_3$-TPMA 40** the nitrogen source is ammonium acetate (NH_4OAc).

Mono-substituted **OCH_3-TPMA 38** presented an initial difficulty due to the low solubility of the aldehyde in the reaction solvent, therefore the solution was left under stirring for 2 hours before adding the reducing agent. However, after washing the organic solution with KOH 0.1 M, the product turned out to be a pure amber oil in good yield as in the case of ligand **35** as shown in the ^{1}H-NMR spectra in Figure 21a. The ligand with two methoxy groups **$(OCH_3)_2$-TPMA 39** presented the same difficulties of solubility of the aldehyde. In this situation the synthesis requires the addition of two equivalents of aldehyde at a distance of 2 hours from each other in order to maximize the solubility and the homogeneity of the solution. The resulting crude, that was a yellow oil, presented several impurities, and it was necessary to purify the **TPMA** ligand through chromatographic column. The stationary phase chosen, as in the other substituted **TPMA** ligands presented so far, is an alumina gel while the eluent always remains gradient DCM:MeOH from 100:0 to 9:1. The final product was a yellow oil characterized by ^{1}H-NMR (Figure 21), ^{13}C-NMR and ESI-MS (Figure 22) in which the molecular ion peak [**39**-H]$^+$ was observed at 351.2 m/z. *Tri*-substituted **$(OCH_3)_3$-TPMA 40** in which the addition of aldehyde is made in three steps has demonstrated the greatest difficulties in terms of solubility. The reaction crude was a green oil with a large quantity of impurities that was removed with a purification on chromatographic column with silica gel and the same eluent as **TPMA 39**. The final product is a stable yellow solid characterized by ^{1}H-NMR (Figure 21c),

ESI-MS and ^{13}C-NMR (Figure 23) which show an additional peak at 3.80 ppm referred to the three equivalent methoxy groups.

The presence of electrondonor substituents like the methoxy groups causes a shift of the signals of six benzylic protons to lower chemical shift than the same signals in previous ligand series where substituents were electron-withdrawing. This is due to increased shielding caused by electron donation of the methoxy group to the pyridine system.

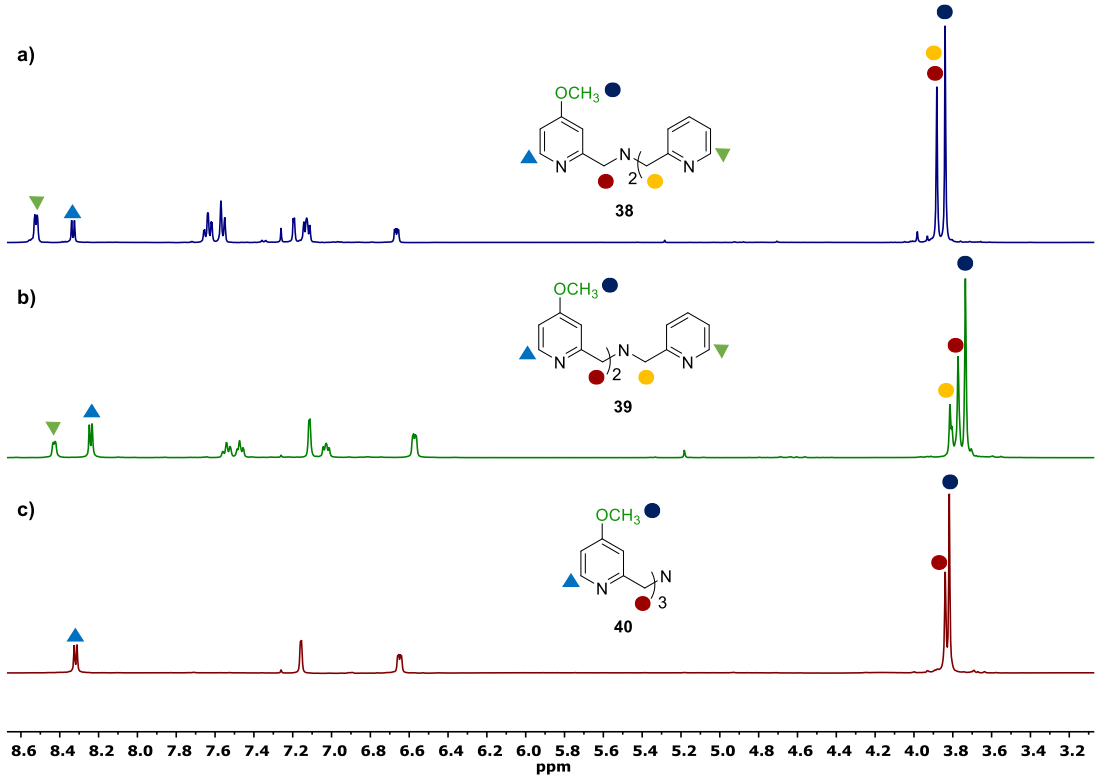

Figure 21: ^{1}H-NMR (400 MHz, $CDCl_3$) of **a) OCH_3-TPMA 38**, **b) $(OCH_3)_2$-TPMA 39,** and **c) $(OCH_3)_3$-TPMA**. **40**.

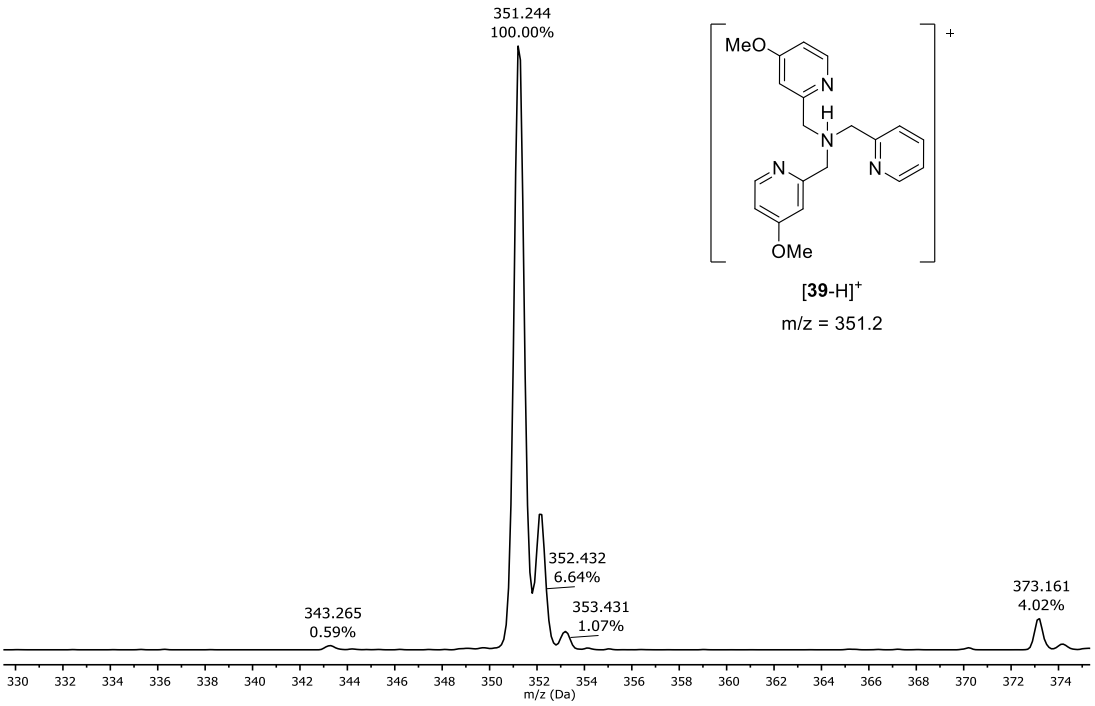

Figure 22: Experimental ESI-MS of protonated ligand [**39**-H]$^+$ at 351.2 m/z in ACN/H$^+$.

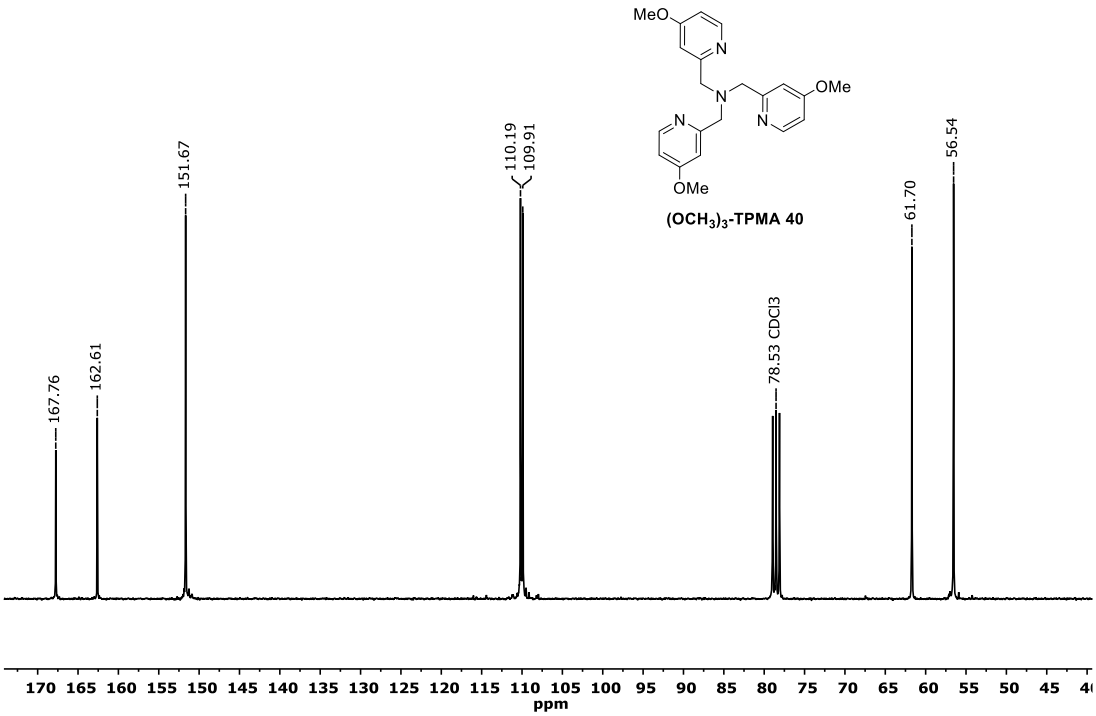

Figure 23: ^{13}C-NMR (75 MHz, $CDCl_3$) of **$(OCH_3)_3$-TPMA 40**.

3.1.5 Pyrrolidine-substituted TPMA

The ligands bearing one to three pyrrolidine substituents were synthesized through a different synthetic pathway (Scheme 12), avoiding the synthesis of corresponding aldehyde.

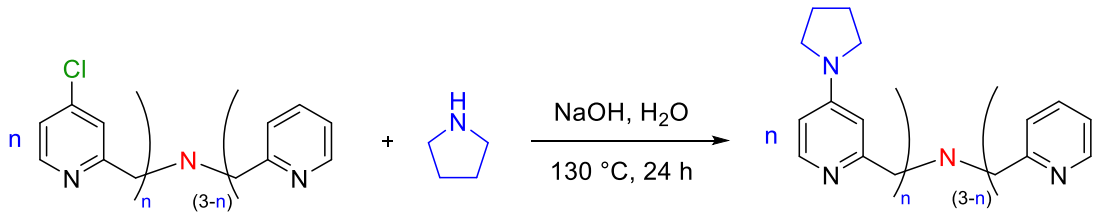

	Yield (%)	Name
n = 1	46	**Pyrr-TPMA 41**
n = 2	98	**Pyrr$_2$-TPMA 42**
n = 3	62	**Pyrr$_3$-TPMA 43**

Scheme 12: Synthesis of **TPMA** ligands with Pyrrolidine as substituent through nucleophilic substitution reaction.

Starting from **TPMAs** substituted with chlorine **32-34**, the synthesis was conducted with a large excess of pyrrolidine in water and NaOH under pressure at 130° according to a procedure developed by Matyjaszewski *et al*[49]. Although it is difficult to change the substituents on the pyridine ring after **TPMA** has already formed, in this case the chlorine in *para*-position is replaced with a pyrrolidine moiety with an aromatic nucleophilic substitution reaction. After removing the excess pyrrolidine with the work up a purification on chromatographic column in alumina gel with DCM:MeOH gradient from 100:0 to 9:1 was required for each **TPMA** ligand **41**, **42**, **43**. All the synthetized products resulted as a light brown solids. The ^{1}H-NMR analysis shows the characteristic peaks of the 6 benzyl protons at 3.79 ppm for **43** and between 3.77 ppm and 3.86 ppm for **41** and **42.** The alpha pyridine protons resulted between 8.04 and 8.47 ppm in all the three ligands. In addition, the two signals of the aliphatic protons of the pyrrolidine unit were identified at 3.28 ppm and 1.98 ppm (Figure 24). The choice to use this stationary phase is necessary because the presence of one or more pyrrolidines on the ligand determines a high interaction with the silica stationary phase and a consequently low retention factor. In alumina gel this phenomenon is less pronounced and allows an optimal separation of the product from the impurities. In this situation, the ESI-MS analysis shows two molecular ion, the first one at 360.1 m/z relative to the species [**41**-H]$^+$ and the second one at 180.5 m/z relative to the di-charge

[**41**-H]$^{2+}$(Figure 25). The first charge is on the aliphatic nitrogen of the **TPMA** skeleton, and the second one is localized in the aminic nitrogen of pyrrolidine moiety. The corresponding two peaks was observed for the other two pyrrolidine derivatives **42** and **43**.

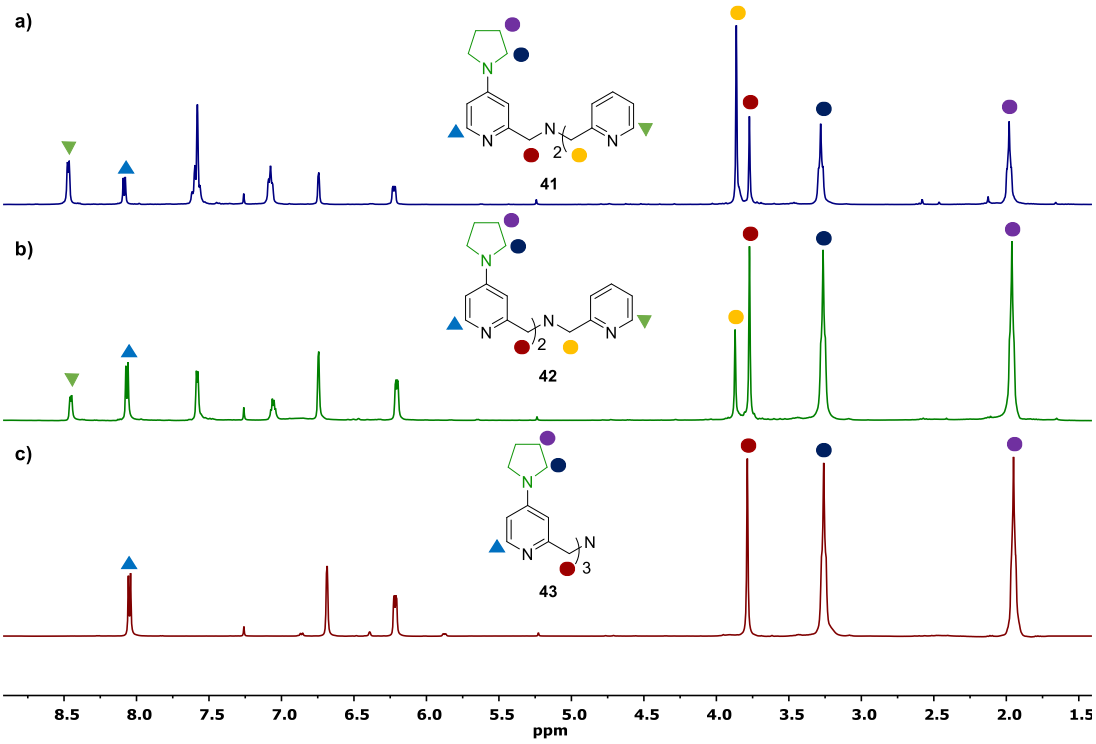

Figure 24: ^{1}H-NMR (400 MHz, $CDCl_3$) of **a) Pyrr-TPMA 41**, **b) Pyrr$_2$-TPMA 42,** and **c) Pyrr$_3$-TPMA 43**.

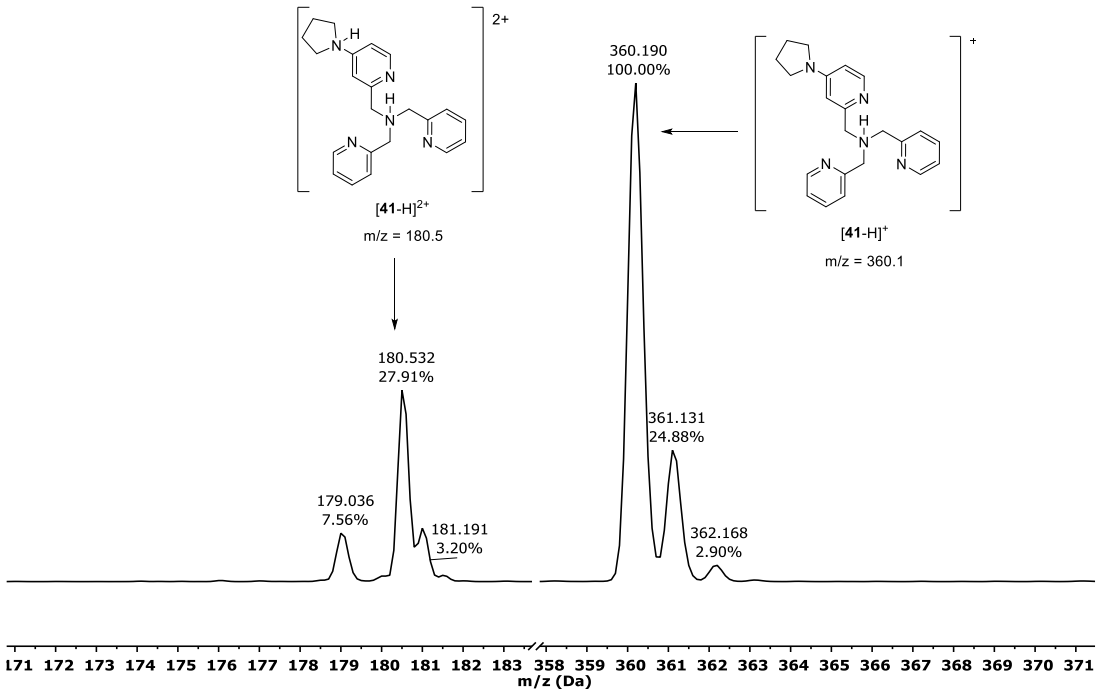

Figure 25: Experimental ESI-MS of protonated ligand [**41**-H]$^+$ at 360.1 m/z and [**41**-H_2]$^{2+}$ at 180.5 m/z in ACN/H^+.

3.1.6 Summary of the *para*-TPMA ligand synthesis

In summary, the synthesis of *para*-substituted **TPMA** with one, two or three substituents were conducted according to Scheme 13, where R = NO_2, Cl, Br, H, OCH_3. The reaction conditions are the same for the synthesis of each ligand: dichloromethane dry as the solvent, room temperature, and a reaction of 12 h. An exception was made for the synthesis of the **TPMA** series equipped with the methoxy group **38-40** due to the low solubility of the aldehyde in dichloromethane that required a reaction time longer than 12 hours. The work-up phase involves three extractions with KOH 0.1M of the product taken in EtOAc where the water-soluble by-products were removed.

For the series of **TPMA** replaced with pyrrolidine was exploited a nucleophilic substitution reaction from the corresponding **TPMA** substituted with chlorine and a large excess of pyrrolidine in the presence of a strong base (Scheme 12).

Generally, in all ligands purification on the chromatographic column was necessary except for **Br-TPMA 35** and **OCH_3-TPMA 38** that were pure after whasing with KOH 0.1 M. After several attempts, an eluent was found to be used, common to all ligands. This is a gradient of DCM:MeOH from 100:0 to 9:1 with the addition of

triethylamine. This is used to avoid the protonation of the pyridine rings and the consequent broadening on the spot of the TLC. The gradual increase in the amount of methanol allows to selectively remove impurities and obtain the pure **TPMA** at the end of the column.

Within the synthesis, **R_3-TPMA** were more challenging due to the higher number of consecutive reductive aminations required for the synthesis. In addition, the ammonium acetate used for the synthesis was not completely anhydrous and this did not only lead to problems of solubility in dichloromethane, but it had an influence on crude impurities. All **R_3-TPMA** have been purified on a chromatographic column using silica gel as a stationary phase. The presence of impurities lowers the reaction yield that in almost all cases is lower for the ligands with three substituents of each series than the ligands with two and one substituent. A difference in the purification of ligands was adopted for **R_2-TPMA** where the best stationary phase to use in the chromatographic column was found to be the alumina gel compared to silica gel. Apart from the series with pyrrolidine as the substituent, where it is necessary to use the alumina gel to avoid the interaction between silica and aliphatic nitrogen that keeps the product in the column.

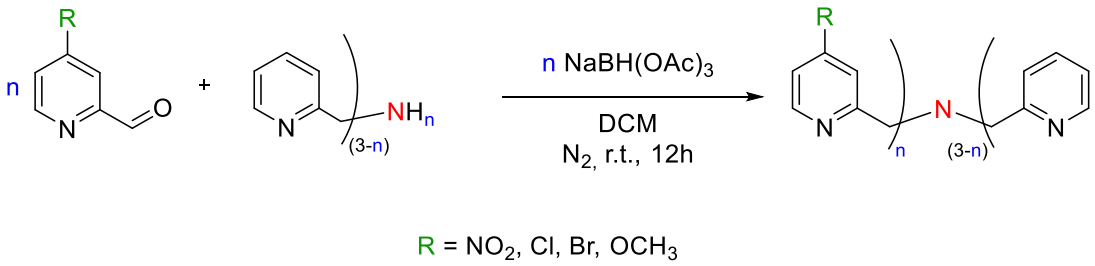

Scheme 13: Reductive amination reaction used for the synthesis of **TPMA** ligands *mono*, *di*, and *tri*-substituted.

Table 1 shows all the experimental yields of *para*-substituted **TPMA** ligands synthetized with reductive amination. Yields are generally higher than 50% except in some cases like **Cl_3-TPMA 34** which has a yield of 32%. The reason why the values are so low is because **34** was the first ligand to be purify in the chromatography column and a part of the product was used to find the suitable eluent for the column.

Ligand	Substitutent (R)	Reductive amination yields (%)
R-TPMA	NO_2	61
	Cl	57
	Br	97
	OCH_3	81
R_2-TPMA	NO_2	/
	Cl	83
	Br	91
	OCH_3	62
R_3-TPMA	NO_2	86
	Cl	32
	Br	74
	OCH_3	58

Table 1: Yields of *para*-substituted **TPMA** ligands synthesized with reductive amination reported in Scheme 13.

In Table 2 is reported the yields of **TPMA** ligands synthetized with nucleophilic substitution reported in Scheme 12. The yields of **Pyrr-TPMA 41** is about 46% because it was the first compound synthesized in the series with Pyrrolidine as substituent and part of the product may have been lost during extractions with water in the work-up in which the excess pyrrolidine was removed.

Ligand	Nucleophilic substitution yields (%)
Pyrr-TPMA	46
Pyrr$_2$-TPMA	98
Pyrr3-TPMA	62

Table 2: Yields of *para*-substituted **TPMA** ligands synthesized with nucleophilic substitution reported in Scheme 12

3.2 SYNTHESIS OF COBALT-TPMA COMPLEXES

The general procedure for the complexation of the Co (II) to the TPMA ligand was already reported in the literature. An adapted procedure was exploited for the synthesis of the metal complexes in this thesis work (Scheme 14).[20] The reaction involves complexation in an anhydrous environment under nitrogen, dissolving the **TPMA**

ligand in anhydrous methanol under stirring for a few minutes. At this point the cobalt salt is added, in our case cobalt chloride hexahydrate, and the reaction is left under stirring for 2h. At the end the methanol is removed under reduced pressure and the solid is dissolved in the minimum amount of acetonitrile. Precipitation is carried out by adding diethyl-ether and left under stirring for a few minutes before separating it by centrifugation. At the end the diethyl-ether was removed and the solid is dried under reduced pressure in a high vacuum pump for 3 hours. This procedure is used for complexation of all synthesized ligands (Table 3).

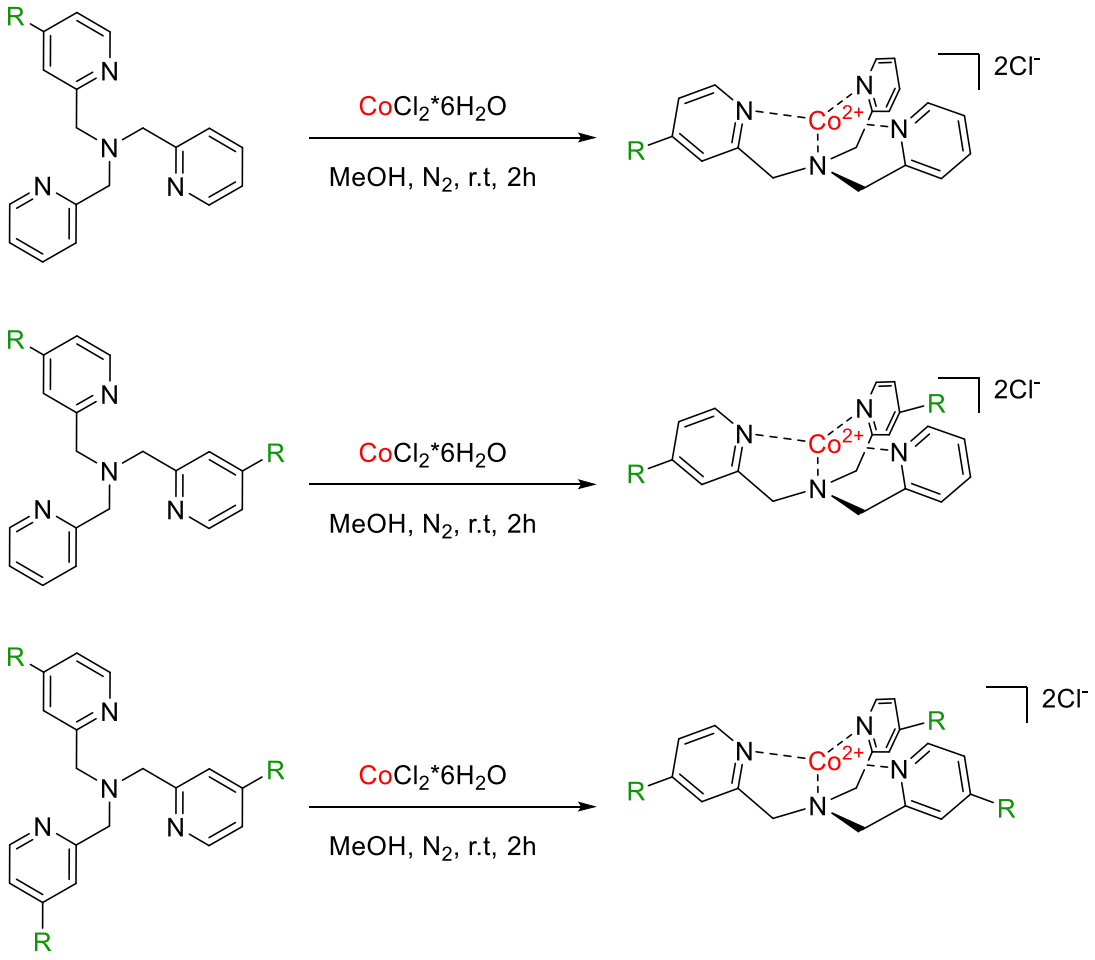

R = NO_2, Cl, Br, H, OCH_3, Pyrr

Scheme 14: Synthesis of cobalt-**TPMA** complexes using cobalt chloride hexahydride in MeOH under nitrogen atmosphere.

Complex	Substituent (R)	Yield (%)
Co-R-TPMA	NO_2	60
	Cl	75
	Br	65
	OCH_3	59
	Pyrrolidine	58
Co-R_2-TPMA	Cl	49
	Br	81
	OCH_3	72
	Pyrrolidine	54
Co-R_3-TPMA	NO_2	53
	Cl	26
	Br	56
	H	43
	OCH_3	53
	Pyrrolidine	48

Table 3: Yields of the complexation reaction reported in Scheme 14.

After the complexation, several crystallization attempts were performed to obtain crystals suitable for X-rays investigation. For this purpose, the vapor diffusion technique was used dissolving the complex in a small amount of acetonitrile and using the diethyl ether as the non-solvent that slowly diffuse into the complex solution. This translates in the use of a small aliquot of the solid which was dissolved in acetonitrile in a vial which in turn is inserted into a larger vial containing diethyl ether.

3.2.1 Characterization of Cobalt-TPMA complexes

The complex synthesis was conducted under the conditions reported in Scheme 16 for all synthesized ligands except for the **$(NO_2)_3$-TPMA 31**. This ligand was not soluble in methanol and complexation was conducted in acetonitrile in which **31** was well dissolved after few minutes. The other ligands once dissolved in methanol were generally pale-yellow-coloured solutions, while the addition of cobalt chloride turned the solution dark with green or blue reflections depending on the type of dissolved

ligand. In general, after the precipitation all the complexes are air stable and not hygroscopic.

The characteristics of cobalt complexes based on **TPMA** ligands have been reported in Table 4 for *mono*-substituted complexes, in Table 5 for *tri*-substituted and in Table 6 for *di*-substitutes. These complexes are colourful due to the absorption of the cobalt-tris-pyridine system, and the colour change is related to the different substituent, and this is reflected in a variation of the electron density of the pyridine rings. Most of the complexes are green or blue while an exception is represented by the complex **Co-$(NO_2)_3$-TPMA 31** in which the presence of three nitro groups causes a variation in colour and the complex turns out to be orange (Table 5). In general, these cobalt-**TPMA** complexes have two typical absorption bands at around 485 nm and 635 nm. In the case of **Co-$(NO_2)_3$-TPMA 31** the second band falls to 645 nm. These two bands can be attributed to transitions of low ε values that are in the order of 200-300 $M^{-1}cm^{-1}$(Figure S72-74). These bands are attributed to d-d transitions coupled to pyridine rings that influences the pure d-d metal transitions.

The formation of the complex is also confirmed by the elemental analysis and by the ESI-MS. The latter showed the cationic complexes [**Co-TPMA**]$^+$ (Figure 26, 27).

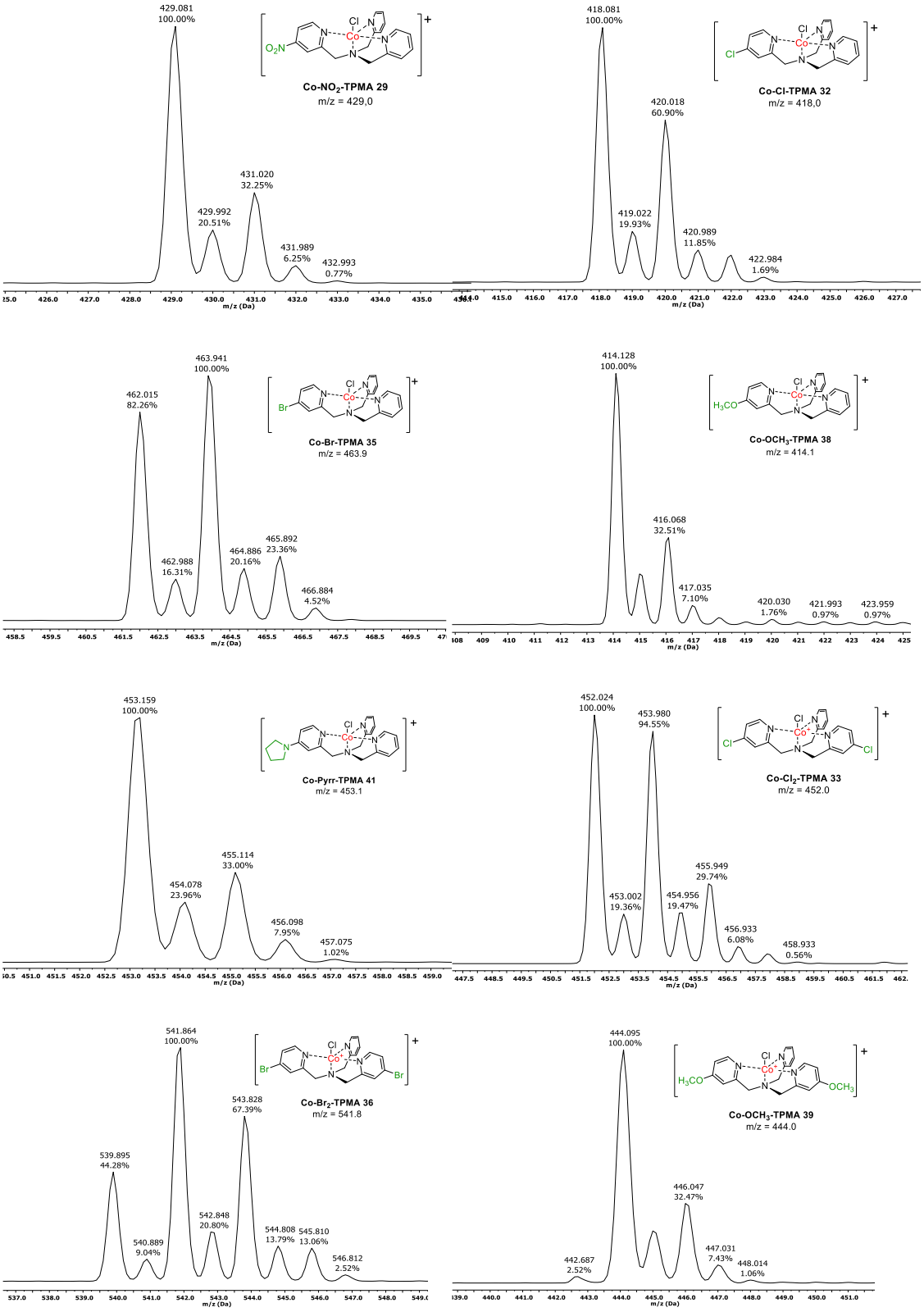

Figure 26: Experimental ESI-MS of **[Co-R_n-TPMA]**$^+$ complexes in ACN/H^+.

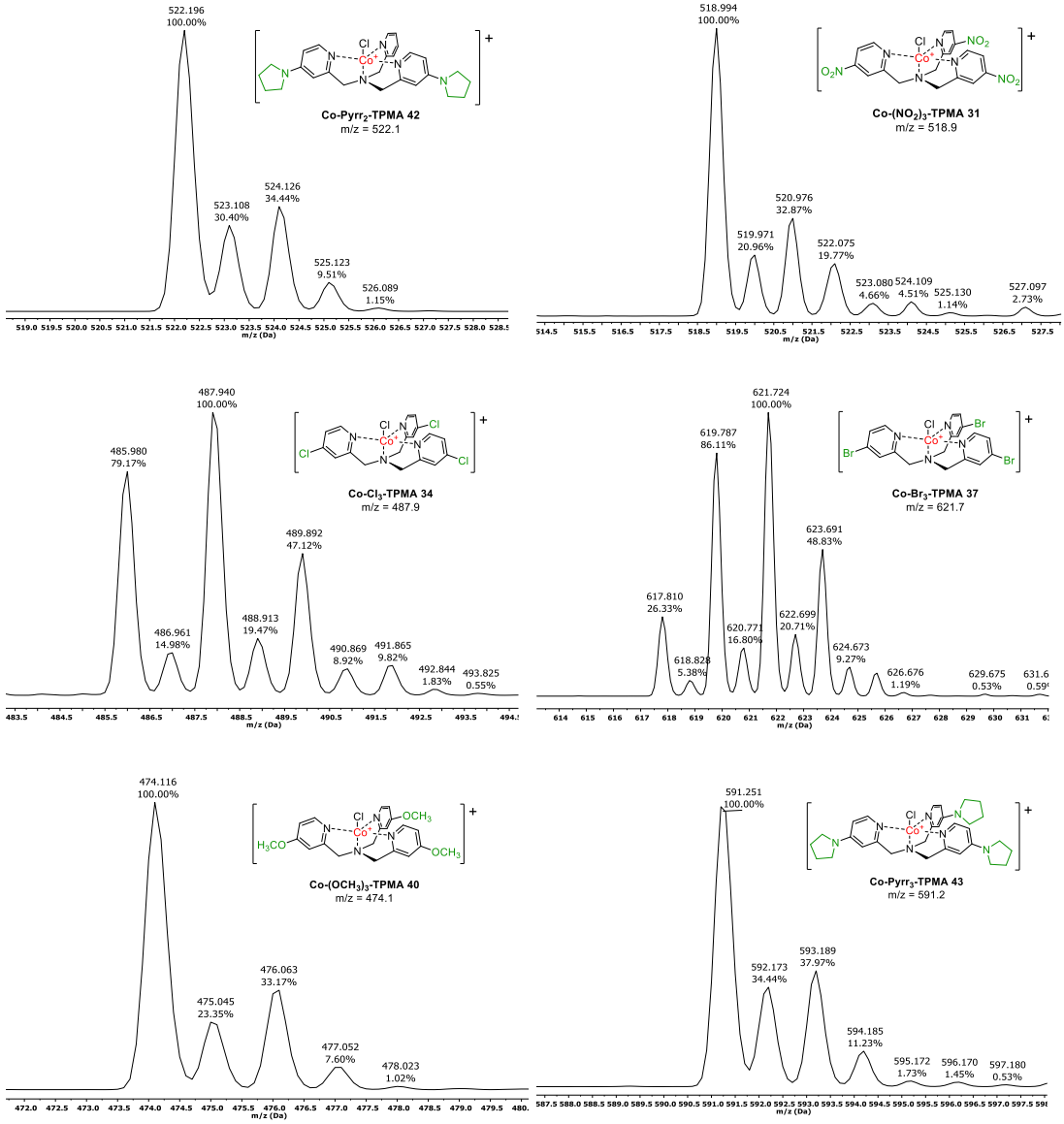

Figure 27: Experimental ESI-MS of **[Co-R$_n$-TPMA]**$^+$ complexes in ACN/H$^+$.

For the characterization of this cobalt (II) complexes, the ^{1}H-NMR analysis was also used despite the paramagnetic feature of the species. In Figure 28 are reported the spectra of the **TPMA** cobalt complexes bearing the chlorine substituents. The spectra have been recorded from -10 ppm to 170 ppm. The characteristic peaks of these systems can be detected. Alpha pyridine protons fall between 140 and 130 ppm, and at lower ppm there are the benzyl protons, between 90 and 110 pm. In the zone between 40 and 60 ppm fall the signals of the aromatic protons of the pyridine ring and finally between 0 and -1 ppm falls the signal of the proton in the para position of the ring not

replaced if one or two para position are not substituted by the chlorine.

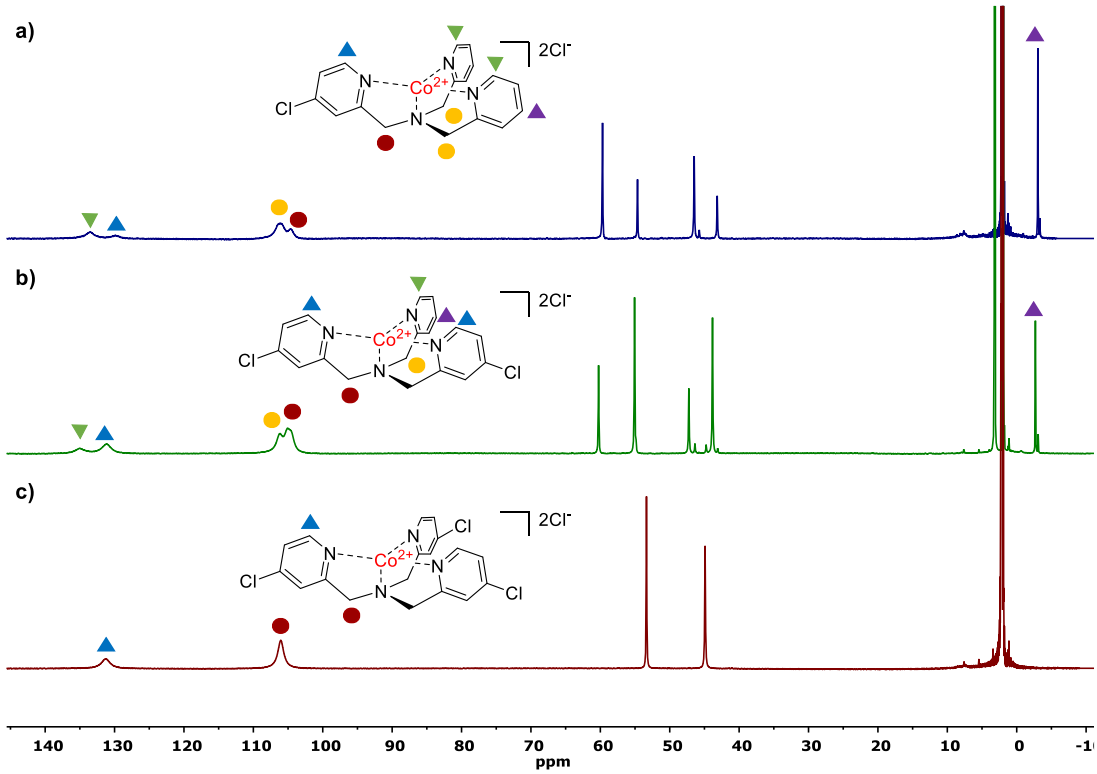

Figure 28: ^{1}H-NMR (400 MHz, CD_3CN) of chlorine substituted cobalt-**TPMA** complexes: **a) Co-Cl-TPMA 32, b) Co-Cl_2 TPMA 33, c) Co-Cl_3-TPMA 34.**

A more detailed inspection of the region between 80 and 145 ppm furnished important information about the complexes. The area of the spectrum where the characteristic peaks fall is between 80 and 145 ppm where resonate the α-pyridine protons and benzylic protons.

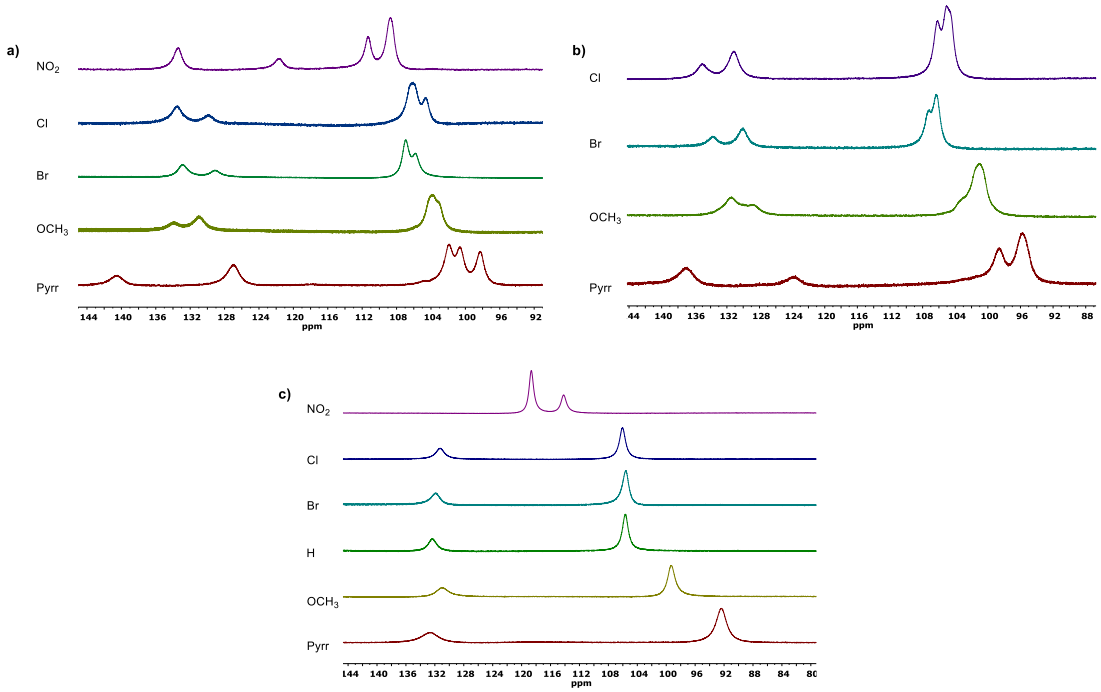

Figure 29: Details of ^{1}H-NMR spectra of cobalt-**TPMA** complexes between 80 ppm and 145 ppm. **a) Co-R-TPMA, b) Co-R$_2$ TPMA, c) Co-R$_3$-TPMA.**

Figure 29 shows the superimposition of the spectra for the a) *mono*, b) *di*, and c) *tri*-substituted complexes. A significant shift of the signals was observed depending on the type and number of substituents on the **TPMA** skeleton. In particular, in the series of *mono*-substituted complexes (Figure 29a), a different shift of the two singlets between 96 ppm and 110 ppm was observed. In the case of the nitro substituent the peaks relative to the arm bearing the substituents was at higher ppm than the two arm with no substitution. An opposite trend was found for the other substituents. A strong effect was found for the α-pyridine protons. The nitro group shift the near protons towards much lower ppm in comparison to the pyridine with no substituents. In the case of electrondonating substituents (OCH_3 and pyrrolidine) the signals of replaced alpha-pyridine protons fall at ppm higher than the unsubstituted pyridine and this effect is more pronounced for pyrrolidine where there also was a separation of this peaks.

As regards the series of *di*-substituted complexes (Figure 29b) there is not a great influence of the substituent on the benzyl protons while the α-pyridine protons undergo the same effect as the *mono*-substituted complexes with the inversion of the peaks referred to the replaced arm of the **TPMA** and the one not replaced. Usually, these two signals fall very close to each other and only in the case of pyrrolidine they undergo an important shift.

The series of *tri*-substituted (Figure 29c) complexes, on the other hand, does not seem to show marked influences of the substituents except in the case of the nitro group and the pyrrolidine, the two substituents at the extremes for characteristics of attraction or electronic donation. In particular, having three nitro groups, the protons resonate even at chemical shift lower than the six benzyl protons, while in the case of pyrrolidine these fall at ppm much higher than the singlet of the six CH_2

Co-R-TPMA	**ESI-MS (m/z)**		**UV-Vis** λ_{Max} **(nm)**	**ELEMENTAL ANALYSIS (%)**	
	Calc.	**Found**		**Calc.**	**Found**
R = NO_2 **Dark Green**	429.0	429.0	486 632	C = 46.47 H = 3.68 N = 15.05	C = 45.47 H = 4.02 N = 15.05
R = Cl **Light Green**	418.0	418.0	486 636	Not available	
[a]**R = Br** **Blue Green**	463.9	463.9	489 631	C = 41.81 H = 3.70 N = 10.83	C = 41.31 H = 3.84 N = 10.20
***R = H** **Green**	384.0	384.0	489 640	Not available	
[b]**R = OCH_3** **Light Green**	414.1	414.1	490 632	C = 48.74 H = 4.74 N = 11.97	C = 47.22 H = 4.88 N = 11.28
R = Pyrrolidine **Dark Green**	453.1	453.1	501 633	Not available	

Table 4: Properties of Cobalt-**TPMA** complexes *mono*-substituted precipitated from ACN/Et_2O. Elemental analysis: a. calculated for **[Co-Br-TPMA]$^+$ [Cl_2]$^-$** + $1H_2O$, b. calculated for **[Co-OCH_3-TPMA]$^+$ [Cl_2]$^-$** + $1H_2O$. *Cobalt **TPMA** complex was synthetized from literature procedure starting from the commercial **TPMA** unsubstituted.

Co-R_3-TPMA	ESI-MS (m/z)		UV-Vis λ_{Max} (nm)	ELEMENTAL ANALYSIS (%)	
	Calc.	Found		Calc.	Found
R = NO_2 **Dark Orange**	519.0	519.0	485 645	C = 38.94 H = 2.72 N = 17.66	C = 38.83 H = 2.87 N = 16.89
R = Cl **Green**	487.9	487.9	485 635	Not Available	
R = Br **Light Blue**	621.7	621.7	490 635	Not Available	
R = OCH_3 **Water Green**	453.1	453.1	495 634	Not Available	
R = Pyrrolidine **Dark Green**	491.2	491.2	510 635	Not Available	

Table 5: Properties of Cobalt-**TPMA** complexes *tri*-substituted precipitated from ACN/Et_2O.

Co-R_2-TPMA	ESI-MS (m/z)		UV-Vis λ_{Max} (nm)	ELEMENTAL ANALYSIS (%)	
	Calc.	Found		Calc.	Found
[a]**R = Cl** **Purple**	452.0	452.0	490 635	C = 42.63 H = 3.58 N = 11.05	C = 42.58 H = 3.39 N = 10.95
[b]**R = Br** **Light Blue**	541.8	541.8	490 635	C = 36.27 H = 3.04 N = 9.40	C = 35.65 H = 2.96 N = 9.12
R = OCH_3 **Water Green**	444.1	444.1	494 635	Not Available	
R = Pyrrolidine **Dark Blue**	522.1	522.1	505 635	Not Available	

Table 6: Properties of Cobalt-**TPMA** complexes *di*-substituted precipitated from ACN/Et_2O. Elemental analysis: a. calculated for **[Co-Cl_2-TPMA]$^+$ [Cl_2]$^-$** + 1H_2O, b. calculated for **[Co-Br_2-TPMA]$^+$ [Cl_2]$^-$** + 1H_2O.

For some of the tri-substituted complexes, crystals suitable for X-ray diffraction analysis have been isolated and there were sent to be analysed by Prof. Klaus Wurst (Innsbruck University). The two structures confirm a bipyramidal trigonal geometry structure in which the central atom achieves penta-coordination by coordinating with the four atoms of nitrogen of the **TPMA** ligand and to a chloride as a counterion (Figure 30).

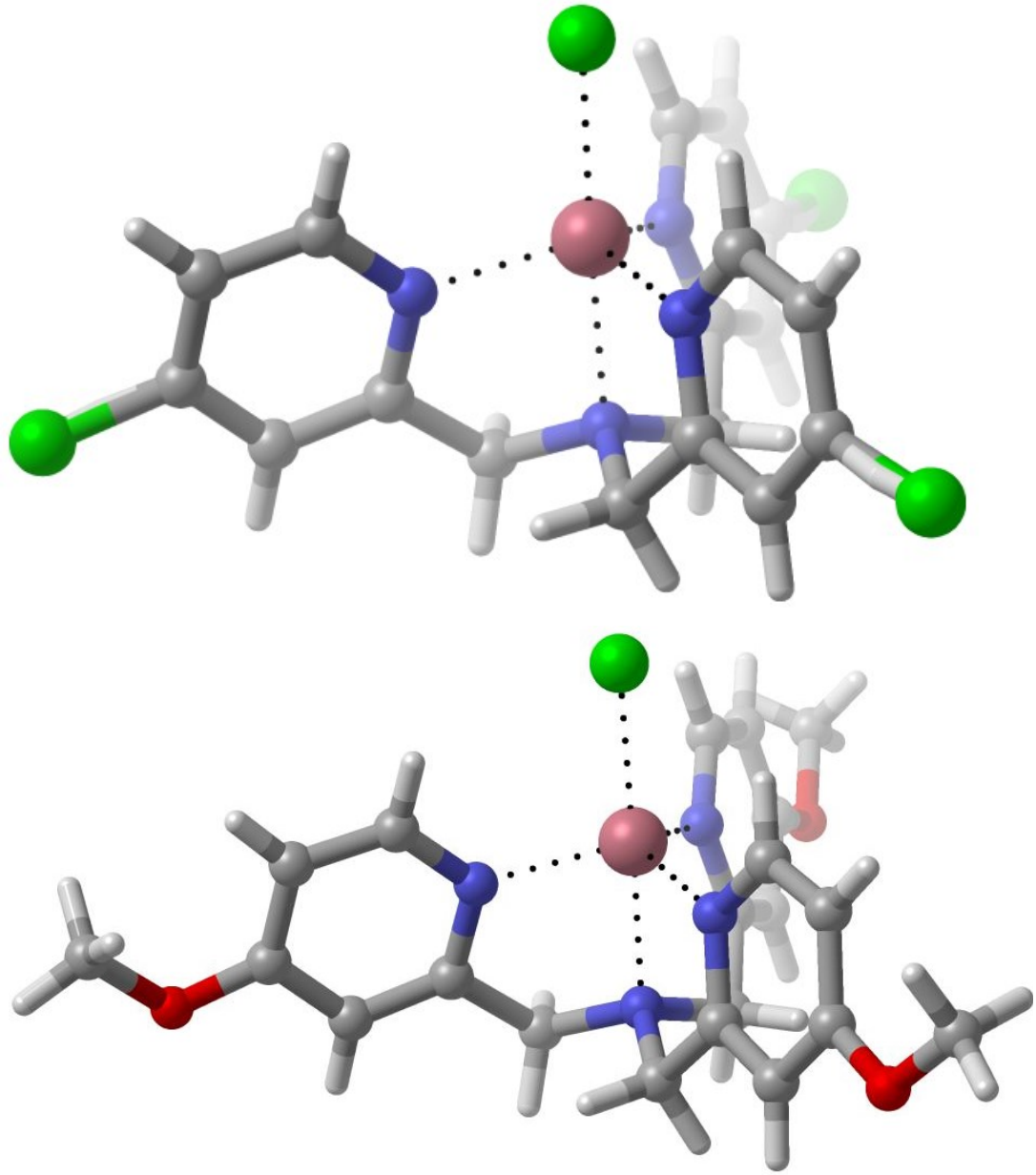

Figure 30: X-Ray crystal structures of **a)** [**Co-Cl$_3$-TPMA**]$^+$[Cl$^-$] **Co-34** and **b)** [**Co-(OCH$_3$)$_3$ TPMA**]$^+$[Cl$^-$] **Co-40.**

3.3 REDUCTION PROPERTIES OF COBALT TPMA COMPLEXES

The synthetized cobalt complexes were also characterized though cyclic voltammetry (CV) to investigate the substituents effect on the Co^{II}/Co^{I} and Co^{I}/Co^{0} reduction potential. As reported in the introduction part (paragraph 1.5.1), the typical CV plot of a **TPMA** cobalt (II) complex shows two characteristic irreversible reduction peaks centred at -1,54 V and -1,76 V vs Ag/AgCl which are assigned as Co^{II}/Co^{I} and Co^{I}/Co^{0} reduction respectively (Figure 32a). The introduction of a *para* substituent on the **TPMA** skeleton have a crucial impact on the electrochemical properties of the metal complex also influencing the reduction peaks of the cobalt. The Figure 32b-f shows

the CV plots for the mono substituted complexes, where one pyridine arm of the **TPMA** has a para substituent. As expected, the two reduction waves of the metal center are influenced by the presence of the substituent. In particular, the electron-withdrawing and electron-donating nature of the substituent is associated to a positive and negative shift of the reduction potential respectively. The potentials of the first reduction wave, which is crucial for the catalysis, are summarized in Table 7. It is possible to observe that an electron-donating substituent such as Pyrr and OCH_3 shifts the Co^{II}/Co^{I} peak toward more negative potential while the opposite results are obtained for the electron-withdrawing chlorine and bromo substituents. For the strong electron-withdrawing nitro group was observed an early reduction peak around -0.54 V, related to the reduction of the nitro group which hampers the right attribution of the reduction peaks of the cobalt. For this reason the relative value of E and ΔE are not present in Table 7. An early third peak is also observed in the bromo derivatives, probably due to the homolytic cleavage of the Br-C bond. Figure 33 shows the Hammett correlation of the first reduction wave shift, with the unsubstituted **TPMA** as the reference, and the σ_p parameter for the different groups. A good linear correlation was obtained in accordance with the electronic effect of the para substituents.

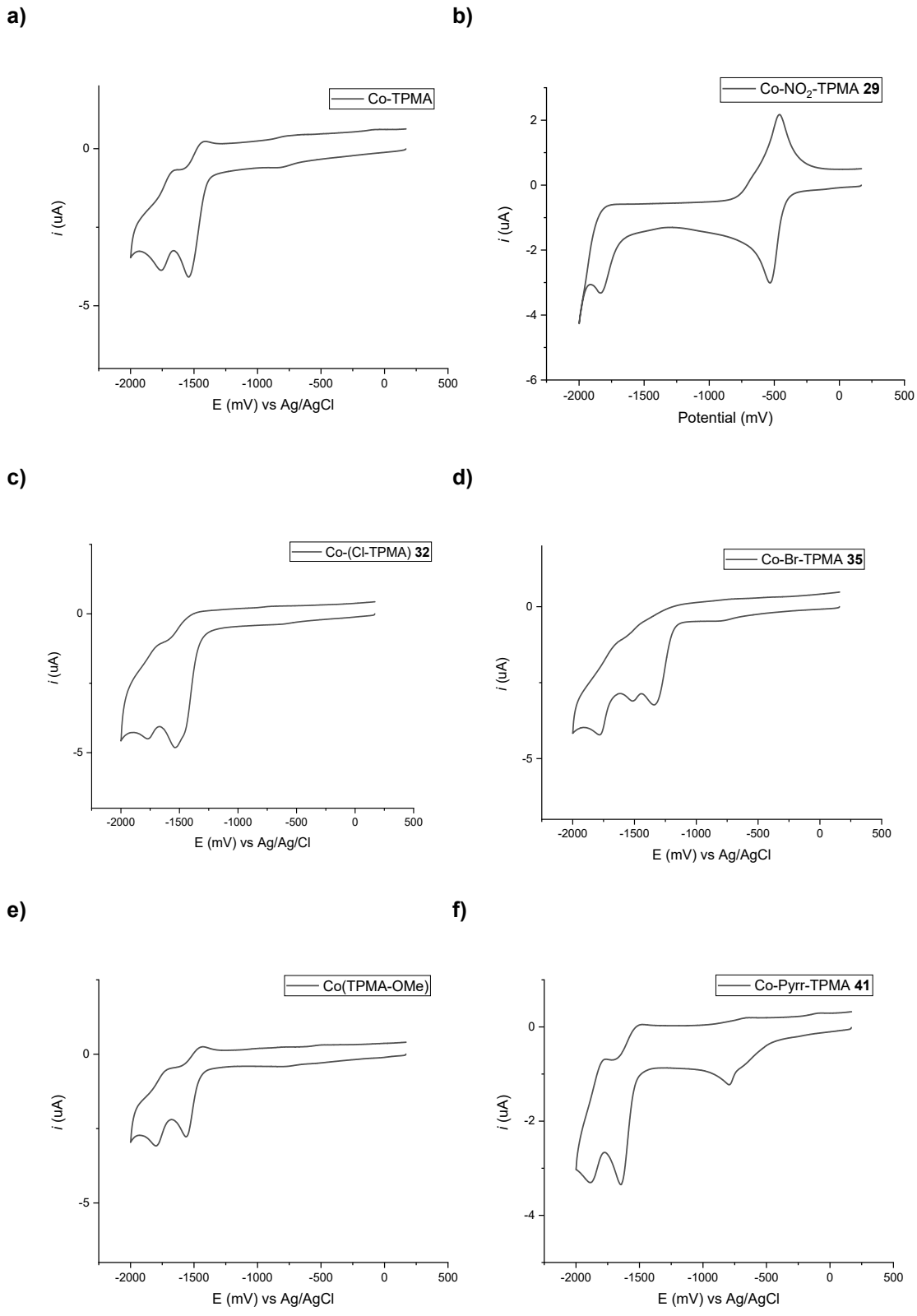

Figure 31: Cyclic voltammetry plots of **Co-R-TPMA** complexes carried out under nitrogen atmosphere in ACN solution. **a)** CV of **Co-TPMA** complex. **b)-f)** CV of **Co-R-TPMA** complexes.

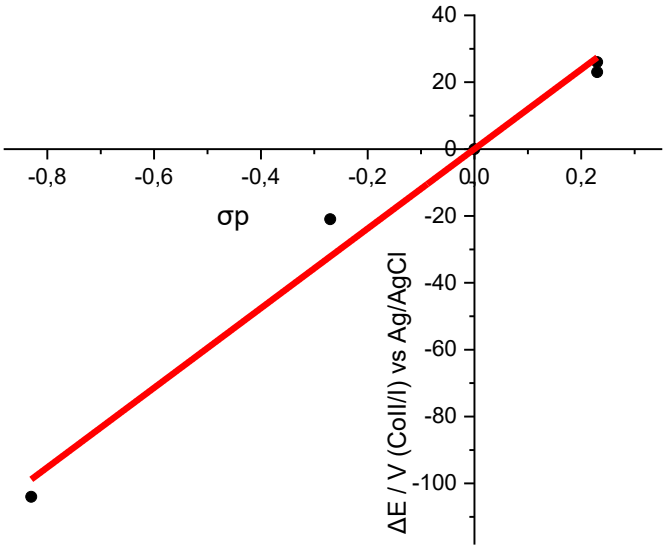

Figure 32: Hammett plot for the first reduction wave shift relative to the Co^{II}/Co^{I} event. The unsubstituted Co-**TPMA** was used as the reference, with a ΔE equal to zero. The fitting equation curve is y=119,05(±8,55)x-0.038(±3,56), R^2=0.9848

Substituent R on the Complex Co-R-TPMA	σ para	E / mV ($Co^{II/I}$) vs Ag/AgCl	ΔE / V ($Co^{II/I}$) vs Ag/AgCl
NO_2	0.78	-	-
Br	0.23	-1515	26
Cl	0.23	-1518	23
H	0.00	-1541	0
OCH_3	-0.27	-1562	-21
Pyr	-0.83	-1645	-104

Table 7: Potential for the reduction of the Co^{II}/Co^{I} species reported in Volt vs the reference Ag/AgCl. The shift of the potential with the unsubstituted Co-(TPMA) as reference is reported on the right column. The σ para value relative to the substituent is also reported reflecting its electron-withdrawing/donating nature.

The introduction of more than one para substituent on pyridine ring of the TPMA has an interesting effect on the reduction potential of the cobalt center. Figure 34 shows the superimposition of CV plots for the *mono*, *di* and *tri* substituted **Co-(R_n-TPMA)** in the case of the chlorine and methoxy substituents. It is possible to notice a different trend for the chlorine and methoxy substituent, due to their opposite electronic effect. For the chlorine, the introduction of two and three para substituents shifts the potential

of the first reduction peak toward higher potential. Opposite trend is observed for the methoxy group that shift the potential towards lower potential.

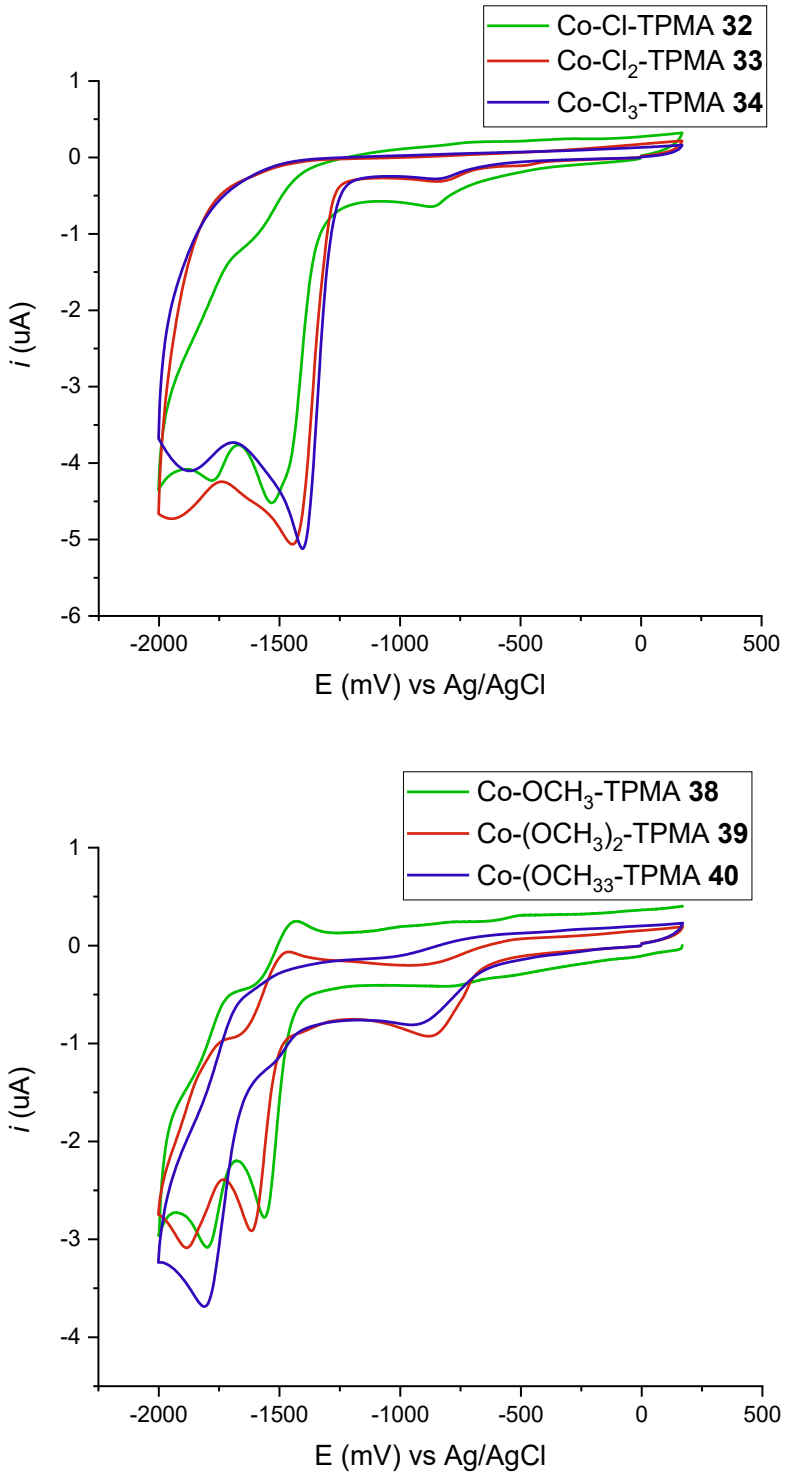

Figure 33: Superimposition CV of **Co-R$_n$-TPMA** complexes where R = Cl, OCH_3 and n = 1, 2, 3. The cyclic voltammetry are conducted under N_2 atmosphere in ACN solution.

4 CONCLUSIONS

In this thesis, 14 different **TPMA**-based ligands were synthesized and the relative Cobalt(II) complexes characterized. In particular, the reductive amino synthetic strategy revealed to by versatile and effective for the synthesis of all these systems. A general methodology for the purification of ligands have been developed and it consists in the use of a chromatographic column using a gradient eluent DCM:MeOH (from DCM to DCM:MeOH 9:1).

TPMA Cobalt (II) complexes were synthetized, and they reveled to be stable solids once precipitated and dried under vacuum. All of the systems were colorful, and the color range is between green and blue with the exception of the complex **Co-$(NO_2)_3$-TPMA 31** which is orange and the complex **Co-Cl_2-TPMA-33** which is purple.

For two of the *tri*-substituted complexes, **Co-Cl_3-TPMA 34** and **Co-$(OCH_3)_3$-TPMA 40** crystalline structures were obtained, and they revealed to be suitable for X-ray diffraction analysis that confirmed the bipyramidal trigonal structure of the Co-**TPMA** complexes where cobalt reaches pentacoordination.

The electrochemical analysis carried out on the series of *mono*-substituted complexes showed the peaks related to the reduction of cobalt: Co^{II}/Co^{I} and Co^{I}/Co^{0}. By increasing the electron-donating nature of the substituents in *para*-position on the pyridine rings, the reduction potential of the first peak of cobalt reduction (Co^{II}/Co^{I}) shifts to more negative potentials. It should be noted that unfortunately some of the substituents seems not stable under reductive catalysis.

However, even if the following work will be directed in their use in reductive catalysis of CO_2 and H_2, other applications such as in sensing can be envisaged.

5 EXPERIMENTAL SECTION

5.1 GENERAL METHODS

NMR spectra were recorded at 301 K on Bruker Avance DMX 400 MHz or Bruker Avance-300 MHz instruments. All the 1H-NMR spectra were referenced to residual isotopic impurity of $CDCl_3$ (7.26 ppm) or CD_3CN (1.94 ppm). The following abbreviations are used in reporting the multiplicity for NMR resonances: s=single, d=doublet, t= triplet, q=quartet, and m=multiplet. The NMR data were processed using Bruker Topspin 3.5 pl2 and MestReNova 12.0.2.

ESI-MS spectra have been acquired with an Agilent Technology LC/MSD Trap SL, interfaced to an Agilent 1100 binary pump. The samples were preventively diluted in acetonitrile and then injected via direct infusion with a Hamilton syringe at a rate of 0.05 ml/min. MS peak intensity for each analysis is reported as monoisotopic mass and the data were processed with Data Explorer 4.2 or with MestReNova 12.0.2. The isotopic distribution simulations have been performed through www.envipat.eawag.ch.

UV-Vis spectra were recorded with a Varian Cary 50 UV-Vis spectrophotometer and processed with Microsoft Excell 365 or OriginPro 2018 (64-bit) SR1 b9.5.1.195.

Cyclic voltammetries were recorded with AUTOLAB PGSTAT101 managed by PC with NOVA 2.1 software interface. All the experiment were conducted using a three-electrode system consisting of a working electrode (WE, *glassy carbon electrode* ϕ = 3 mm, Basi), reference electrode (RE, *Ag/AgCl, 3M NaCl*) and counter electrode (CE, *platinum electrode* ϕ = 1.6 mm, Basi).

Chemicals were purchased from Aldrich or FluoroChem and used without further purification.

5.2 ABBREVIATIONS

ACN	Acetonitrile
DCM	Dichloromethane
EtOAc	Etil Acetate
Et_2O	Diethyl Ether
MeOH	Methanol
K_2CO_3	Potassium Carbonate
THF	Tetrahydrofuran
TPMA	Tris((pyridin-2-yl)methyl)amine
R-TPMA	1-(pyridin-2-yl)-N,N-bis((4-(R-1-yl)pyridin-2-yl)methyl)methanamine
R_2-TPMA	1-(4-methoxypyridin-2-yl)-N-((4-R-pyridin-2-yl)methyl)-N-(pyridin-2-ylmethyl)methanamine
R_3-TPMA	Tris((4-R-pyridin-2-yl)methyl)amine
r.t	Room temperature
$(CF_3CO)_2O$	Trifluoroacetic anhydride

5.3 SYNTHESIS OF (4-NITROPIRYDIN-2-YL)METHANOL 27

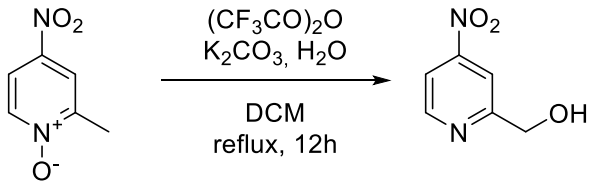

26 **27**

In a 250 mL double neck flask, 4-nitro-2-picoline-N-oxide **26** (3.01 g, 19.53 mmol) were dissolved in DCM (40 mL) and a solution of $(CF_3CO)_2O$ (6.76 mL) mixed with DCM (7.45 mL) was added dropwise. The red solution was left under stirring for 12 hours to reflux. Solvent was evaporated under reduced pressure. Methanol (60 mL) and a saturated aqueous solution of K_2CO_3 (32 mL) were added and the mixture was stirred at room temperature for 4 hours. Methanol was evaporated and the compound was extracted with DCM (3 x 25 mL). Combined organic phases were washed with brine solution (25mL), dried over Na_2SO_4, and the solvent was removed under reduced pressure. A yellow solid was isolated (1.53 g, 9.94 mmol, 51 %).

^{1}H NMR: (300 MHz, $CDCl_3$) δ 8.87 (d, *J* = 5.4 Hz, 1H, PyrH), 8.18 – 7.78 (m, 2H, PyrH), 4.94 (s, 2H, CH_2).

5.4 SYNTHESIS OF 4-NITROPICOLINALDEHYDE 28

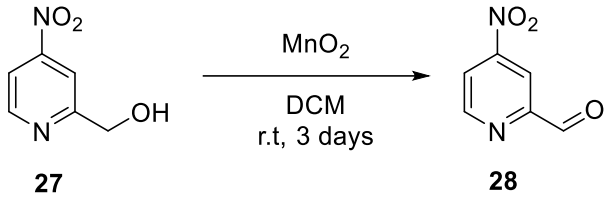

27 **28**

In a 500 mL flask, (4-nitropirydin-2-yl)methanol **27** (1.53 g, 9.94 mmol), DCM (250 mL) and MnO_2 (5.14 g, 59.10 mmol) was stirring at room temperature for three days. The heterogeneous solution was filtrated through celite and DCM was evaporated under reduced pressure. The crude was purified by column chromatography (silica gel, DCM) to give compound **3** as a yellow oil (0.85 g, 5.58 mmol, 56 %).

^{1}H NMR: (300 MHz, $CDCl_3$) δ 10.19 (s, 1H, CHO), 9.11 (d, *J* = 5.3 Hz, 1H, PyrH), 8.63 (d, *J* = 2.2 Hz, 1H, PyrH), 8.26 (dd, *J* = 5.3, 2.1 Hz, 1H, PyrH).

5.5 SYNTHESIS OF 1-(4-NITROPYRIDIN-2-YL)-N,N-BIS(PYRIDIN-2-YLMETHYL)METHANAMINE 29

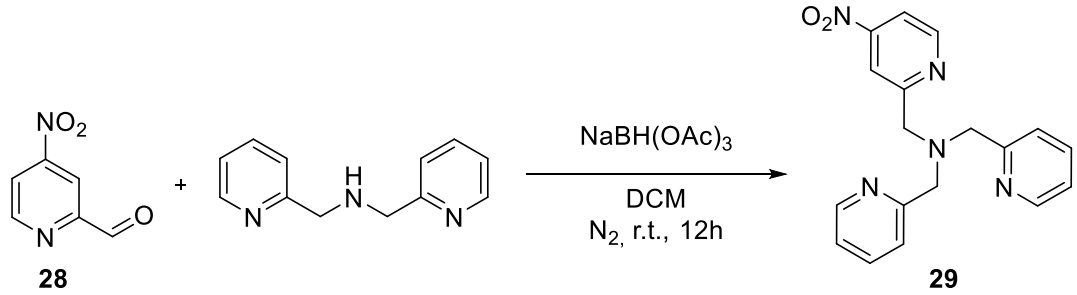

28 **29**

In a 50 ml double neck flask, 4-nitropicolinaldehyde **28** (1.00 g, 6.48 mmol) and bis(pyridin-2-ylmethyl)amine (1.29 g, 6.48 mmol) were dissolved in dry DCM (22 mL) under N_2 and left under stirring for 1 hour. $NaBH(OAc)_3$ (1.38 g, 6.48 mmol) was added in three aliquots waiting 20 minutes between each other. After that the reaction was stirred for 12 hours at room temperature. The solvent was removed under reduced pressure. The resulting black solid was dissolved in EtOAc (about 30 ml) and the solution extracted with 0.1 M solution of KOH (3x100 ml) and brine (20 mL). The organic phases were dried on anhydrous Na_2SO_4, and the solvent was removed under

reduced pressure. The crude was purified through column chromatography (silica gel, DCM/MeOH from 100:0 to 9:1) to give purple wine red oil (2.00 g, 5.42 mmol, 61%).

^{1}H NMR: (400 MHz, $CDCl_3$) δ 8.79 (d, *J* = 5.4 Hz, 1H, PyrH), 8.55 (d, *J* = 4.9 Hz, 2H, PyrH), 8.34 (d, *J* = 2.3 Hz, 1H, PyrH), 7.83 (dd, *J* = 5.5, 2.3 Hz, 1H, PyrH), 7.60 (dd, *J* = 51.2, 8.1 Hz, 4H, PyrH), 7.17 (dd, *J* = 7.4, 4.9 Hz, 2H, PyrH), 4.06 (s, 2H, CH_2), 3.95 (s, 4H, CH_2).

^{13}C NMR: (75 MHz, $CDCl_3$) δ 165.38, 160.18, 155.94, 152.59, 150.76, 138.03, 124.58, 123.72, 116.89, 115.87, 62.04, 61.21.

ESI-MS (m/z): calcd 336.1$[M+H]^+$, found 336.1$[M+H]^+$

5.6 SYNTHESIS OF 1-(4-CHLOROPYRIDIN-2-YL)-N,N-BIS(PYRIDIN-2-YLMETHYL) METHANAMINE 32

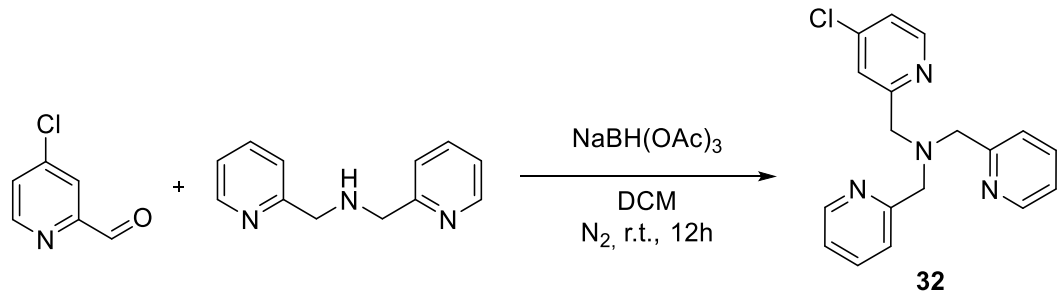

32

In a 50 ml double neck flask, 4-chloropicolinaldehyde (1.00 g, 7.06 mmol) and bis(pyridin-2-ylmethyl)amine (1.40 g, 7.06 mmol) were dissolved in dry DCM (22 mL) under N_2 and left under stirring for 1 hour. $NaBH(OAc)_3$ (1.50 g, 7.06 mmol) was added in three aliquots waiting 20 minutes between each other. After that the reaction was stirred for 12 hours at room temperature. The solvent was removed under reduced pressure. The resulting orange solid was dissolved in EtOAc (about 30 ml) and the solution extracted with 0.1 M solution of KOH (3x100 ml) and a solution of brine (20 mL). The organic phases were dried on anhydrous Na_2SO_4, and the solvent was removed under reduced pressure. The crude was purified through column chromatography (silica gel, DCM/MeOH from 100:0 to 9:1) to give orange oil (1.30 g, 4.00 mmol, 57%).

^{1}H NMR: (300 MHz, $CDCl_3$) δ 8.58 – 8.45 (m, 2H, PyrH), 8.38 (d, *J* = 5.3 Hz, 1H, PyrH), 7.62 (ddd, *J* = 15.1, 7.6, 1.9 Hz, 3H, PyrH), 7.51 (d, *J* = 7.8 Hz, 2H, PyrH), 7.12 (td, *J* = 6.0, 5.2, 2.3 Hz, 3H, PyrH), 3.86 (d, *J* = 3.4 Hz, 6H, CH_2).

^{13}C NMR: (75 MHz, $CDCl_3$) δ 162.81, 160.32, 151.35, 150.53, 146.13, 138.10, 124.74, 124.61, 123.97, 123.67, 61.72, 61.23.

ESI-MS (m/z): calcd 325.2 $[M+H]^+$, found 325.2 $[M+H]^+$

5.7 SYNTHESIS OF 1-(4-BROMOPYRIDIN-2-YL)-N,N-BIS(PYRIDIN-2-YLMETHYL) METHANAMINE 35

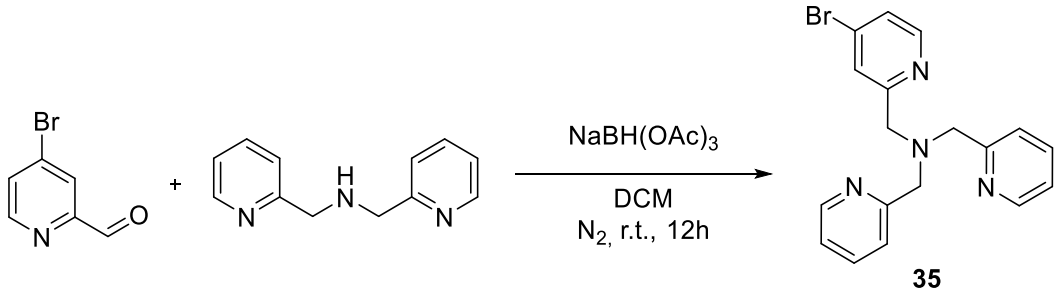

In a 50 ml double neck flask, 4-bromopicolinaldehyde (1.00 g, 5.38 mmol) and bis(pyridin-2-ylmethyl)amine (1.07 g, 5.38 mmol) were dissolved in dry DCM (22 mL) under N_2 and left under stirring for 1 hour. $NaBH(OAc)_3$ (1.14 g, 5.38 mmol) was added in three aliquots waiting 20 minutes between each other. After that the reaction was stirred for 12 hours at room temperature. The solvent was removed under reduced pressure. The resulting amber solid was dissolved in EtOAc (about 30 ml) and the solution extracted with 0.1 M solution of KOH (3x100 ml) and brine (20 mL). The organic phases were dried on anhydrous Na_2SO_4, and the solvent was removed under reduced pressure to give an amber oil (1.93 g, 5.22 mmol, 97%).

^{1}H NMR: (400 MHz, $CDCl_3$) δ 8.53 (dd, *J* = 4.9, 1.8 Hz, 2H, PyrH), 8.31 (d, *J* = 5.3 Hz, 1H, PyrH), 7.75 (d, *J* = 1.9 Hz, 1H, PyrH), 7.65 (td, *J* = 7.7, 1.8 Hz, 2H, PyrH), 7.52 (d, *J* = 7.8 Hz, 2H, PyrH), 7.29 (dd, *J* = 5.3, 1.9 Hz, 1H, PyrH), 7.14 (ddd, *J* = 7.5, 4.9, 1.2 Hz, 2H, PyrH), 3.87 (d, *J* = 7.9 Hz, 6H, CH_2).

^{13}C NMR: (75 MHz, $CDCl_3$) δ 162.67, 160.33, 151.25, 150.62, 138.01, 134.85, 127.80, 126.90, 124.58, 123.63, 61.77, 61.18.

ESI-MS (m/z): calcd 369.1 $[M+H]^+$, found 369.1 $[M+H]^+$

5.8 SYNTHESIS OF 1-(4-METHOXYPYRIDIN-2-YL)-N,N-BIS(PYRIDIN-2-YLMETHYL)METHANAMINE 38

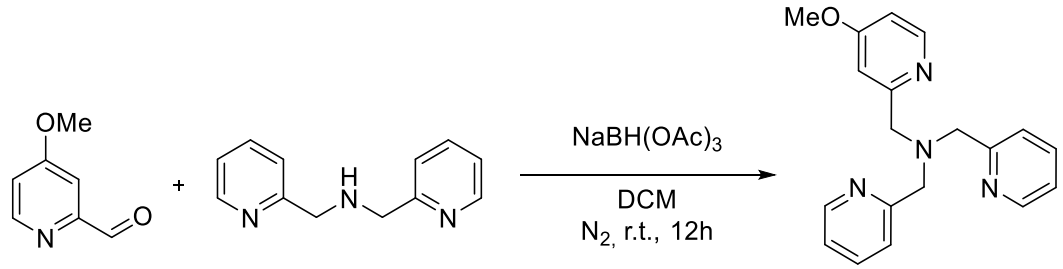

38

In a 50 ml double neck flask, 4-bromopicolinaldehyde (1.00 g, 7.29 mmol) and bis(pyridin-2-ylmethyl)amine (1.45 g, 7.29 mmol) were dissolved in dry DCM (22 mL) under N_2 and left under stirring for 2 hour. $NaBH(OAc)_3$ (1.55 g, 7.29 mmol) was added in three aliquots waiting 20 minutes between each other. After that the reaction was stirred for 12 hours at room temperature. The solvent was removed under reduced pressure. The resulting yellow solid was dissolved in EtOAc (about 30 ml) and the solution extracted with 0.1 M solution of KOH (3x100 ml) and a solution of brine (20 mL). The organic phases were dried on anhydrous Na_2SO_4, and the solvent was removed under reduced pressure to give an amber oil (1.91 g, 5.97 mmol, 81%).

^{1}H NMR: (400 MHz, $CDCl_3$) δ 8.57 – 8.47 (m, 2H, PyrH), 8.33 (d, *J* = 5.7 Hz, 1H, PyrH), 7.64 (td, *J* = 7.6, 1.8 Hz, 2H, PyrH), 7.56 (d, *J* = 7.8 Hz, 2H, PyrH), 7.19 (d, *J* = 2.6 Hz, 1H, PyrH), 7.13 (ddd, *J* = 7.4, 4.9, 1.3 Hz, 2H, PyrH), 6.67 (dd, *J* = 5.8, 2.6 Hz, 1H, PyrH), 3.86 (d, *J* = 17.3 Hz, 6H, CH_2).

^{13}C NMR: (75 MHz, $CDCl_3$) δ 167.86, 162.65, 160.78, 151.60, 150.60, 137.88, 124.45, 123.48, 110.19, 109.85, 61.67, 61.48, 56.60.

ESI-MS (m/z): calcd 321.2 $[M+H]^+$, found 321.2 $[M+H]^+$

5.9 SYNTHESIS OF 1-(PYRIDIN-2-YL)-N-(PYRIDIN-2-YLMETHYL)-N-((4-(PYRROLIDIN-1-YL)PYRIDIN-2-YL)METHYL)METHANAMINE 41

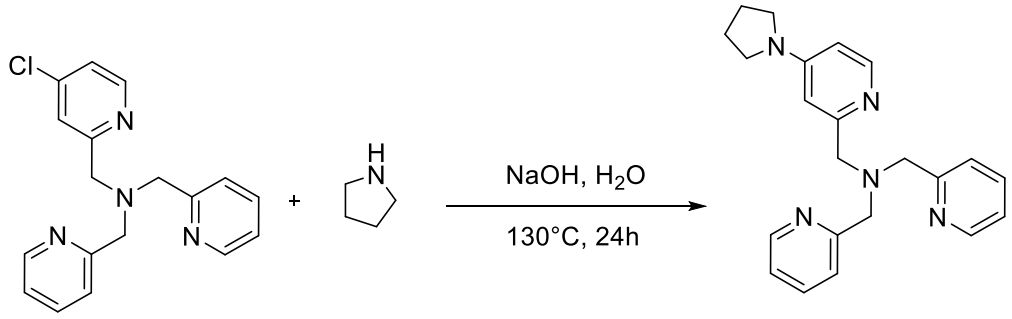

32 **41**

In a 15 mL pressure vessel, **29** (0.300 g, 0.924 mmol) was dissolved in a 5 mL solution of deionized water containing an excess of pyrrolidine (2.30 g, 32.33 mmol). The solution was stirred at room temperature for 5 minutes. Then a pellet of NaOH (0.14 g, 3.43 mmol) was added to reaction mixture and the stirring continued for another 5 minutes at room temperature. The mixture was heated at 130 °C with a strong stirring for 24 hours. Then was cooled at room temperature and dissolved in DCM (12 mL) and extract with deionized water (3 x 20 mL). The organic layer was dried over Na_2SO_4 and after solvent evaporation under reduced pressure a brown solid was recovered. The crude was purified through a column chromatography (neutral alumina gel, DCM:MeOH from 100:0 to 98:2) to give a brown solid (0.151 g, 0.420 mmol, 46%).

^{1}H NMR: (400 MHz, $CDCl_3$) δ 8.47 (d, *J* = 4.9 Hz, 2H, PyrH), 8.08 (d, *J* = 6.0 Hz, 1H, PyrH), 7.89 – 7.40 (m, 5H, PyrH), 7.08 (ddd, *J* = 6.8, 4.8, 2.1 Hz, 2H, PyrH), 6.74 (d, *J* = 2.5 Hz, 1H, PyrH), 6.22 (dd, *J* = 6.1, 2.5 Hz, 1H, PyrH), 3.86 (s, 4H, CH_2), 3.77 (s, 2H, CH_2), 3.43 – 3.04 (m, 4H, Pyrr-CH_2), 2.43 – 1.58 (m, 4H, Pyrr-CH_2).

^{13}C NMR: (75 MHz, $CDCl_3$) δ 161.12, 160.05, 153.88, 150.47, 150.04, 137.78, 124.28, 123.31, 107.07 (d, *J* = 4.0 Hz), 61.62, 54.91, 48.45, 30.78, 26.76.

ESI-MS (m/z): calcd 360.2 $[M+H]^+$, 180.5 $[M+H]^{2+}$, found 360.2 $[M+H]^+$, 180.5 $[M+H]^{2+}$

5.10 SYNTHESIS OF TRIS((4-NITROPYRIDIN-2-YL)METHYL)AMINE 31

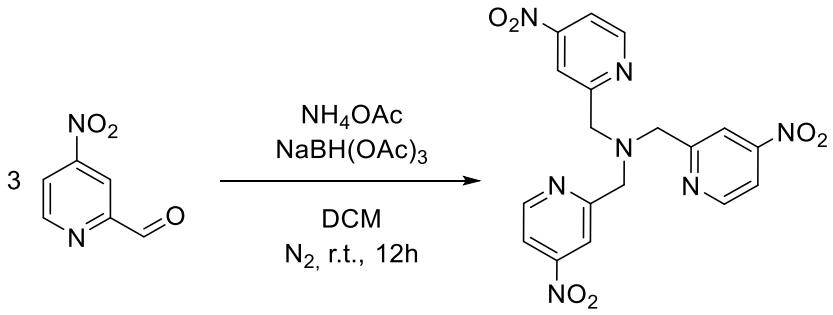

28 **31**

In a 50 ml double neck flask, 4-nitropicolinaldehyde **28** (0.28 g, 1.86 mmol) and ammonium acetate (0.14 g, 1.86 mmol) were dissolved in dry DCM (22 mL) under N_2 and left under stirring for 1 hour. Three aliquots of $NaBH(OAc)_3$ (in total 0.394 g, 1.86 mmol) were added waiting 20 minutes between each other. The reactions were repeated twice with the same amount of **28** and $NaBH(OAc)_3$. After that the reaction was stirred for 12 hours at room temperature. The solvent was removed under reduced pressure. The resulting black solid was dissolved in EtOAc (about 30 ml) and the solution extracted with 0.1 M solution of KOH (3x100 ml) and a solution of brine (20 mL). The organic phases were dried on anhydrous Na_2SO_4, and the solvent was removed under reduced pressure to give black oil. The crude was purified through a column chromatography (alumina gel, DCM:MeOH from 100:0 to 98:2) to give an orange solid (0.681 g, 1.60 mmol, 86%).

^{1}H NMR: (400 MHz, $CDCl_3$) δ 8.88 (d, J = 5.4 Hz, 3H), 8.27 (d, J = 2.2 Hz, 3H), 7.90 (dd, J = 5.5, 2.1 Hz, 3H), 4.17 (s, 6H).

^{13}C NMR: (75 MHz, $CDCl_3$) δ 163.72, 155.96, 153.11, 117.17, 116.39, 61.29.

ESI-MS (m/z): calcd 426.1 $[M+H]^+$, found 426.1 $[M+H]^+$

5.11 SYNTHESIS OF TRIS((4-CHLOROPYRIDIN-2-YL)METHYL)AMINE 34

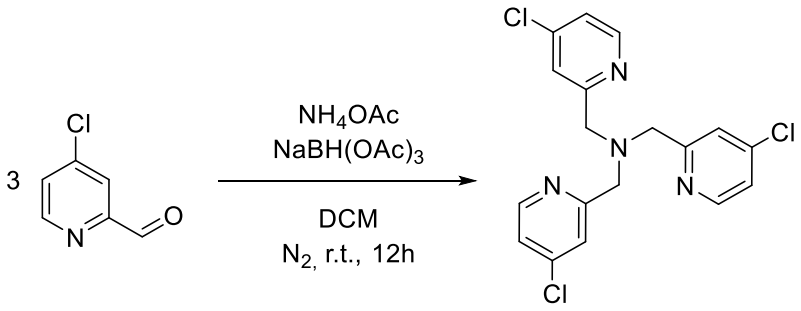

34

In a 50 ml double neck flask, 4-chloropicolinaldehyde (0.333 g, 2.35 mmol) and ammonium acetate (0.181 g, 2.35 mmol) were dissolved in dry DCM (22 mL) under N_2 and left under stirring for 1 hour. Three aliquots of $NaBH(OAc)_3$ (in total 0.500 g, 2.35 mmol) were added waiting 20 minutes between each other. The reactions were repeated twice with the same amount of 4-chloropicolinaldehyde and $NaBH(OAc)_3$. After that the reaction was stirred for 12 hours at room temperature. The solvent was removed under reduced pressure. The resulting orange solid was dissolved in EtOAc (about 30 ml) and the solution extracted with 0.1 M solution of KOH (3x100 ml) and a solution of brine (20 mL). The organic phases were dried on anhydrous Na_2SO_4, and the solvent was removed under reduced pressure to give orange oil. The crude was purified through a column chromatography (silica gel, DCM:MeOH from 100:0 to 9:1) to give an orange solid (0.300 g, 0.762 mmol, 32%).

^{1}H NMR: (400 MHz, $CDCl_3$) δ 8.41 (d, J = 5.4 Hz, 3H, PyrH), 7.50 (d, J = 2.0 Hz, 3H, PyrH), 7.15 (dd, J = 5.4, 2.0 Hz, 3H, PyrH), 3.88 (s, 6H, CH_2).

^{13}C NMR: (75 MHz, $CDCl_3$) δ 162.04, 151.49, 146.18, 124.96, 124.16, 61.42.

ESI-MS (m/z): calcd 393.0 $[M+H]^+$, found 393.1 $[M+H]^+$

5.12 SYNTHESIS OF TRIS((4-BROMOPYRIDIN-2-YL)METHYL)AMINE 37

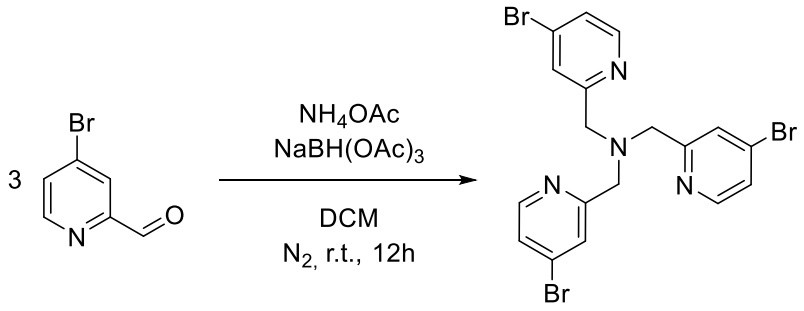

37

In a 50 ml double neck flask, 4-bromopicolinaldehyde (0.333 g, 1.80 mmol) and ammonium acetate (0.138 g, 1.80 mmol) were dissolved in dry DCM (22 mL) under N_2 and left under stirring for 1 hour. Three aliquots of $NaBH(OAc)_3$ (in total 0.380 g, 1.80 mmol) were added waiting 20 minutes between each other. The reactions were repeated twice with the same amount of 4-bromopicolinaldehyde and $NaBH(OAc)_3$. After that the reaction was stirred for 12 hours at room temperature. The solvent was removed under reduced pressure. The resulting amber solid was dissolved in EtOAc (about 30 ml) and the solution extracted with 0.1 M solution of KOH (3x100 ml) and a solution of brine (20 mL). The organic phases were dried on anhydrous Na_2SO_4, and the solvent was removed under reduced pressure to give amber oil. The crude was purified through a column chromatography (silica gel, DCM:MeOH from 100:0 to 9:1) to give an amber solid (0.700 g, 1.33 mmol, 74%).

^{1}H NMR: (400 MHz, $CDCl_3$) δ 8.35 (d, J = 5.3 Hz, 3H, PyrH), 7.66 (d, J = 1.9 Hz, 3H, PyrH), 7.32 (dd, J = 5.4, 1.9 Hz, 3H, PyrH), 3.89 (s, 6H, CH_2).

^{13}C NMR: (75 MHz, $CDCl_3$) δ 161.90, 151.36, 134.89, 128.11, 127.13, 61.49.

ESI-MS (m/z): calcd 526.9 $[M+H]^+$, found 526.9 $[M+H]^+$

5.13 SYNTHESIS OF TRIS((4-METHOXYPYRIDIN-2-YL)METHYL)AMINE 40

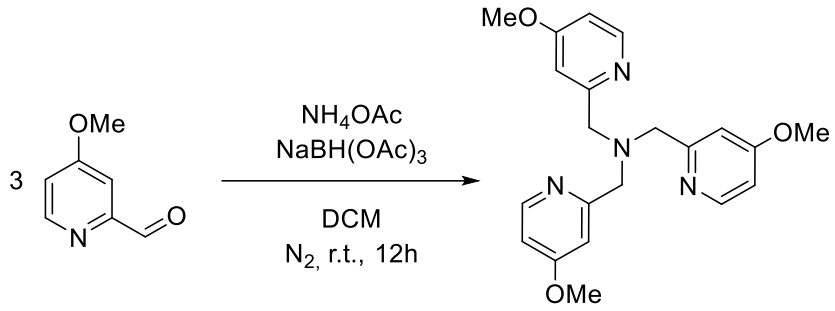

40

In a 50 ml double neck flask, 4-methoxypicolinaldehyde (0.333 g, 2.43 mmol) and ammonium acetate (0.187 g, 2.43 mmol) were dissolved in dry DCM (22 mL) under N_2 and left under stirring for 2 hour. Three aliquots of $NaBH(OAc)_3$ (in total 0.515 g, 2.43 mmol) were added waiting 20 minutes between each other. The reactions were repeated twice with the same amount of 4-methoxypicolinaldehyde and $NaBH(OAc)_3$. After that the reaction was stirred for 12 hours at room temperature. The solvent was removed under reduced pressure. The resulting yellow solid was dissolved in EtOAc (about 30 ml) and the solution extracted with 0.1 M solution of KOH (3x100 ml) and a solution of brine (20 mL). The organic phases were dried on anhydrous Na_2SO_4, and the solvent was removed under reduced pressure to give green oil. The crude was purified through a column chromatography (silica gel, DCM:MeOH from 100:0 to 9:1) to give a yellow solid (0.536 g, 1.41 mmol, 58%).

^{1}H NMR: (400 MHz, $CDCl_3$) δ 8.32 (d, J = 5.7 Hz, 3H, PyrH), 7.16 (d, J = 2.6 Hz, 3H, PyrH), 6.65 (dd, J = 5.8, 2.5 Hz, 3H, PyrH), 3.84 (s, 6H), 3.82 (s, 9H).

^{13}C NMR: (75 MHz, $CDCl_3$) δ 167.76, 162.61, 151.67, 110.19, 109.91, 61.70, 56.54.

ESI-MS (m/z): calcd 381.2 $[M+H]^+$, found 381.2 $[M+H]^+$

5.14 SYNTHESIS OF TRIS((4-(PYRROLIDIN-1-YL)PYRIDIN-2-YL)METHYL)AMINE 43

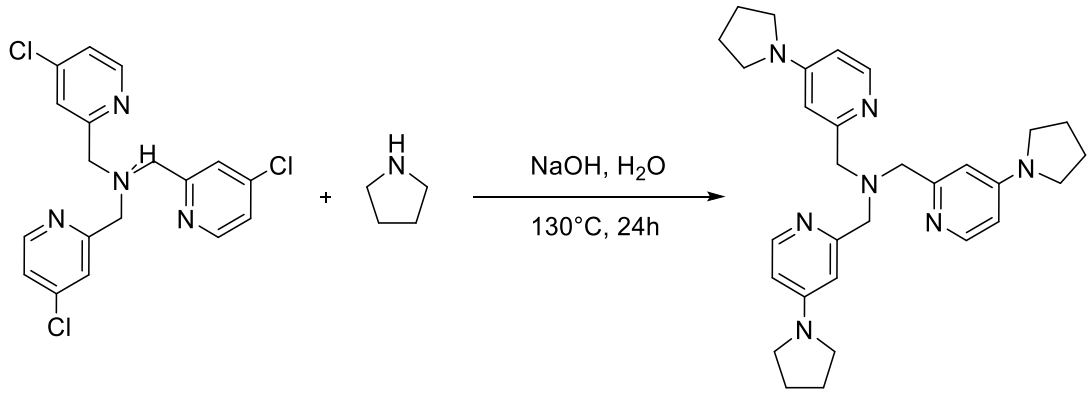

34 **43**

In a 9 mL pressure vessel, **34** (0.120 g, 0.305 mmol) was dissolved in a solution containing an excess of pyrrolidine (0.759 g, 10.67 mmol) and 2 mL of deionized water. The solution was stirred at room temperature for 5 minutes. Then a pellet of NaOH (0.037 g, 1.00 mmol) was added to reaction mixture and the stirring continued for another 5 minutes at room temperature. The mixture was heated at 130 °C with a strong stirring for 24 hours. Then was cooled at room temperature and dissolved in DCM (5 mL) and extract with deionized water (3 x 20 mL). The organic layer was dried over Na_2SO_4 and after solvent evaporation under reduced pressure a brown solid was recovered. The crude was purified through a column chromatography (alumina gel, DCM:MeOH from 100:0 to 98:2) to give a brown solid (0.094 g, 0.189 mmol, 62%).

^{1}H NMR: (400 MHz, $CDCl_3$) δ 8.05 (d, J = 6.0 Hz, 3H, PyrH), 6.69 (d, J = 2.5 Hz, 3H, PyrH), 6.22 (dd, J = 6.1, 2.5 Hz, 3H, PyrH), 3.79 (s, 6H, CH_2), 3.26 (m, 12H, Pyrr-CH_2), 1.95 (m, J = 3.4 Hz, 12H, Pyrr-CH_2).

^{13}C NMR: (75 MHz, $CDCl_3$) δ 159.12, 154.19, 148.54, 107.56, 107.13, 61.09, 48.71, 26.75.

ESI-MS (m/z): calcd 249.7 $[M+H]^{2+}$, 498.3 $[M+H]^+$, found 249.7 $[M+H]^{2+}$, 498.3 $[M+H]^+$

5.15 SYNTHESIS OF 1-(4-NITROPYRIDIN-2-YL)-N-((4-NITROPYRIDIN-2 YL)METHYL) -N-(PYRIDIN-2-YLMETHYL)METHANAMINE 30

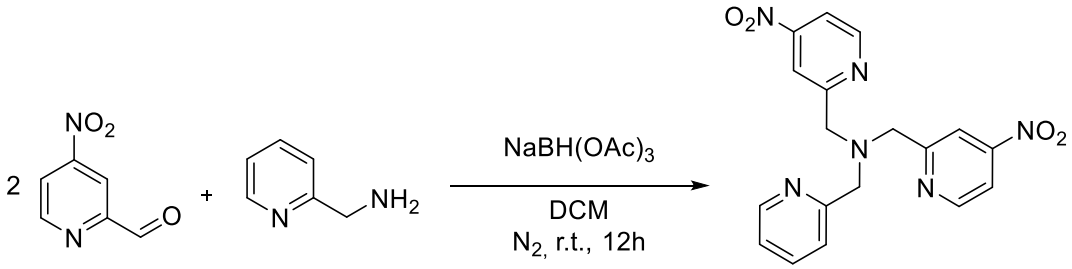

28 **30**

In a 50 ml double neck flask, 4-nitropicolinaldehyde **28** (0.343 g, 2.25 mmol) and pyridin-2-ylmethanamine (0.244 g, 2.25 mmol) were dissolved in dry DCM (22 mL) under N_2 and left under stirring for 1 hour. Three aliquots of $NaBH(OAc)_3$ (in total 0.478 g, 2.25 mmol) were added waiting 20 minutes between each other. The reactions were repeated once with the same amount of **28** and $NaBH(OAc)_3$. After that the reaction was stirred for 12 hours at room temperature. The solvent was removed under reduced pressure. The resulting black solid was dissolved in EtOAc (about 30 ml) and the solution extracted with 0.1 M solution of KOH (3x100 ml) and a solution of brine (20 mL). The organic phases were dried on anhydrous Na_2SO_4, and the solvent was removed under reduced pressure to give black oil. The crude was purified through a column chromatography (allumina gel, DCM:MeOH from 100:0 to 99:1) to give a purple-wine oil.

ESI-MS (m/z): calcd 381.1 $[M+H]^+$, found 381.1 $[M+H]^+$

5.16 SYNTHESIS OF 1-(4-CHLOROPYRIDIN-2-YL)-N-((4-CHLOROPYRIDIN-2-YL) METHYL)-N-(PYRIDIN-2-YLMETHYL)METHANAMINE 33

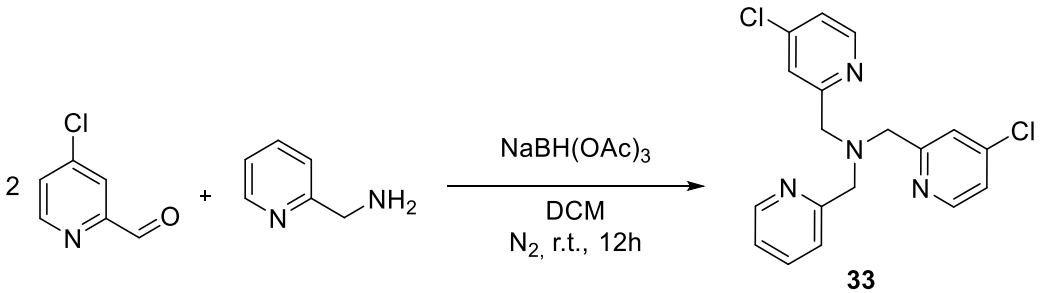

33

In a 50 ml double neck flask, 4-chloropicolinaldehyde (0.500 g, 3.53 mmol) and pyridin-2-ylmethanamine (0.382 g, 3.53 mmol) were dissolved in dry DCM (22 mL)

under N_2 and left under stirring for 1 hour. Three aliquots of $NaBH(OAc)_3$ (in total 0.515 g, 2.43 mmol) were added waiting 20 minutes between each other. The reactions were repeated once with the same amount of 4-chloropicolinaldehyde and $NaBH(OAc)_3$. After that the reaction was stirred for 12 hours at room temperature. The solvent was removed under reduced pressure. The resulting orange solid was dissolved in EtOAc (about 30 ml) and the solution extracted with 0.1 M solution of KOH (3x100 ml) and a solution of brine (20 mL). The organic phases were dried on anhydrous Na_2SO_4, and the solvent was removed under reduced pressure to give orange oil. The crude was purified through a column chromatography (allumina gel, DCM:MeOH from 100:0 to 99:1) to give an orange oil (0.700 g, 1.95 mmol, 83%).

^{1}H NMR: (400 MHz, $CDCl_3$) δ 8.55 (m, 1H; PyrH), 8.42 (d, *J* = 5.4 Hz, 2H, PyrH), 7.67 (qd, *J* = 6.5, 5.3, 1.7 Hz, 1H, PyrH), 7.56 (d, *J* = 2.0 Hz, 2H, PyrH), 7.50 (d, *J* = 8.0 Hz, 1H, PyrH), 7.16 (dd, *J* = 5.3, 2.1 Hz, 3H, PyrH), 3.89 (d, *J* = 5.6 Hz, 6H, CH_2).

^{13}C NMR: (75 MHz, $CDCl_3$) δ 162.50, 160.11, 151.47, 150.72, 146.11, 138.03, 124.82, 124.59, 124.04, 123.72, 61.93, 61.37.

ESI-MS (m/z): calcd 359.1 $[M+H]^+$, found 359.1 $[M+H]^+$

5.17 Synthesis of 1-(4-bromopyridin-2-yl)-N-((4-bromopyridin-2-yl) methyl)-N-(pyridin-2-ylmethyl)methanamine 36

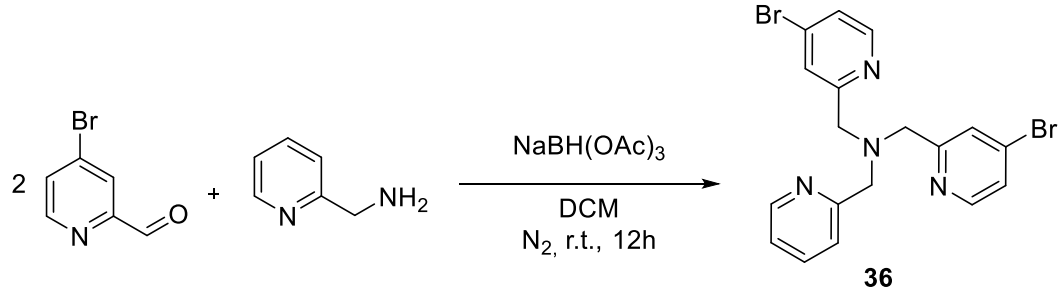

36

In a 50 ml double neck flask, 4-bromopicolinaldehyde (0.500 g, 2.69 mmol) and pyridin-2-ylmethanamine (0.291 g, 2.69 mmol) were dissolved in dry DCM (22 mL) under N_2 and left under stirring for 1 hour. Three aliquots of $NaBH(OAc)_3$ (in total 0.570 g, 2.69 mmol) were added waiting 20 minutes between each other. The reactions were repeated once with the same amount of 4-bromopicolinaldehyde and $NaBH(OAc)_3$. After that the reaction was stirred for 12 hours at room temperature.

The solvent was removed under reduced pressure. The resulting amber solid was dissolved in EtOAc (about 30 ml) and the solution extracted with 0.1 M solution of KOH (3x100 ml) and a solution of brine (20 mL). The organic phases were dried on anhydrous Na_2SO_4, and the solvent was removed under reduced pressure to give amber oil. The crude was purified through a column chromatography (allumina gel, DCM:MeOH from 100:0 to 99:1) to give an amber oil (1.100 g, 2.45 mmol, 91%).

^{1}H NMR: (400 MHz, $CDCl_3$) δ 8.60 – 8.50 (m, 1H, PyrH), 8.34 (d, *J* = 5.3 Hz, 2H, PyrH), 7.69 (dd, *J* = 13.3, 1.8 Hz, 3H, PyrH), 7.49 (d, *J* = 7.8 Hz, 1H, PyrH), 7.31 (dd, *J* = 5.3, 1.9 Hz, 2H, PyrH), 7.20 – 7.13 (m, 1H, PyrH), 3.89 (d, *J* = 10.5 Hz, 6H, CH_2).

^{13}C NMR: (75 MHz, $CDCl_3$) δ 162.34, 160.09, 151.33, 150.72, 138.02, 134.85, 127.94, 127.00, 124.62, 123.73, 61.99, 61.36.

ESI-MS (m/z): calcd 449.0 $[M+H]^+$, found 449.0 $[M+H]^+$

5.18 Synthesis of 1-(4-methoxypyridin-2-yl)-N-((4-methoxypyridin-2-yl) methyl)-N-(pyridin-2-ylmethyl)methanamine 39

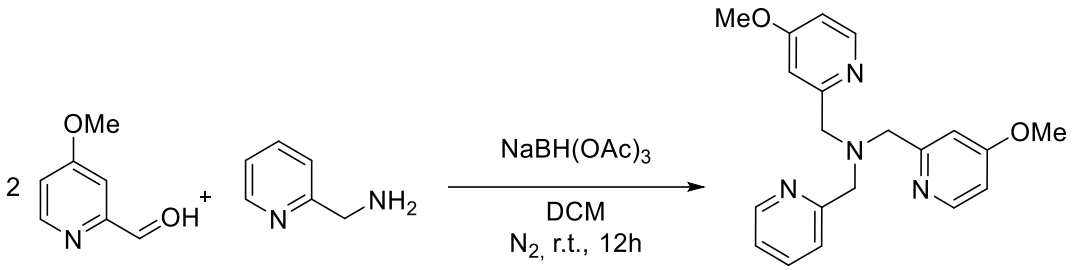

39

In a 50 ml double neck flask, 4-methoxypicolinaldehyde (0.500 g, 3.65 mmol) and pyridin-2-ylmethanamine (0.394 g, 3.65 mmol) were dissolved in dry DCM (22 mL) under N_2 and left under stirring for 2 hour. Three aliquots of $NaBH(OAc)_3$ (in total 0.772 g, 3.65 mmol) were added waiting 20 minutes between each other. The reactions were repeated once with the same amount of and $NaBH(OAc)_3$. After that the reaction was stirred for 12 hours at room temperature. The solvent was removed under reduced pressure. The resulting yellow solid was dissolved in EtOAc (about 30 ml) and the solution extracted with 0.1 M solution of KOH (3x100 ml) and a solution of brine (20 mL). The organic phases were dried on anhydrous Na_2SO_4, and the solvent was removed under reduced pressure to give yellow oil. The crude was purified through a

column chromatography (allumina gel, DCM:MeOH from 100:0 to 99:1) to give green oil (0.800 g, 2.28 mmol, 62%).

^{1}H NMR: (400 MHz, $CDCl_3$) 8.43 (d, *J* = 5.0 Hz, 1H, PyrH), 8.24 (d, *J* = 5.7 Hz, 2H, PyrH), 7.67 – 7.34 (m, 2H, PyrH), 7.11 (d, *J* = 2.6 Hz, 2H, PyrH), 7.08 – 6.93 (m, 1H, PyrH), 6.57 (dd, *J* = 5.8, 2.6 Hz, 2H, PyrH), 3.79 (d, *J* = 16.7 Hz, 6H, CH_2), 3.73 (s, 6H, CH_3).

^{13}C NMR: (75 MHz, $CDCl_3$) δ 167.71, 162.60, 160.70, 151.61, 150.53, 137.81, 124.34, 123.42, 110.07, 109.80, 61.52, 56.49.

ESI-MS (m/z): calcd 351.2 $[M+H]^+$, found 351.2 $[M+H]^+$

5.19 SYNTHESIS OF 1-(PYRIDIN-2-YL)-N,N-BIS((4-(PYRROLIDIN-1-YL)PYRIDIN-2-YL)METHYL)METHANAMINE 42

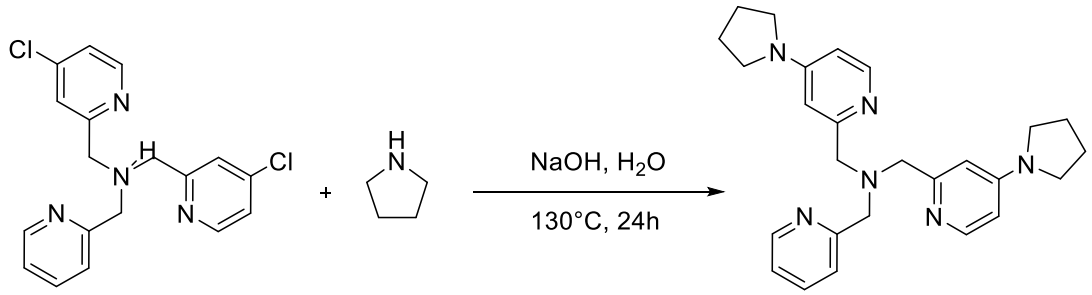

33 **42**

In a 9 mL pressure vessel, **33** (0.222 g, 0.618 mmol) was dissolved in a solution containing an excess of pyrrolidine (0.1.54 g, 21.63 mmol) and 3 mL of deionized water. The solution was stirred at room temperature for 5 minutes. Then a pellet of NaOH (0.080 g, 2.00 mmol) was added to reaction mixture and the stirring continued for another 5 minutes at room temperature. The mixture was heated at 130 °C with a strong stirring for 24 hours. Then was cooled at room temperature and dissolved in DCM (8 mL) and extract with deionized water (3 x 20 mL). The organic layer was dried over Na_2SO_4 and after solvent evaporation under reduced pressure a brown solid was recovered. The crude was purified through a column chromatography (alumina gel, DCM:MeOH from 100:0 to 98:2) to give a brown solid (0.260 g, 0.606 mmol, 98%).

^{1}H NMR: (400 MHz, $CDCl_3$) δ 8.45 (d, *J* = 4.8 Hz, 1H, PyrH), 8.07 (d, *J* = 5.9 Hz, 2H, PyrH), 7.58 (d, *J* = 4.3 Hz, 2H, PyrH), 7.06 (q, *J* = 4.5 Hz, 1H, PyrH), 6.75 (d, *J* = 2.5 Hz, 2H, PyrH), 6.21 (dd, *J* = 6.1, 2.5 Hz, 2H, PyrH), 3.82 (d, *J* = 39.6 Hz, 6H, CH_2), 3.42 – 3.04 (m, 8H,CH_2-Pyrrolidine), 2.14 – 1.76 (m, 8H,CH_2-Pyrrolidine).

^{13}C NMR: (75 MHz, $CDCl_3$) δ 161.16, 159.73, 154.04, 150.43, 149.33, 137.82, 124.38, 123.29, 107.30, 107.03, 61.70, 61.38, 48.57, 26.76.

ESI-MS (m/z): calcd 215.1 $[M+H]^{2+}$, 429.3 $[M+H]^+$, found 215.1 $[M+H]^{2+}$, 429.3 $[M+H]^+$

5.20 Synthesis of Co (II) –TPMA complexes Co-29-43

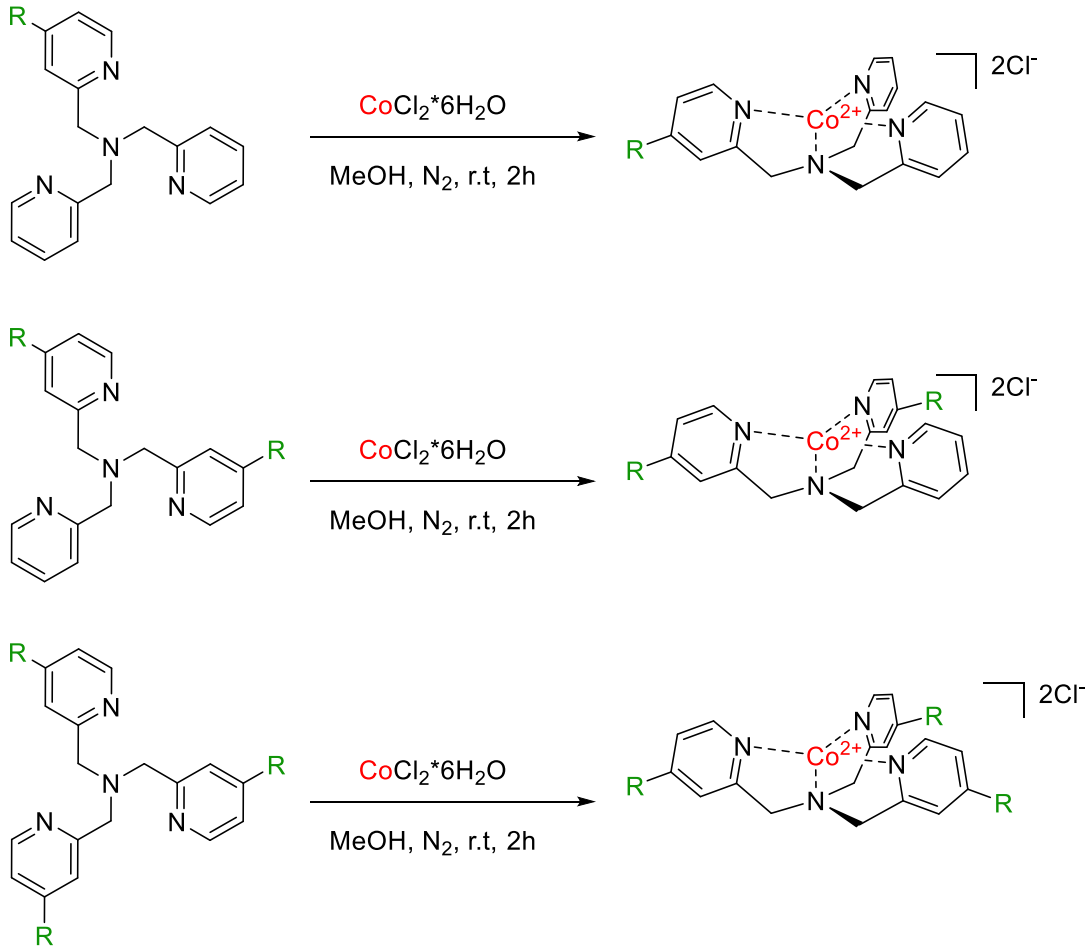

R = NO_2, Cl, Br, H, OCH_3, Pyrr

In a 25 mL double neck flask, **29-43** (50 mg) were dissolved in 5 mL of anhydrous MeOH. Then, cobalt (II) chloride hexahydrate was added in equimolar amount and the reaction was stirred at room temperature, under N_2 for 2 hours. Methanol was

evaporated under reduced pressure. The green solid was dissolved in a small amount of ACN and Et_2O was added. The resulting precipitate was separated by centrifugation and dried in a vacuum pump for 3 hours.

5.20.1 Co-NO_2-TPMA 29 (dark green, solid)

^{1}H NMR: (400 MHz, CD_3CN) δ 133.40 (s, 2H, PyrH), 121.67 (s, 1H, PyrH), 111.32 (s, 2H, CH_2), 108.60 (s, 4H, CH_2), 56.47 (s, 2H, PyrH), 49.26 (s, 2H, PyrH), 48.37 (s, 1H, PyrH), 44.49 (s, 1H, PyrH), -1.16 (s, 2H, PyrH).

ESI-MS (m/z): calcd 429.0 $[M+H]^+$, found 429.0 $[M+H]^+$
ANAL. CALC. ($C_{18}H_{17}Cl_2CoN_5O_2$): calcd. C 46,47%, H 3.68%, N 15.05% found C 45.47%, H 4.02%, N 15.05%

UV-Vis: (CH_3CN) λ_{max} (nm) ($\varepsilon/M^{-1}cm^{-1}$) = 486 (143) (d-d transition), 616 (92), 632 (89) (d-d transition)

5.20.2 Co-Cl-TPMA 32 (light green, solid)

^{1}H NMR: (400 MHz, CD_3CN) δ 133.55 (s, 2H, PyrH), 129.93 (s, 1H, PyrH), 106.04 (s, 4H, CH_2), 104.61 (s, 2H, CH_2), 59.68 (s, 2H, PyrH), 54.64 (s, 1H, PyrH), 46.47 (s, 2H, PyrH), 43.15 (s, 1H, PyrH), -3.04 (s, 2H, PyrH).

ESI-MS (m/z): calcd 418.0 $[M+H]^+$, found 418.0 $[M+H]^+$

ELEM. ANAL.: Not Available

UV-Vis: (CH_3CN) λ_{max} (nm) ($\varepsilon/M^{-1}cm^{-1}$) = 486 (209) (d-d transition), 592 (181), 636 (228) (d-d transition)

5.20.3 Co-Br-TPMA 35 (blue green, solid)

^{1}H NMR: (400 MHz, CD_3CN) δ 132.86 (s, 2H, PyrH), 129.18 (s, 1H, PyrH), 106.93 (s, 4H, CH_2), 105.85 (s, 2H, CH_2), 58.17 (s, 2H, PyrH), 53.17 (s, 1H, PyrH), 47.39 (s, 2H, PyrH), 43.93 (tt, J = 8.2, 4.2 Hz, 1H, PyrH), -2.23 (tt, J = 8.7, 4.2 Hz, 2H, PyrH).

ESI-MS (m/z): calcd 463.9 $[M+H]^+$, found 463.9 $[M+H]^+$

ELEM. ANAL. ($C_{18}H_{17}BrCl_2CoN_4$) + 1H_2O: calcd. C 41.81%, H 3.70%, N 10.83% found C 41.31%, H 3.84%, N 10.20%

UV-Vis: (CH_3CN) λ_{max} (nm) ($\varepsilon/M^{-1}cm^{-1}$) = 489 (197) (d-d transition), 616 (169), 631 (148) (d-d transition)

5.20.4 Co-TPMA (green solid)

^{1}H NMR: (400 MHz, CD_3CN) δ 105.66 (s, 6H, CH_2), 59.83 (s, 3H, PyrH), 45.67 (s, 3H, PyrH), 3.39 (s, 3H, PyrH).

ESI-MS (m/z): calcd 384.0 $[M+H]^+$, found 384.0 $[M+H]^+$

ELEM. ANAL.: Not Available

UV-Vis: (CH_3CN) λ_{max} (nm) ($\varepsilon/M^{-1}cm^{-1}$) = 489 (110) (dd transition), 591 (124), 640 (133) (d-d transition)

5.20.5 Co-OCH_3-TPMA 38 (light green, solid)

^{1}H NMR: (400 MHz, CD_3CN) δ 133.92 (s, 1H, PyrH), 130.99 (s, 2H, PyrH), 104.05 – 103.07 (m, 6H, CH_2) 59.18 (s, 2H, PyrH), 55.00 (s, 1H, PyrH), 45.72 (s, 2H, PyrH), 40.42 (t, J = 7.8 Hz, 1H, PyrH), -3.25 (s, 2H, PyrH).

ESI-MS (m/z): calcd 414.1 $[M+H]^+$, found 414.1 $[M+H]^+$

ELEM. ANAL. ($C_{19}H_{20}Cl_2CoN_4O$) + 1H_2O: calcd. C 48.74%, H 4.48%, N 12.44% found C 47.22%, H 4.88%, N 11.28%

UV-Vis: (CH_3CN) λ_{max} (nm) ($\varepsilon/M^{-1}cm^{-1}$) = 490 (115) (dd transition), 615 (91), 632 (70) (d-d transition)

5.20.6 Co-Pyrr-TPMA 41 (dark green, solid)

^{1}H NMR: (400 MHz, CD_3CN) δ 140.53 (s, 1H, PyrH), 127.13 (s, 2H, PyrH), 101.91-98.23 (m, 6H, CH_2), 58.35 (s, 2H, PyrH), 56.03 (s, 1H, PyrH), 44.62 (s, 2H, PyrH), 35.56 (s, 1H, PyrH), -3.42 (m, 2H, PyrH).

ESI-MS: (m/z): calcd 453.1 $[M+H]^+$, found 453.1 $[M+H]^+$

ELEM. ANAL.: Not Available

UV-Vis: (CH_3CN) λ_{max} (nm) ($\varepsilon/M^{-1}cm^{-1}$) = 501 (106) (dd transition), 591 (158), 633 (125) (d-d transition)

5.20.7 Co-$(NO_2)_3$-TPMA 31 (dark orange, solid)

^{1}H NMR: (400 MHz, CD_3CN) δ 118.66 (s, 6H, CH_2), 114.18 (s, 3H, PyrH), 54.45 (s, 3H, PyrH), 42.13 (s, 3H, PyrH).

ESI-MS (m/z): calcd 519.0 $[M+H]^+$, found 519.0 $[M+H]^+$

ELEM. ANAL. ($C_{18}H_{15}Cl_2CoN_7O_6$): calc. C 38.94%, H 2.72%, N 17.66% found C 38.83%, H 2.87%, N 16.89%

UV-Vis: (CH_3CN) λ_{max} (nm) ($\varepsilon/M^{-1}cm^{-1}$) = 485 (157) (d-d transition), 620 (77), 645 (86) (d-d transition)

5.20.8 Co-Cl_3-TPMA 34 (green, solid)

^{1}H NMR: (400 MHz, CD_3CN) δ 131.23 (s, 3H, PyrH), 106.07 (s, 6H, CH_2), 53.35 (s, 3H, PyrH), 44.90 (s, 3H, PyrH).

ESI-MS (m/z): calcd 487.9 $[M+H]^+$, found 487.9 $[M+H]^+$

ELEM. ANAL.: Not Available

UV-Vis: (CH_3CN) λ_{max} (nm) ($\varepsilon/M^{-1}cm^{-1}$) = 485 (229) (d-d transition), 590 (177), 635 (230) (d-d transition)

5.20.9 Co-Br_3-TPMA 37 (light blue, solid)

^{1}H NMR: (400 MHz, CD_3CN) δ 131.80 (s, 3H, PyrH) 105.66 (s, 6H, CH_2), 54.28 (s, 3H, PyrH), 45.04 (s, 3H, PyrH).

ESI-MS (m/z): calcd 621.7 $[M+H]^+$, found 621.7 $[M+H]^+$

ELEM. ANAL.: Not Available

UV-Vis: (CH_3CN) λ_{max} (nm) ($\varepsilon/M^{-1}cm^{-1}$) = 490 (222) (d-d transition), 615 (160), 635 (172) (d-d transition)

5.20.10Co-$(OCH_3)_3$-TPMA 40 (water green, solid)

^{1}H NMR: (400 MHz, CD_3CN) δ 131.03 (s, 3H, PyrH), 99.28 (s, 6H, CH_2), 54.23 (s, 3H, PyrH), 39.38 (d, J = 16.0 Hz, 3H, PyrH).

ESI-MS (m/z): calcd 453.1 $[M+H]^+$, found 453.1 $[M+H]^+$

ELEM. ANAL.: Not Available

UV-Vis: (CH_3CN) λ_{max} (nm) ($\varepsilon/M^{-1}cm^{-1}$) = 495 (293) (dd transition), 590 (269), 634 (229) (d-d transition)

5.20.11Co-$Pyrr_3$-TPMA 43 (dark green, solid)

^{1}H NMR: (400 MHz, CD_3CN) δ 132.55 (s, 3H, PyrH), 92.37 (s, 6H, CH_2), 53.95 (s, 3H, PyrH), 34.99 (s, 3H, PyrH).

ESI-MS (m/z): calcd 491.2 $[M+H]^+$, found 491.2 $[M+H]^+$

ELEM. ANAL.: Not Available

UV-Vis: (CH_3CN) λ_{max} (nm) ($\varepsilon/M^{-1}cm^{-1}$) = 510 (321) (dd transition), 590 (336), 635 (189) (d-d transition)

5.20.12Co-Cl_2-TPMA 33 (purple, solid)

^{1}H NMR: (400 MHz, CD_3CN) δ 134.98 (s, 1H, PyrH), 131.12 (s, 2H, PyrH), 106.15-105.08 (d, *J* = 470.8 Hz, 6H, CH_2), 60.25 (s, 1H, PyrH), 55.07 (s, 2H, PyrH), 47.24 (s, 1H, PyrH), 43.83 (s, 2H, PyrH), -2.69 (s, 1H, PyrH).

ESI-MS (m/z): calcd 452.0 $[M+H]^+$, found 452.0 $[M+H]^+$

ELEM. ANAL. ($C_{18}H_{16}Cl_4CoN_4$) + 1 H_2O: calc. C 42.63%, H 3.58%, N 11.05% found C 42.58%, H 3.39%, N 10.95%

UV-Vis: (CH_3CN) λ_{max} (nm) ($\varepsilon/M^{-1}cm^{-1}$) = 490 (241) (d-d transition), 620 (210), 635 (208) (d-d transition)

5.20.13Co-Br_3-TPMA 36 (light blue, solid)

^{1}H NMR: (400 MHz, CD_3CN) δ 133.75 (s, 1H, PyrH), 130.13 (s, 2H, PyrH), 107.23-106.33 (d, *J* = 379.5 Hz, 6H, CH_2), 57.86 (s, 1H, PyrH), 52.87 (s, 2H, PyrH), 48.25 (s, 1H, PyrH), 44.62 (s, 2H, PyrH), -1.90 (s, 1H, PyrH).

ESI-MS (m/z): calcd 541.8 $[M+H]^+$, found 541.8 $[M+H]^+$

ELEM. ANAL. ($C_{18}H_{16}Br_2Cl_2CoN_4$) + 1 H_2O: calc. C 36.27%, H 3.04%, N 9.40% found C 35.65%, H 2.96%, N 9.12%

UV-Vis: (CH_3CN) λ_{max} (nm) ($\varepsilon/M^{-1}cm^{-1}$) = 490 (245) (d-d transition), 620 (210), 635 (208) (d-d transition)

5.20.14 Co-$(OCH_3)_2$-TPMA 39 (Petrol blue, solid)

^{1}H NMR: (400 MHz, CD_3CN) δ 131.53-128.27 (d, *J* = 1378.3 Hz, 2H, PyrH), 103.66-101.09 (d, *J* = 1004.2 Hz, 6H, CH_2), 58.52 (s, 1H, PyrH), 54.38 (s, 2H, PyrH), 45.18 (s, 1H, PyrH), 39.84 (s, 2H, PyrH), -3.29 (s, 1H, PyrH).

ESI-MS (m/z): calcd $[M+H]^+$, found 444.1 $[M+H]^+$

ELEM. ANAL.: Not Available

UV-Vis: (CH_3CN) λ_{max} (nm) ($\varepsilon/M^{-1}cm^{-1}$) = 494 (217) (dd transition), 610 (209), 635 (192) (d-d transition)

5.20.15Co-Pyrr$_2$-TPMA 42 (dark blue, solid)

^{1}H NMR: (400 MHz, CD_3CN) δ 137.07 (s, 2H, PyrH), 123.90 (s, 1H, PyrH), 98.59-95.75 (d, J = 1176.3 Hz, 6H, CH_2), 57.62 (s, 1H, PyrH), 55.13 (s, 2H, PyrH), 44.19 (s, 1H, PyrH), 35.47 (s, 2H, PyrH), -3.70 (s, 1H, PyrH).

ESI-MS (m/z): calcd 522.1 $[M+H]^+$, found 522.1 $[M+H]^+$

ELEM. ANAL.: Not Available

UV-Vis: (CH_3CN) λ_{max} (nm) ($\varepsilon/M^{-1}cm^{-1}$) = 505 (243) (d-d transition), 590 (290), 635 (195) (d-d transition)

5.21 UV-VIS MEASUREMENTS

The solutions for the UV-Vis measurements were prepared from the **Co-R$_n$-TPMA 29-43** complexes by dilution to obtain a final concentration of equal to $1 \cdot 10^{-3}$ M in ACN. The spectra were collected with a 0.1 cm cuvette path length in the range of 350 – 700 nm at room temperature.

5.22 CYCLIC VOLTAMMETRY MEASUREMENTS

Electrochemical properties of TPMA complexes **Co-R$_n$-TPMA 29-43** under nitrogen atmosphere were investigated using cyclic voltammetry (CV) in 0.1 M $[^nBu_4N]ClO_4$, CH_3CN solutions $1*10^{-3}$ M. Scan rate were 0.1 V/s and the CV the applied potentials range were from 0 V to -2 V vs Ag/AgCl.

6 SPECTRA

6.1 CHARACTERIZATION OF *PARA*-TPMA LIGANDS

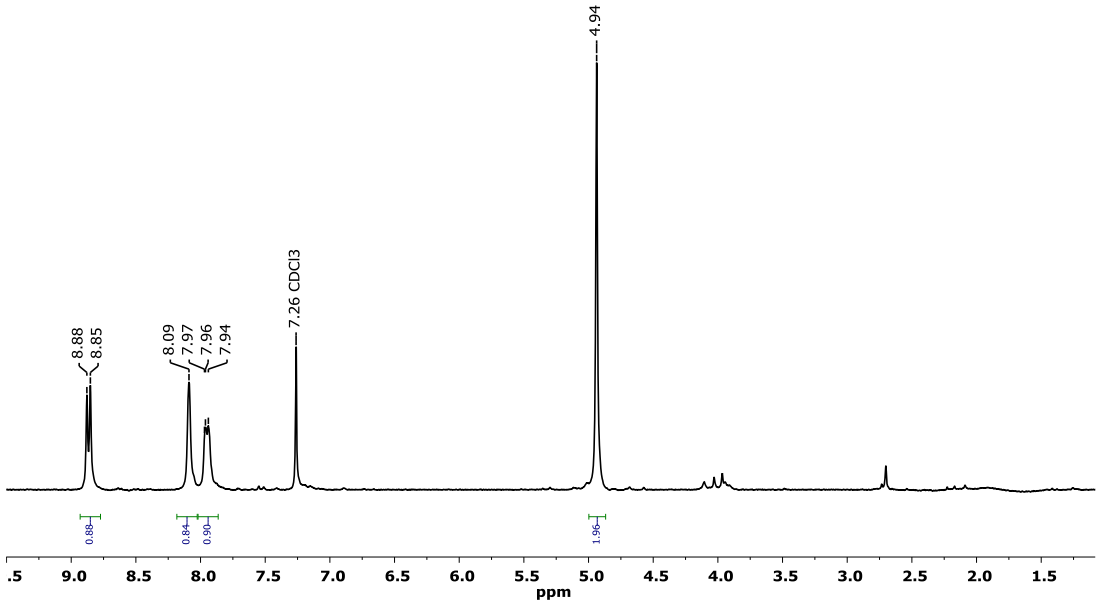

Figure S1: ^{1}H-NMR (300 MHz, $CDCl_3$) of (4-nitropirydin-2-yl)methanol **27**

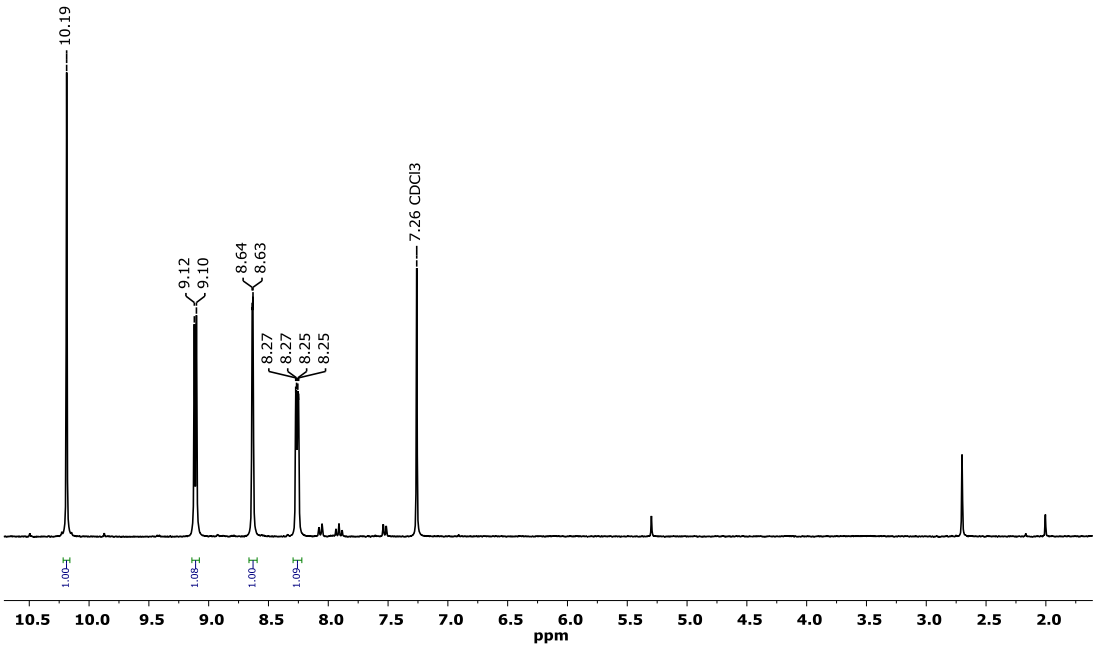

Figure S2: ^{1}H-NMR (300 MHz, $CDCl_3$) of 4-nitropicolinaldehyde **28**

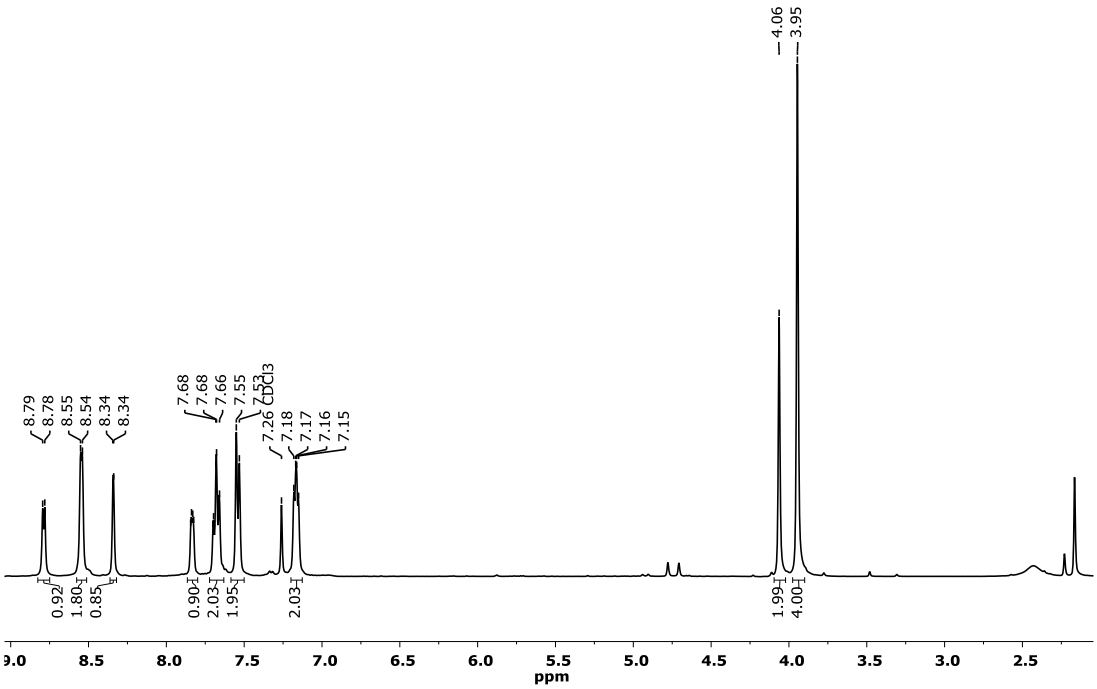

Figure S3: ^{1}H-NMR (400 MHz, $CDCl_3$) of **NO_2-TPMA 29**

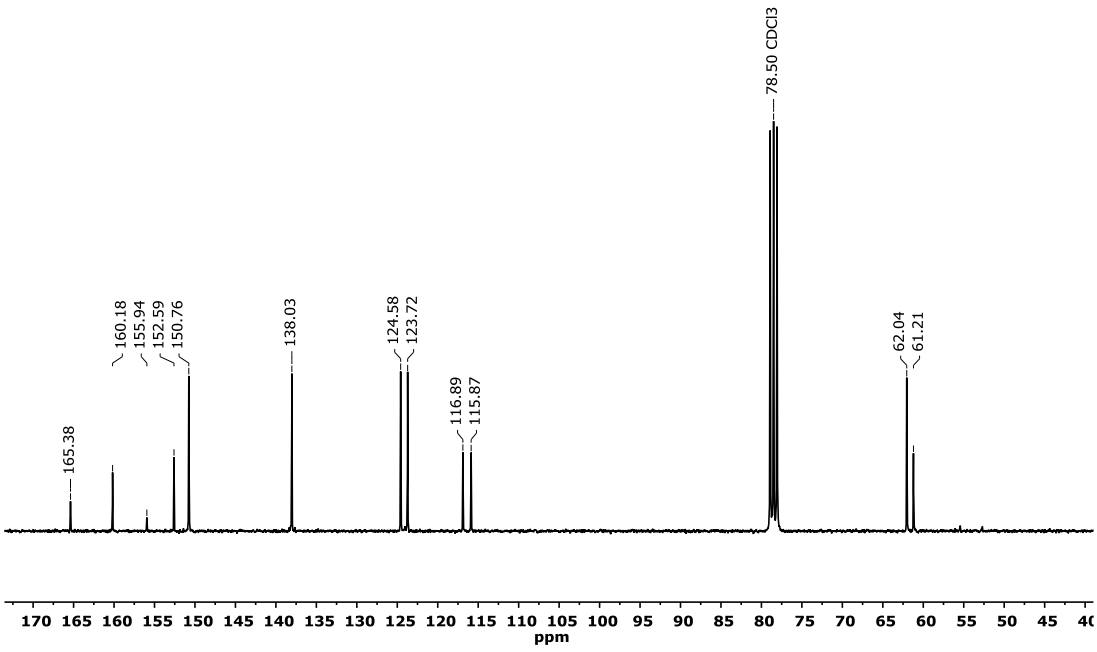

Figure S4: ^{13}C-NMR (75 MHz, $CDCl_3$) of **NO_2-TPMA 29**

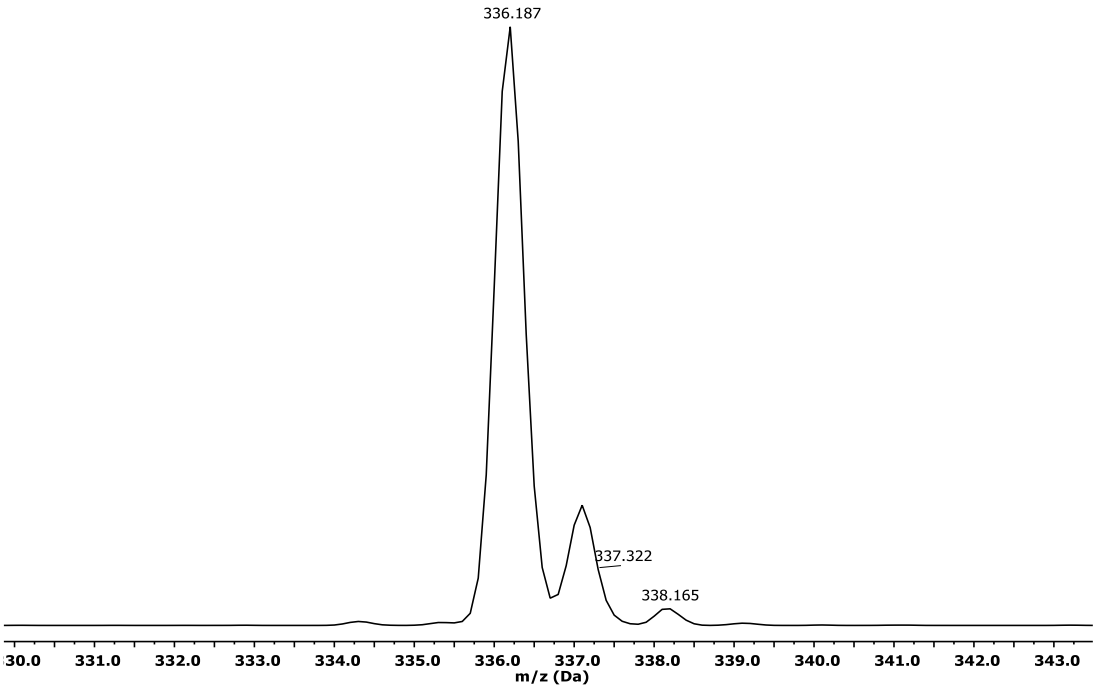

Figure S5: Experimental ESI-MS (ACN/H^+) of **NO_2-TPMA 29**

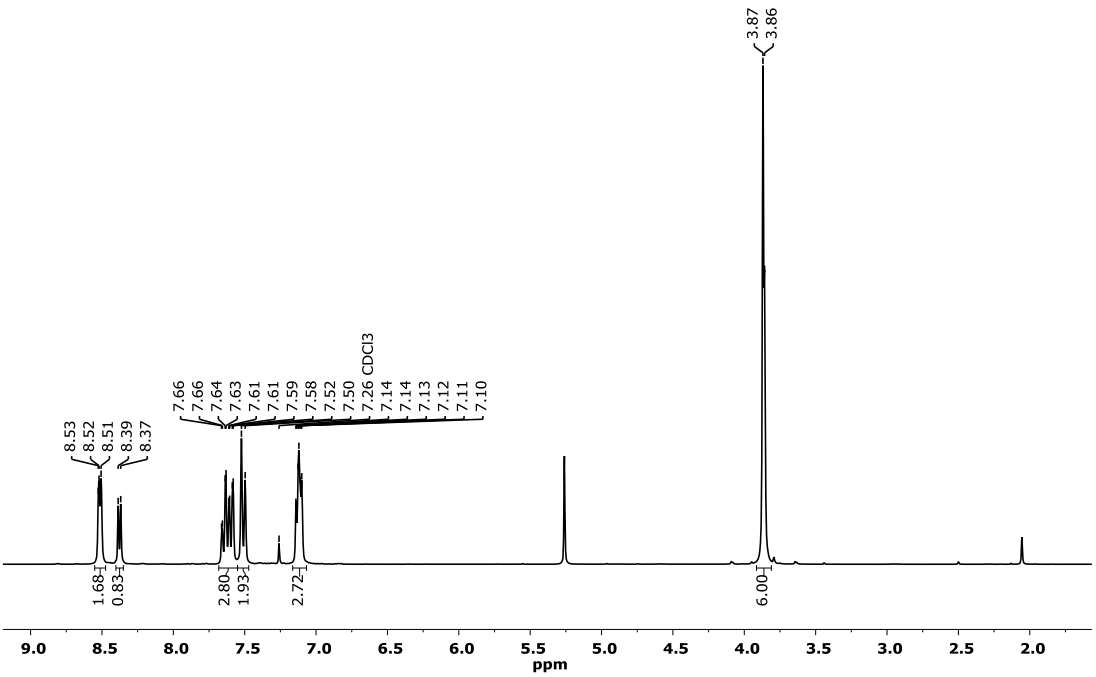

Figure S6: ^{1}H-NMR (400 MHz, $CDCl_3$) of **Cl-TPMA 32**

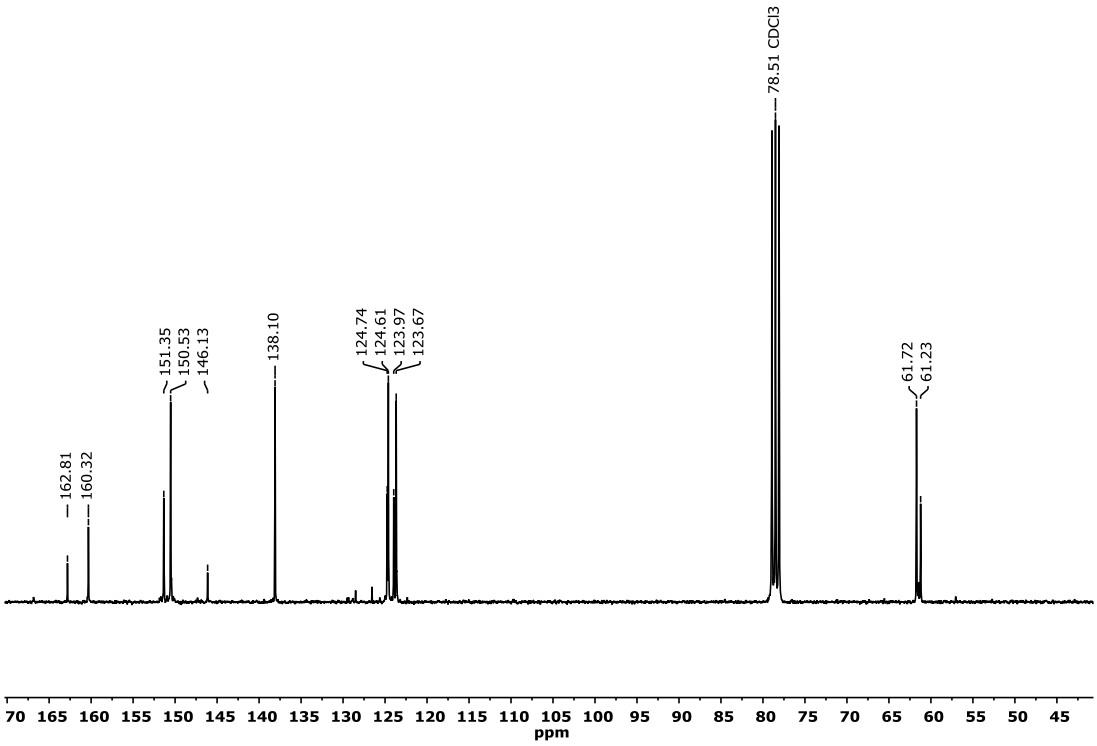

Figure S7: ^{13}C-NMR (75 MHz, $CDCl_3$) of **Cl-TPMA 32**

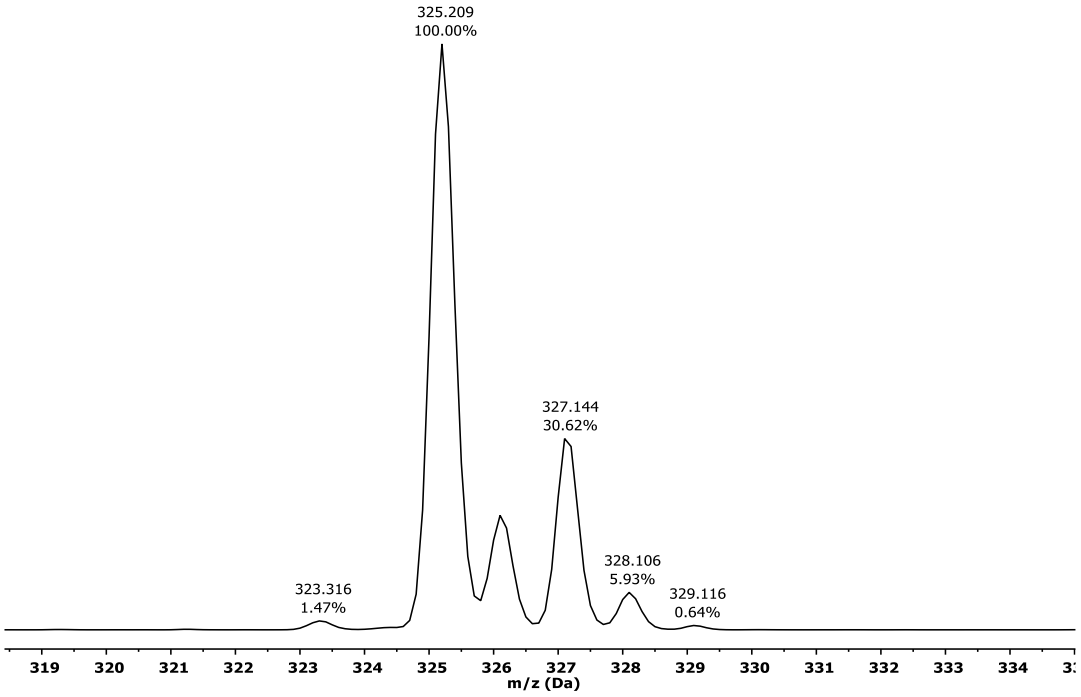

Figure S8: Experimental ESI-MS (ACN/H^+) of **Cl-TPMA 32**

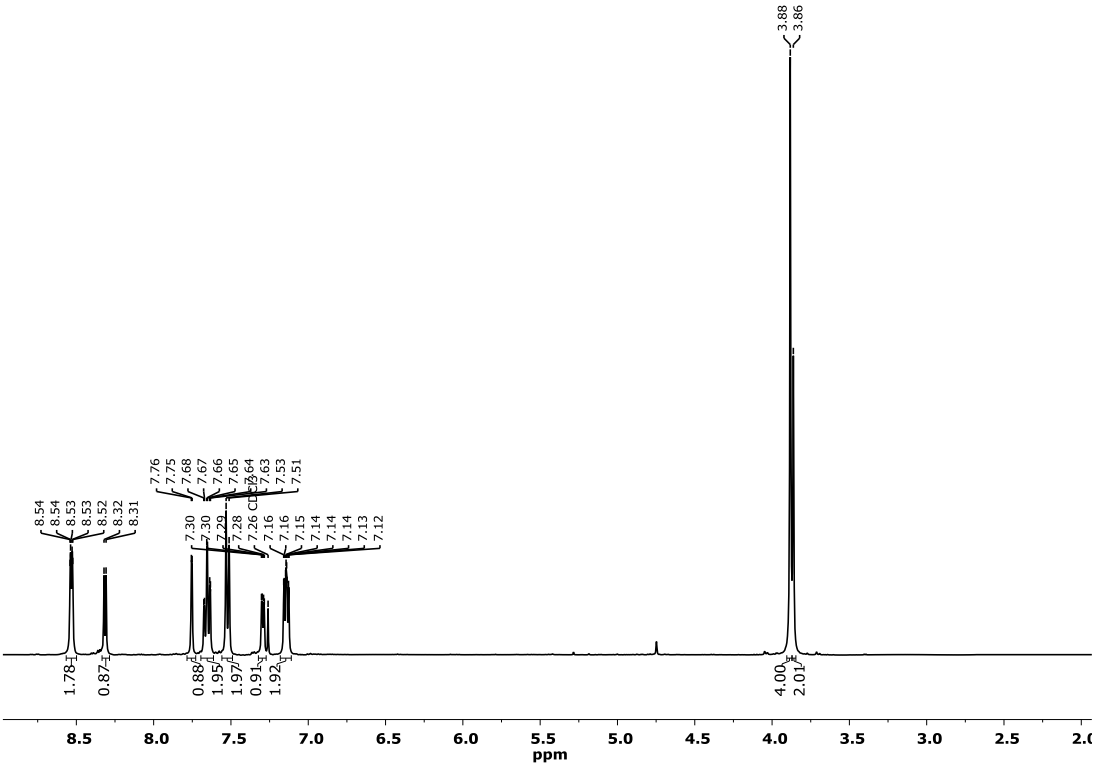

Figure S9: ^{1}H-NMR (400 MHz, $CDCl_3$) of **Br-TPMA 35**

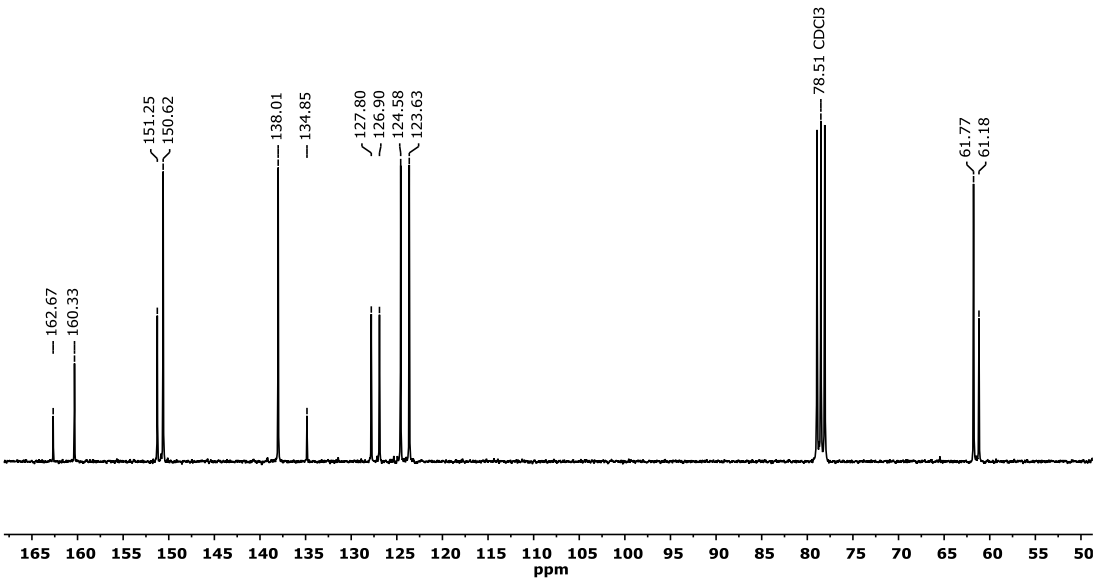

Figure S10: ^{13}C-NMR (75 MHz, $CDCl_3$) of **Br-TPMA 35**

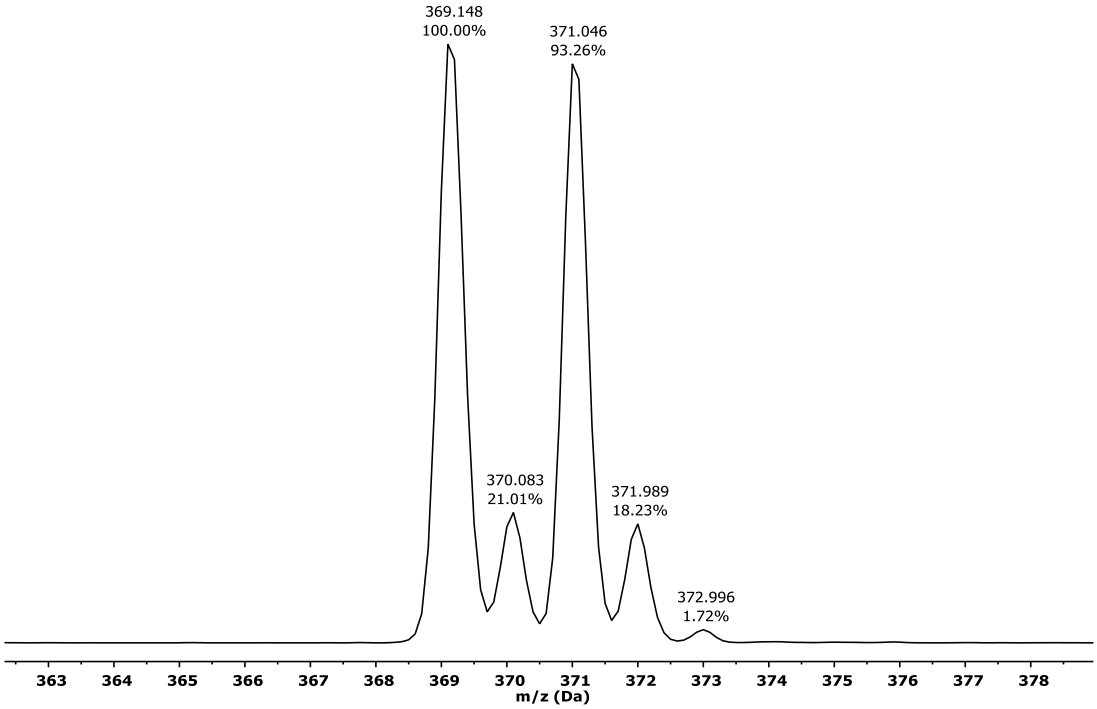

Figure S11: Experimental ESI-MS (ACN/H^+) of **Br-TPMA 35**

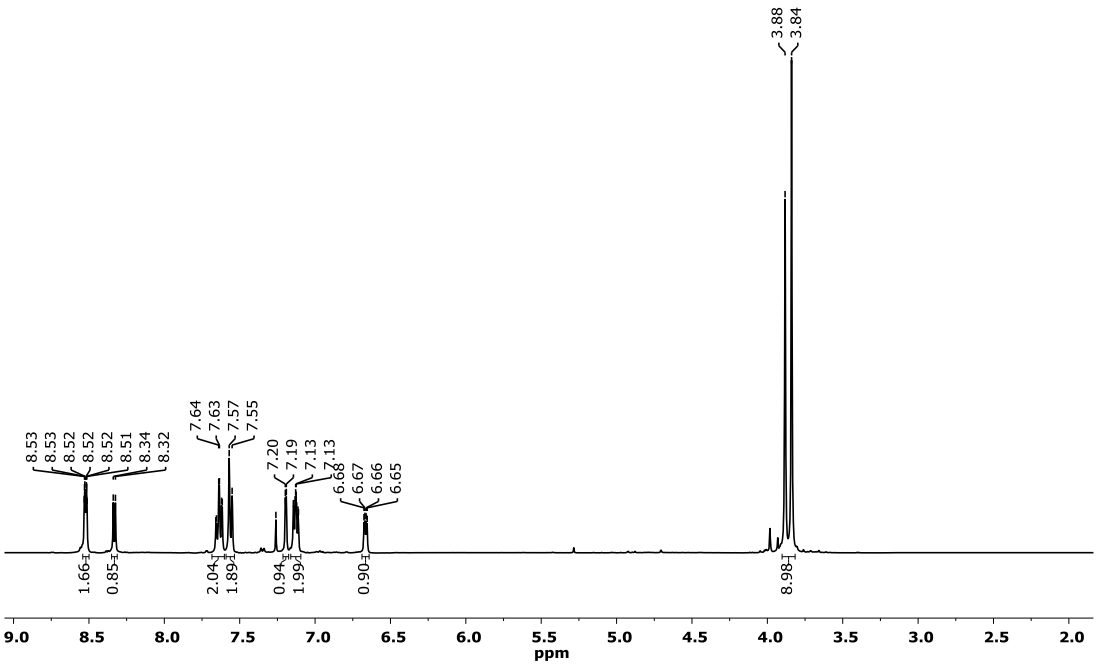

Figure S12: ^{1}H-NMR (400 MHz, $CDCl_3$) of **OCH_3-TPMA 38**

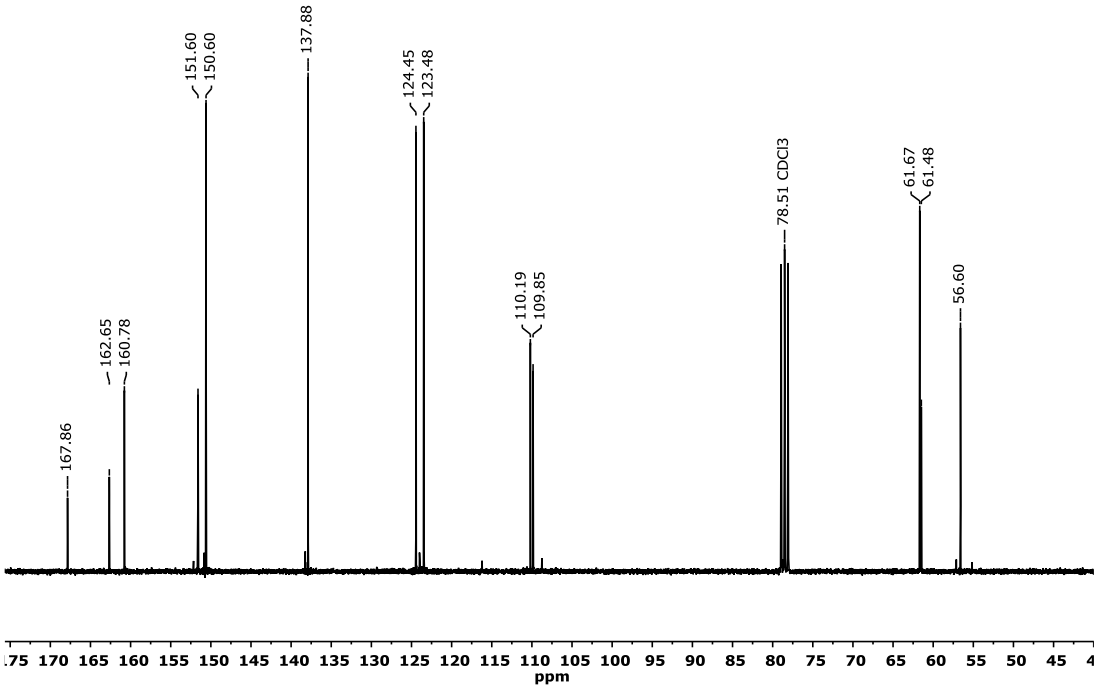

Figure S13: ^{13}C-NMR (75 MHz, $CDCl_3$) of **OCH_3-TPMA 38**

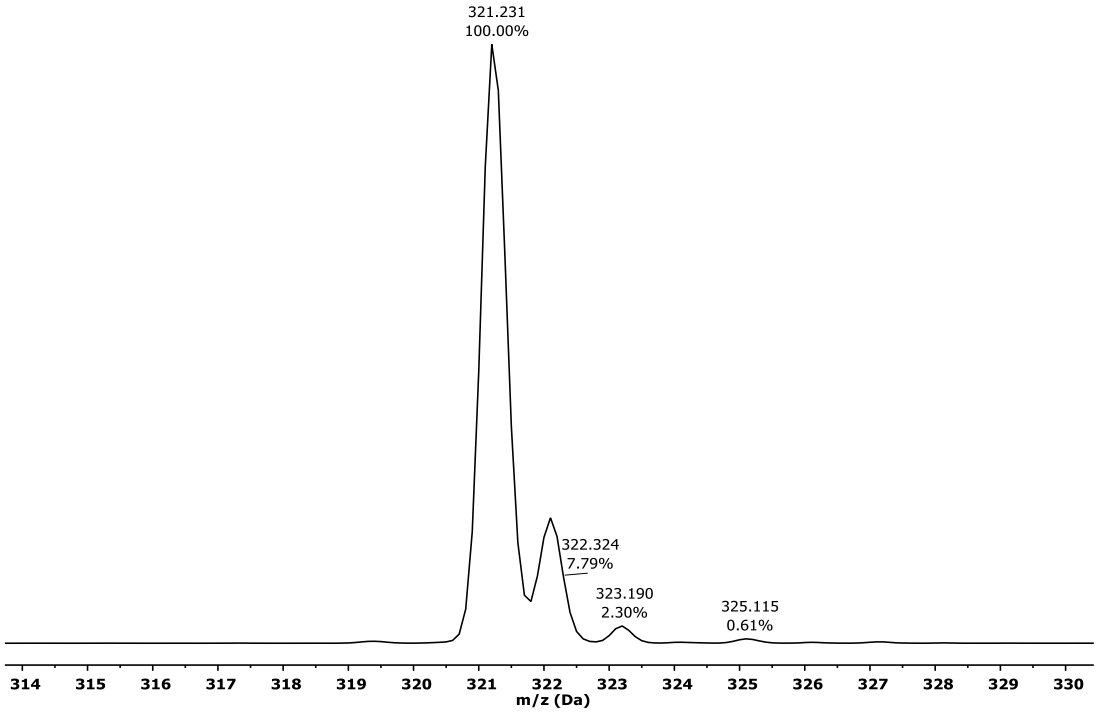

Figure S14: Experimental ESI-MS (ACN/H^+) of **OCH_3-TPMA 38**

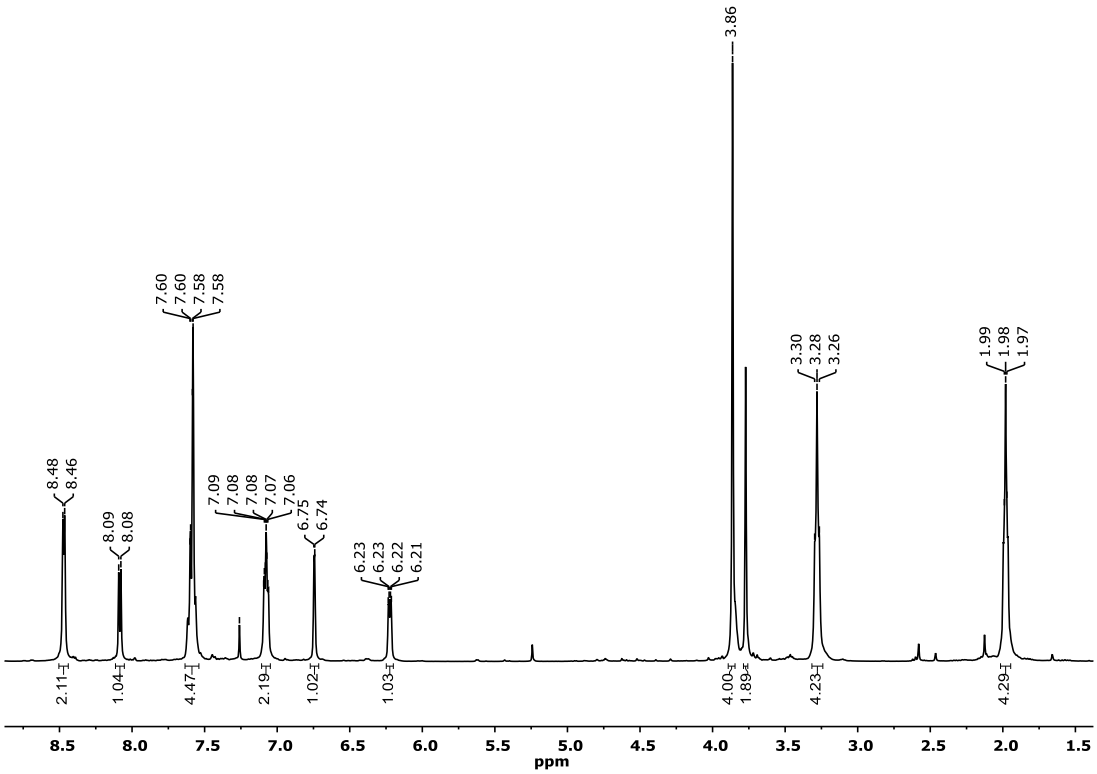

Figure S15: ^{1}H-NMR (400 MHz, $CDCl_3$) of **Pyrr-TPMA 41**

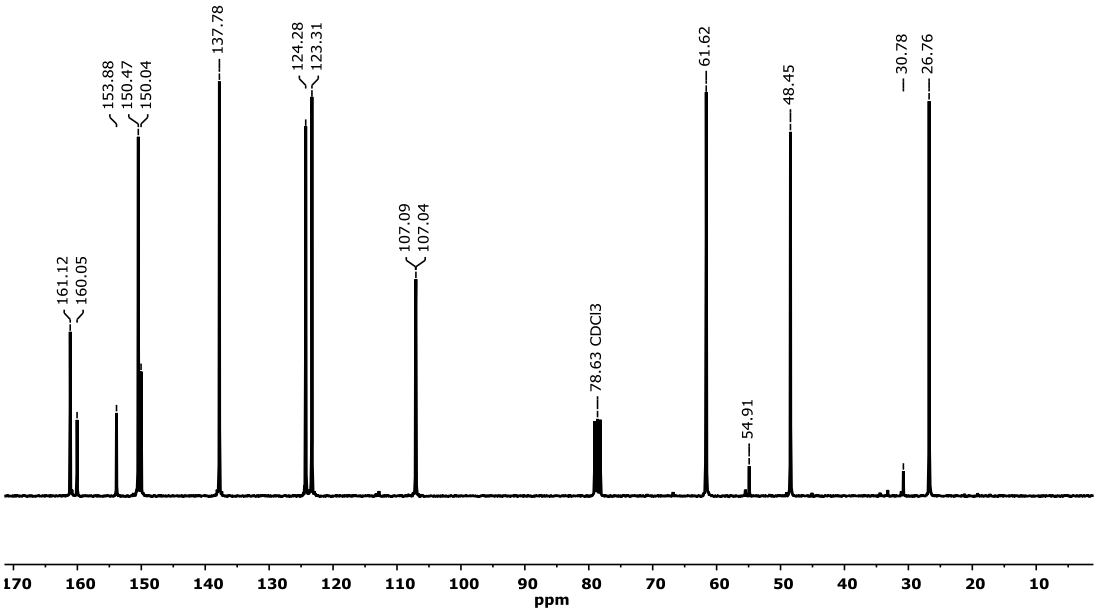

Figure S16: ^{13}C-NMR (75 MHz, $CDCl_3$) of **Pyrr-TPMA 41**

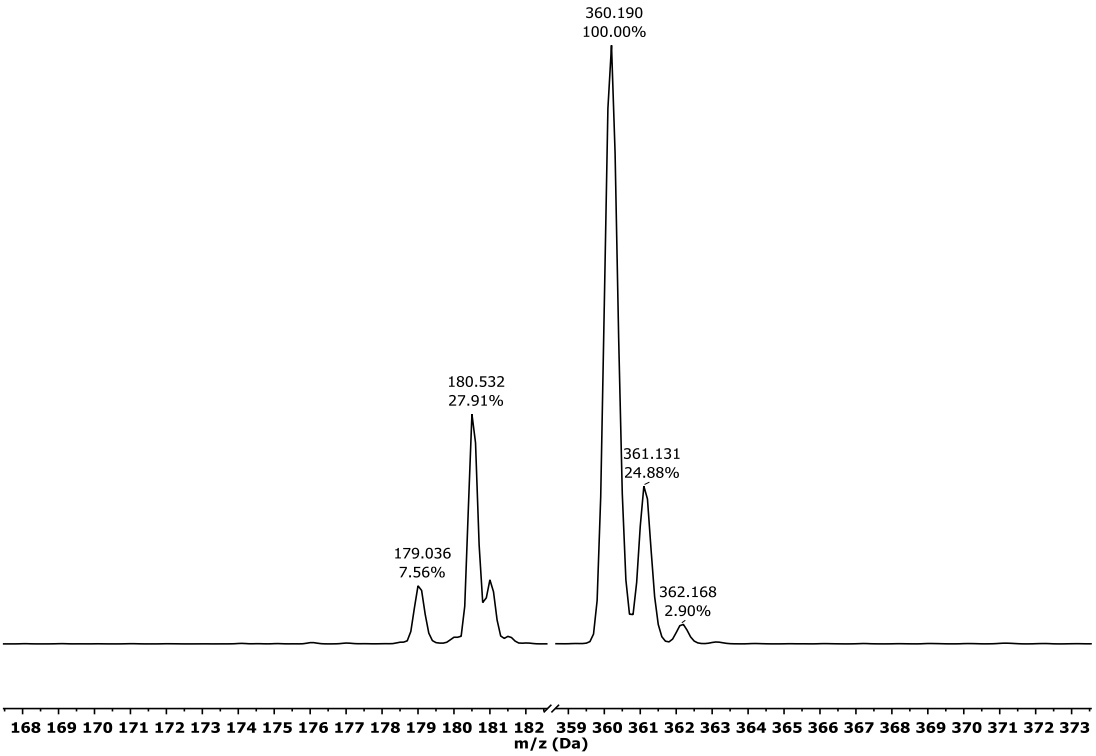

Figure S17: Experimental ESI-MS (ACN/H^+) of **Pyrr-TPMA 41**

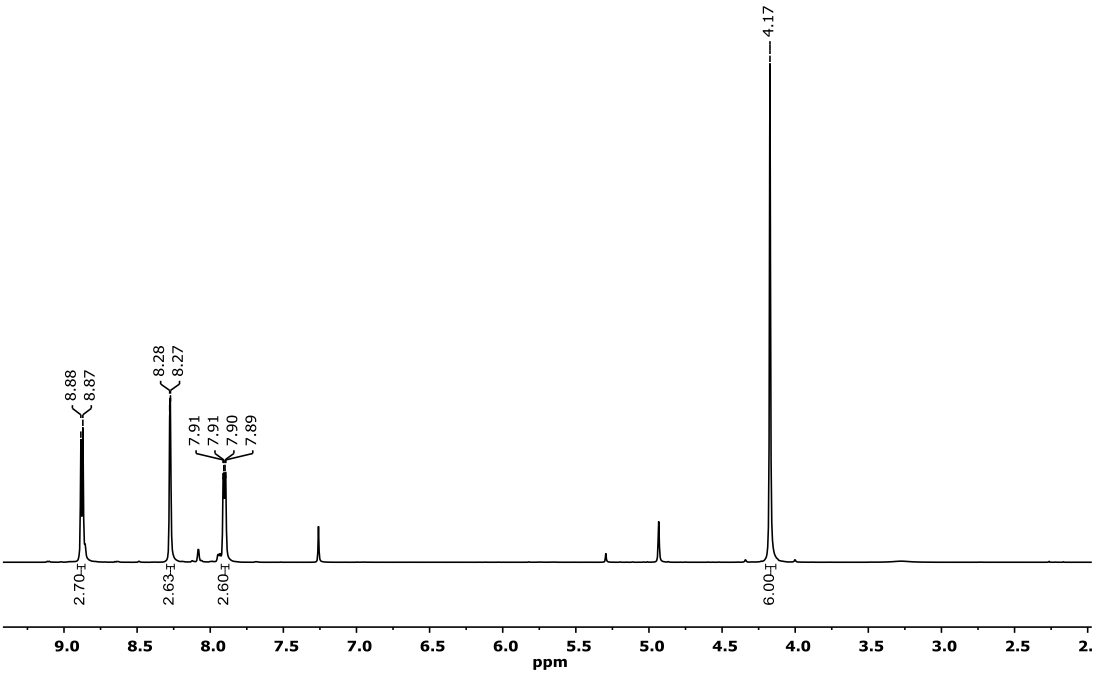

Figure S18: ^{1}H-NMR (400 MHz, $CDCl_3$) of **$(NO_2)_3$-TPMA 31**

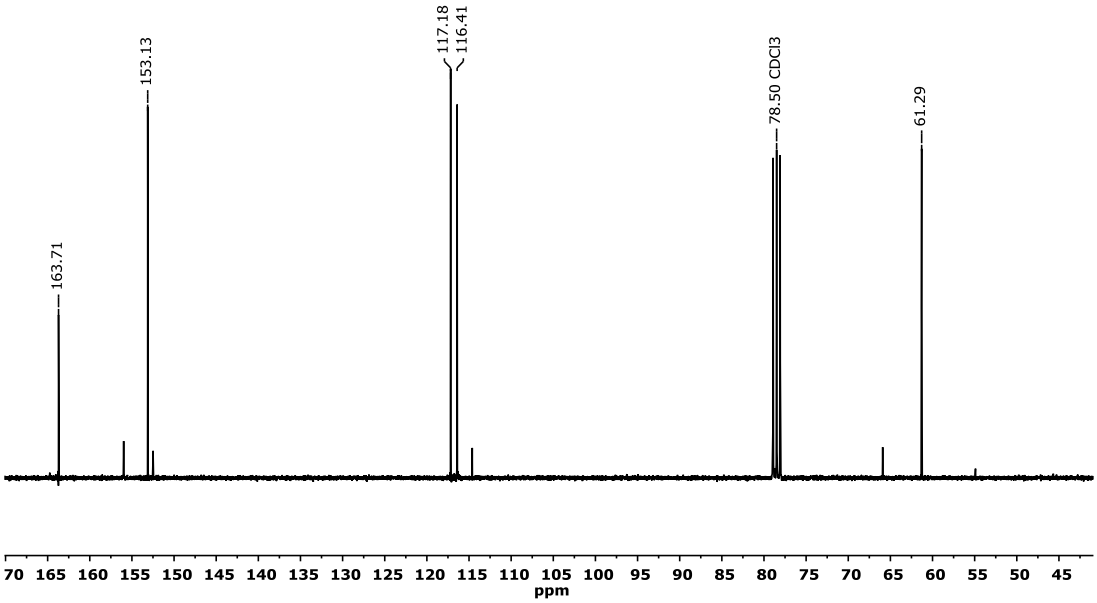

Figure S19: ^{13}C-NMR (75 MHz, $CDCl_3$) of **$(NO_2)_3$-TPMA 31**

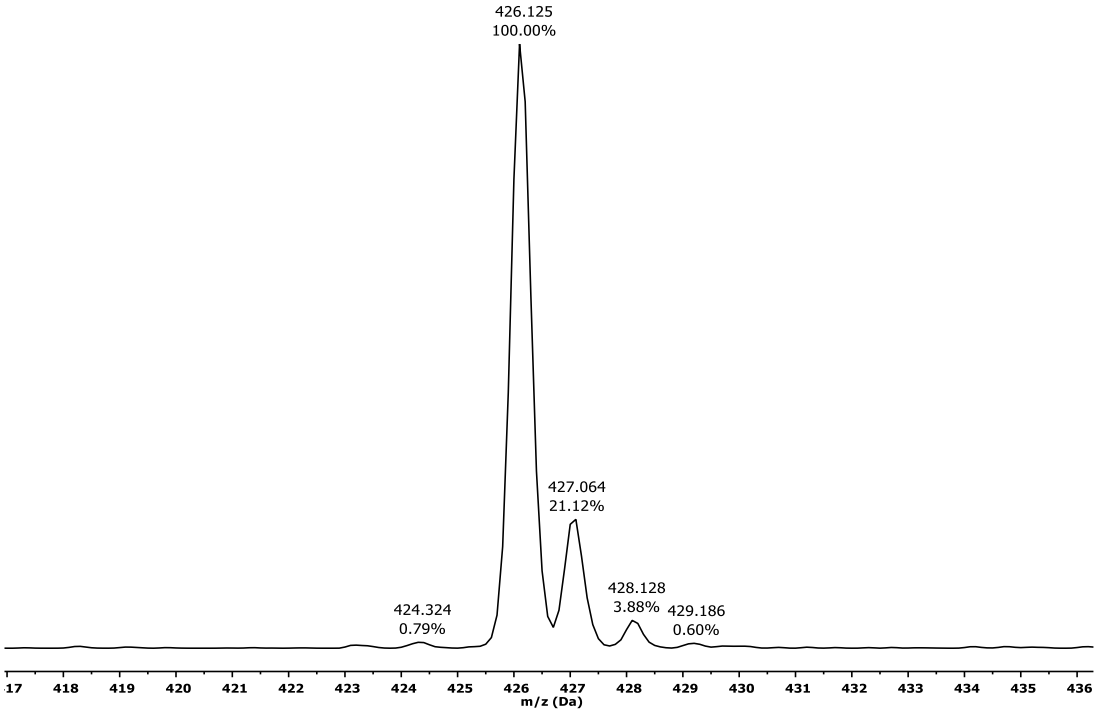

Figure S20: Experimental ESI-MS (ACN/H^+) of **$(NO_2)_3$-TPMA 31**

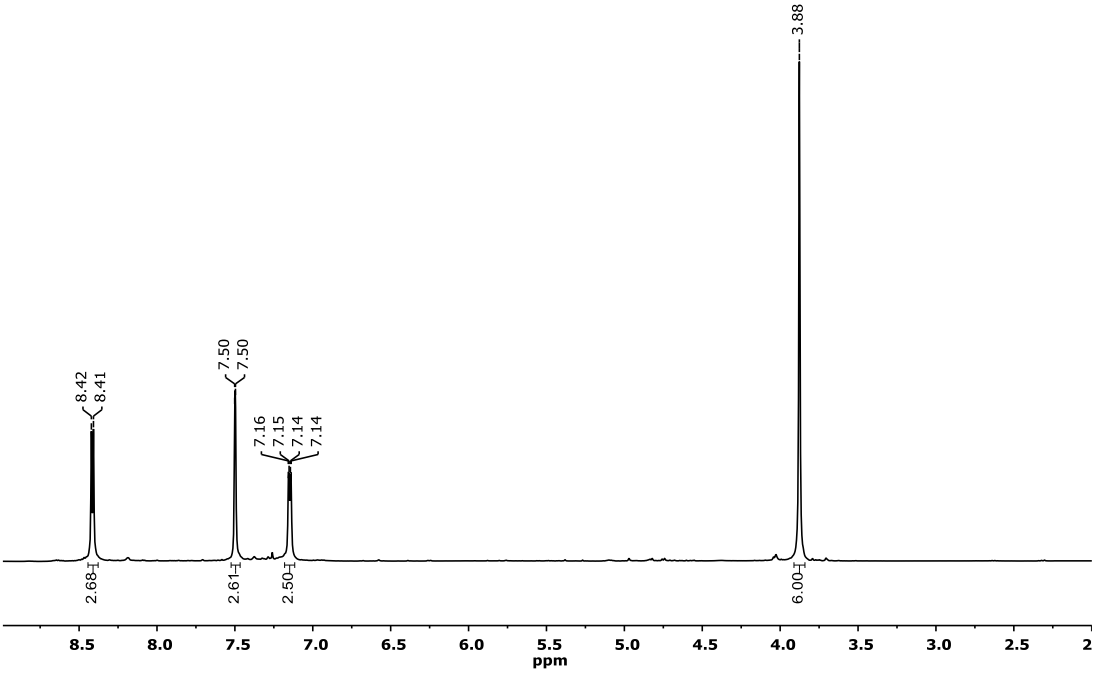

Figure S21: ^{1}H-NMR (400 MHz, $CDCl_3$) of **Cl_3-TPMA 34**

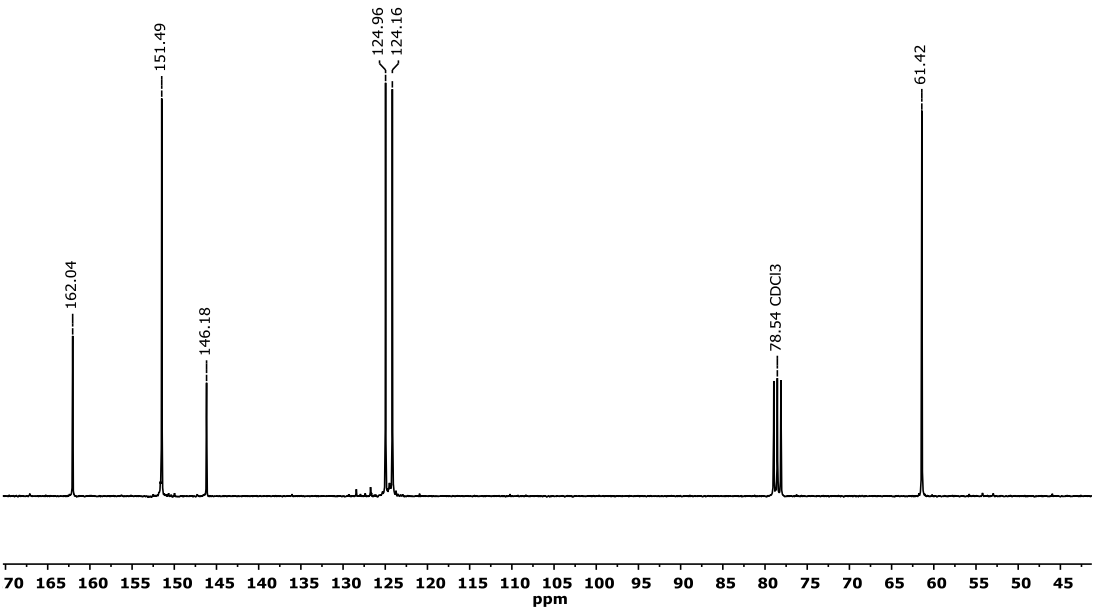

Figure S22: ^{13}C-NMR (75 MHz, $CDCl_3$) of **Cl_3-TPMA 34**

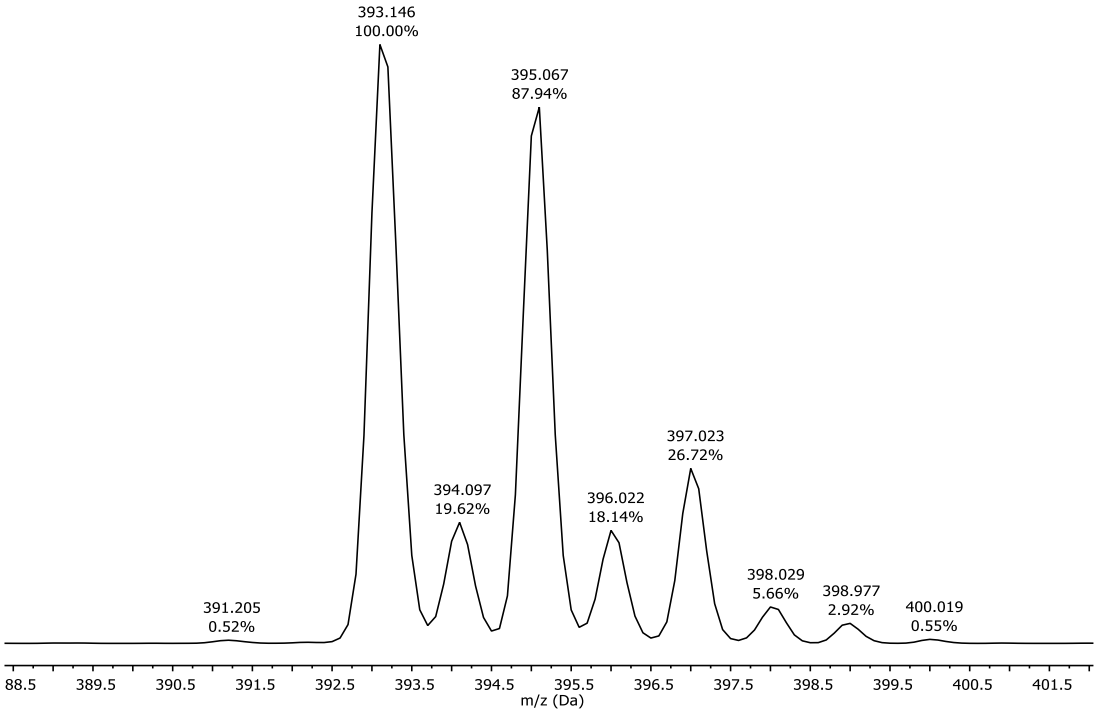

Figure S23: Experimental ESI-MS (ACN/H^+) of **Cl_3-TPMA 34**

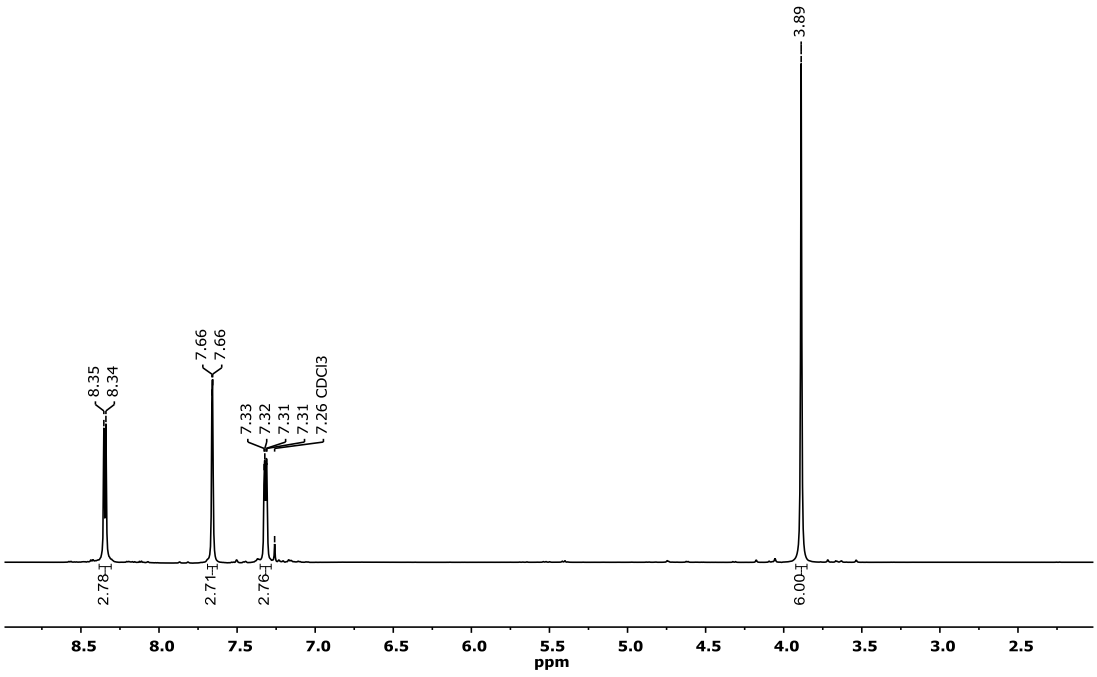

Figure S24: ^{1}H-NMR (400 MHz, $CDCl_3$) of **Br_3-TPMA 37**

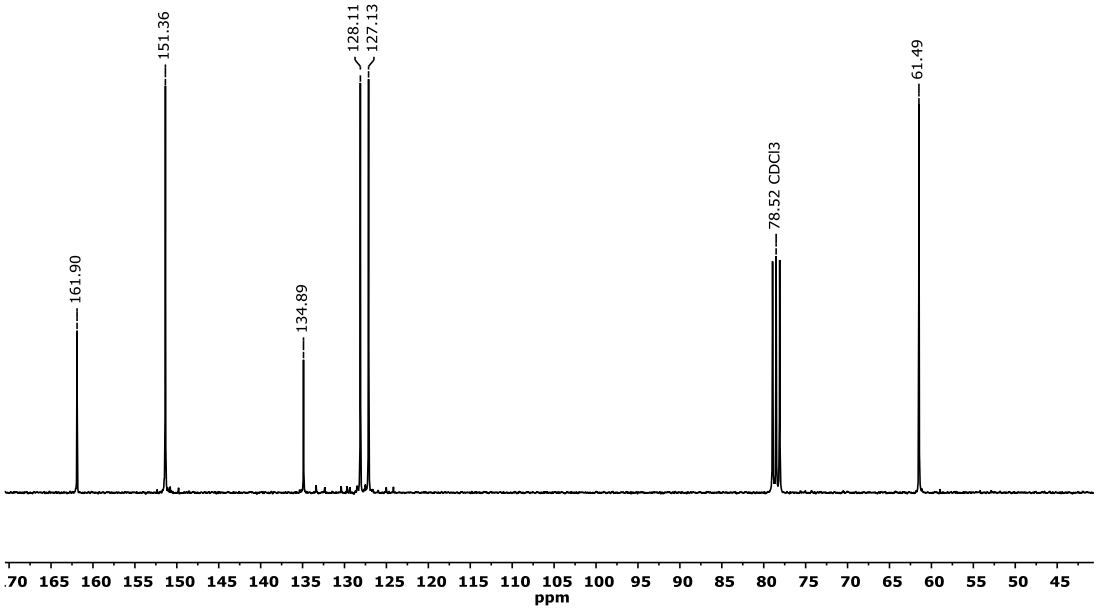

Figure S25: ^{13}C-NMR (75 MHz, $CDCl_3$) of **Br_3-TPMA 37**

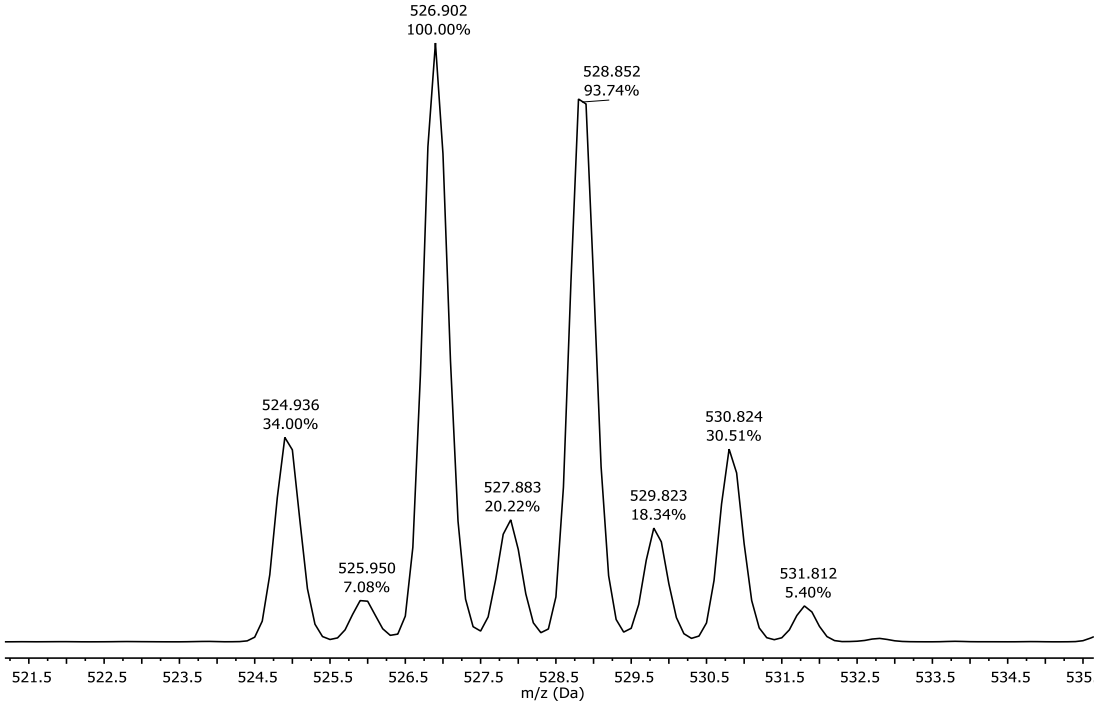

Figure S26: Experimental ESI-MS (ACN/H^+) of **Br_3-TPMA 37**

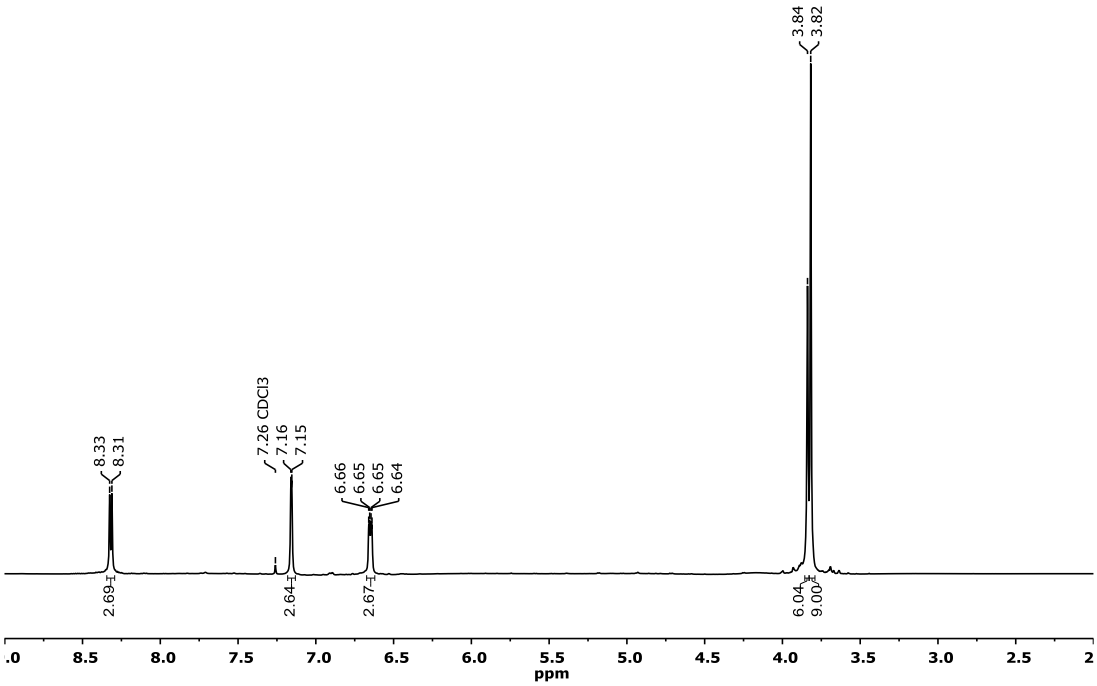

Figure S27: ^{1}H-NMR (400 MHz, $CDCl_3$) of **$(OMe)_3$-TPMA 40**

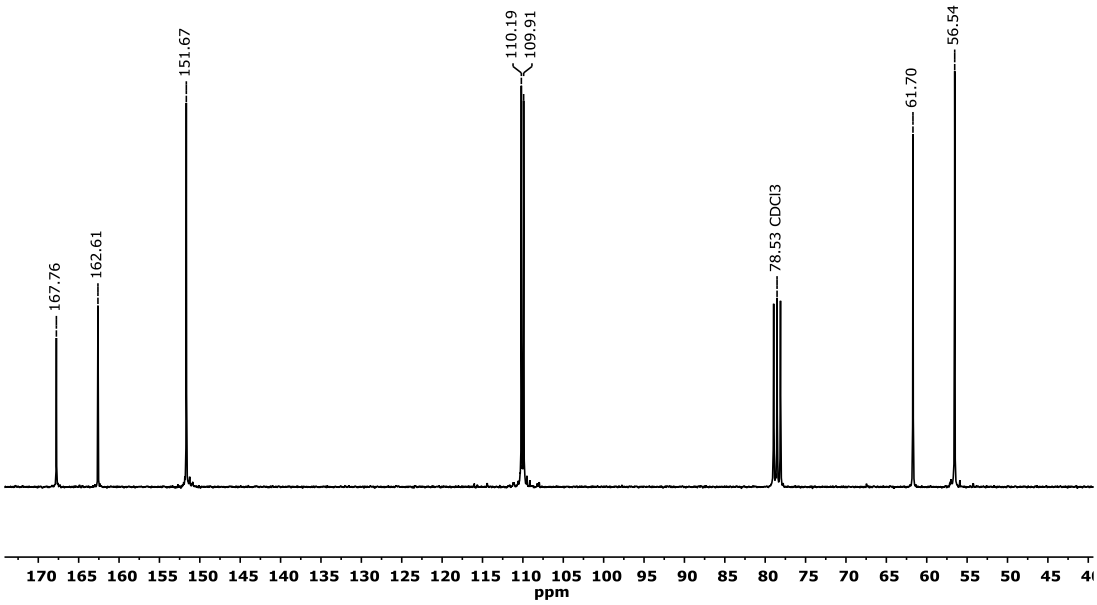

Figure S28: ^{13}C-NMR (75 MHz, $CDCl_3$) of **$(OMe)_3$-TPMA 40**

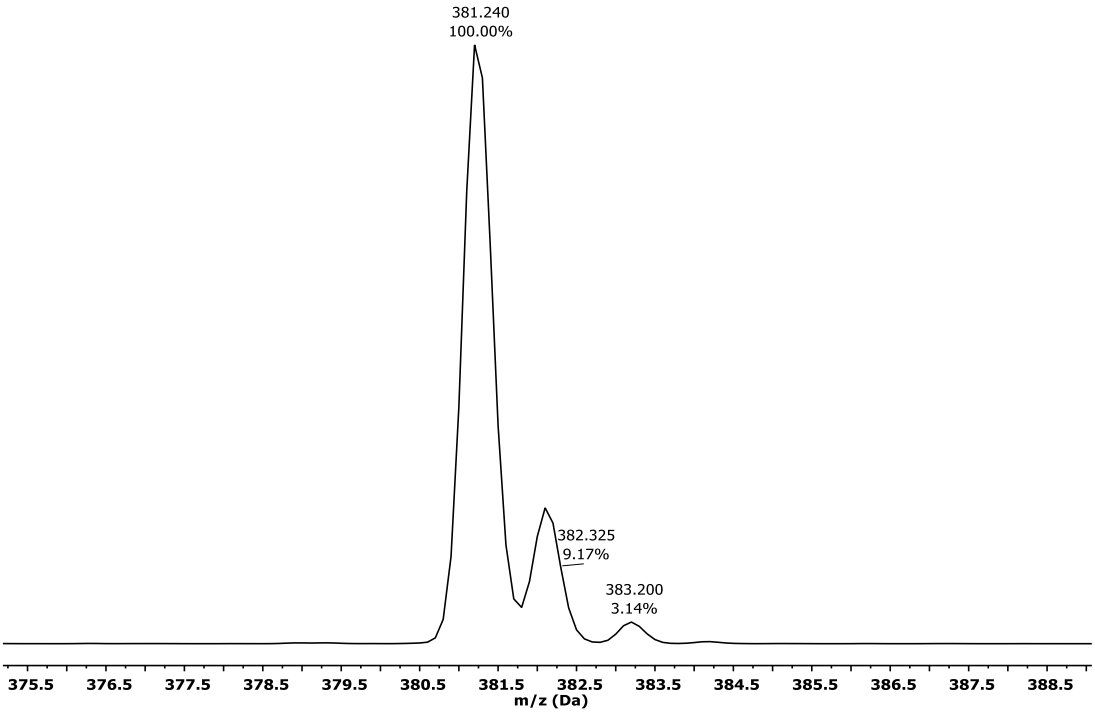

Figure S29: Experimental ESI-MS (ACN/H^+) of **$(OMe)_3$-TPMA 40**

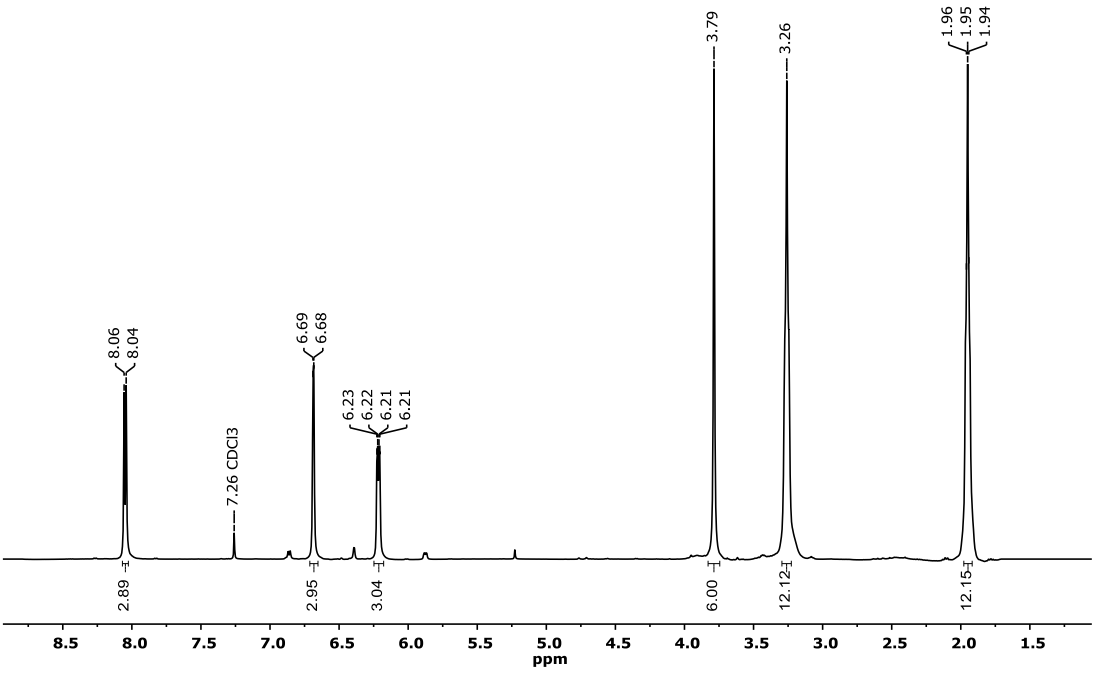

Figure S30: ^{1}H-NMR (400 MHz, $CDCl_3$) of **$Pyrr_3$-TPMA 40**

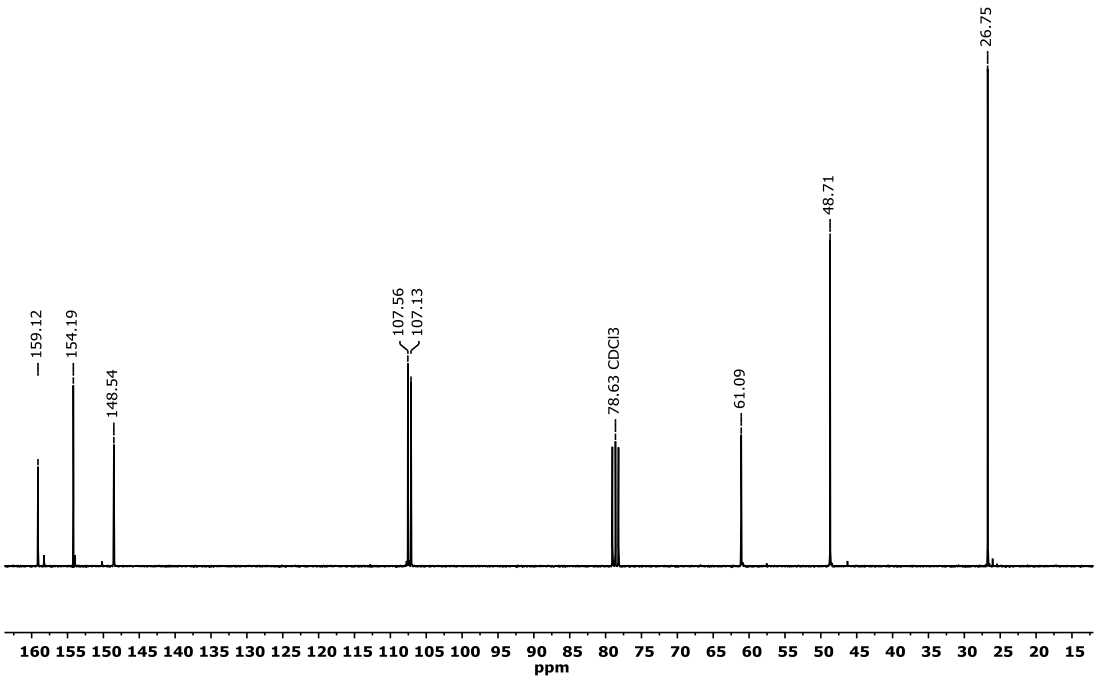

Figure S31: ^{13}C-NMR (75 MHz, $CDCl_3$) of **Pyrr$_3$-TPMA 40**

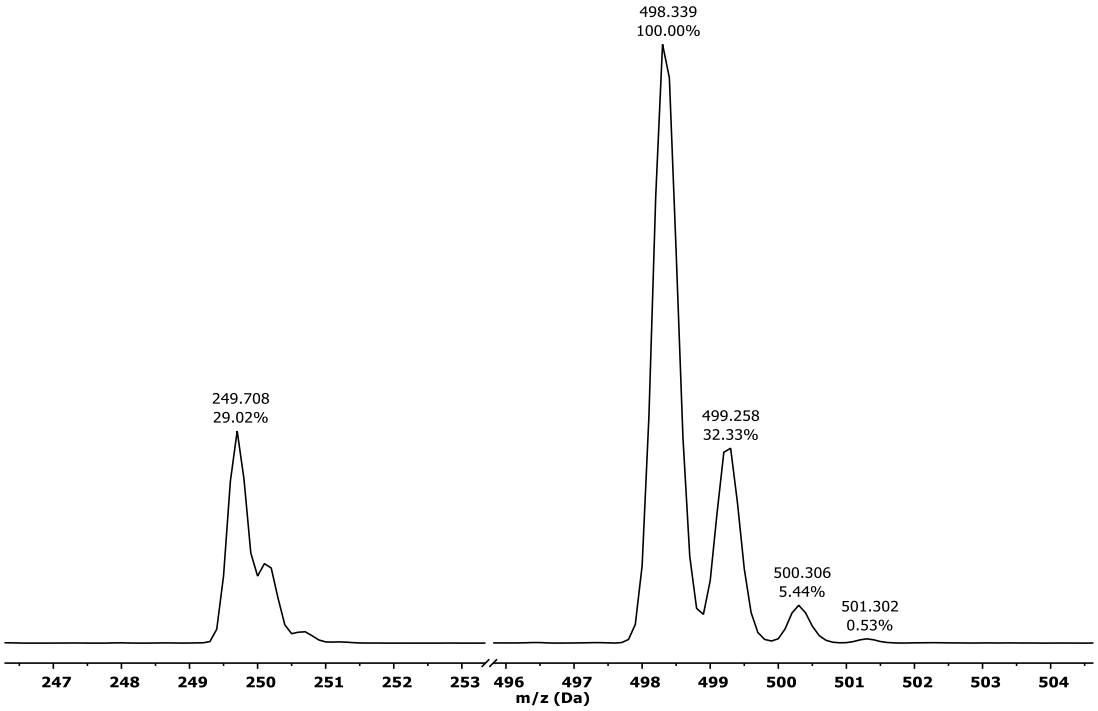

Figure S32: Experimental ESI-MS (ACN/H^+) of **Pyrr$_3$-TPMA 40**

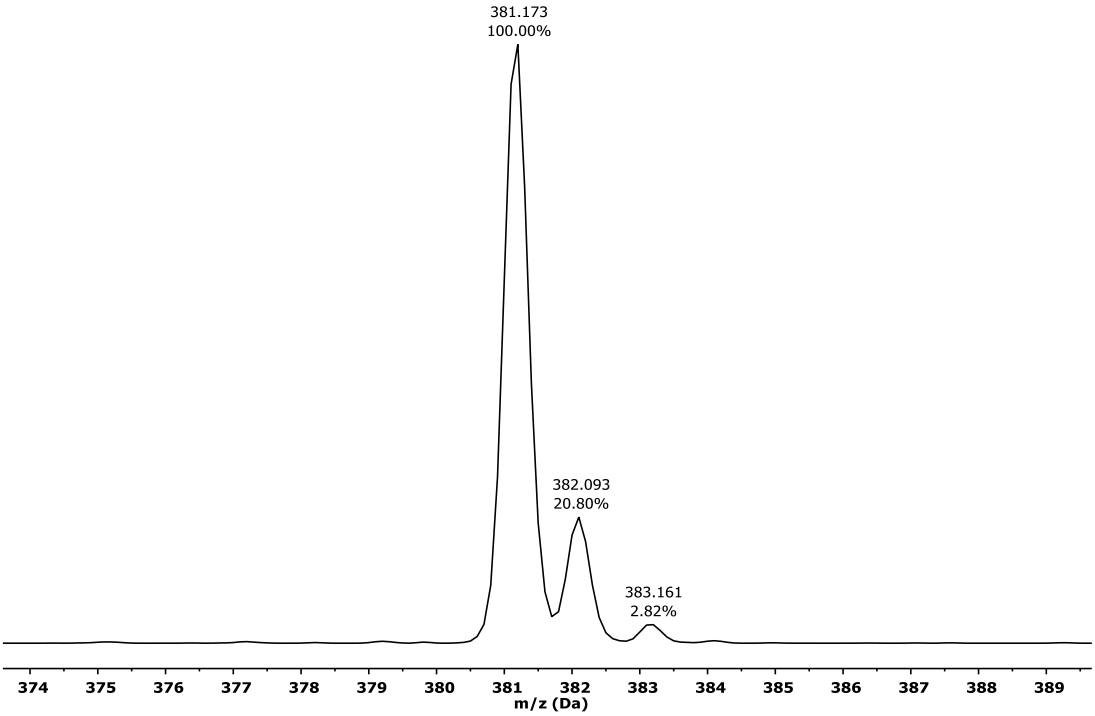

Figure S 33: Experimental ESI-MS (ACN/H^+) of **$(NO_2)_2$-TPMA 30**

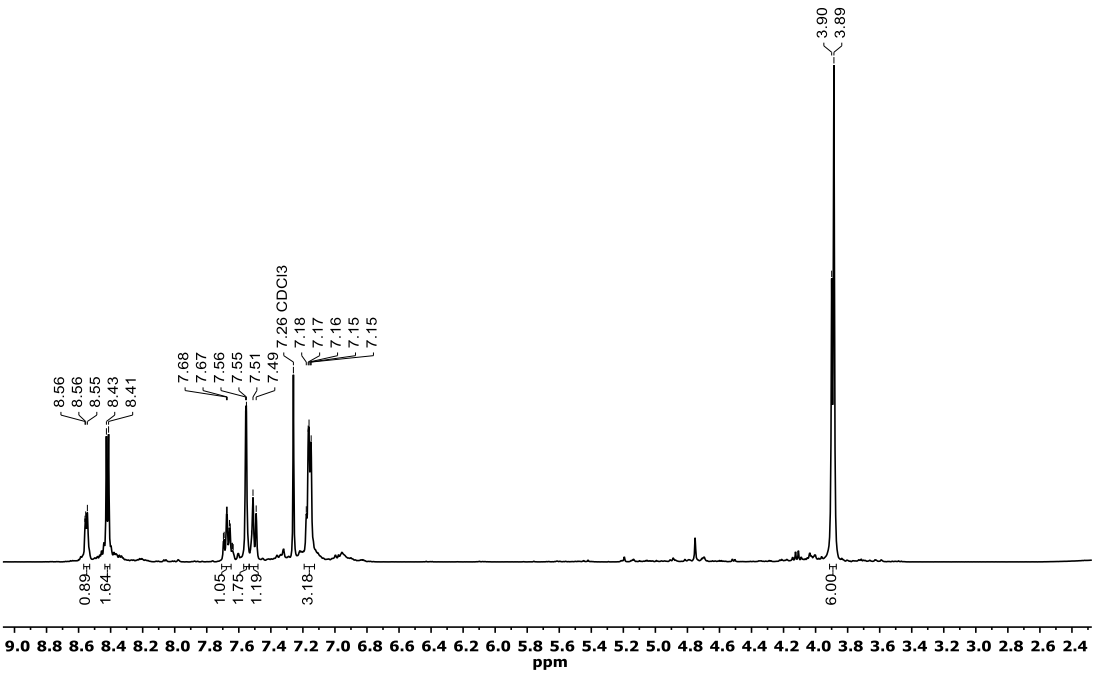

Figure S34: ^{1}H-NMR (400 MHz, $CDCl_3$) of **Cl_2-TPMA 33**

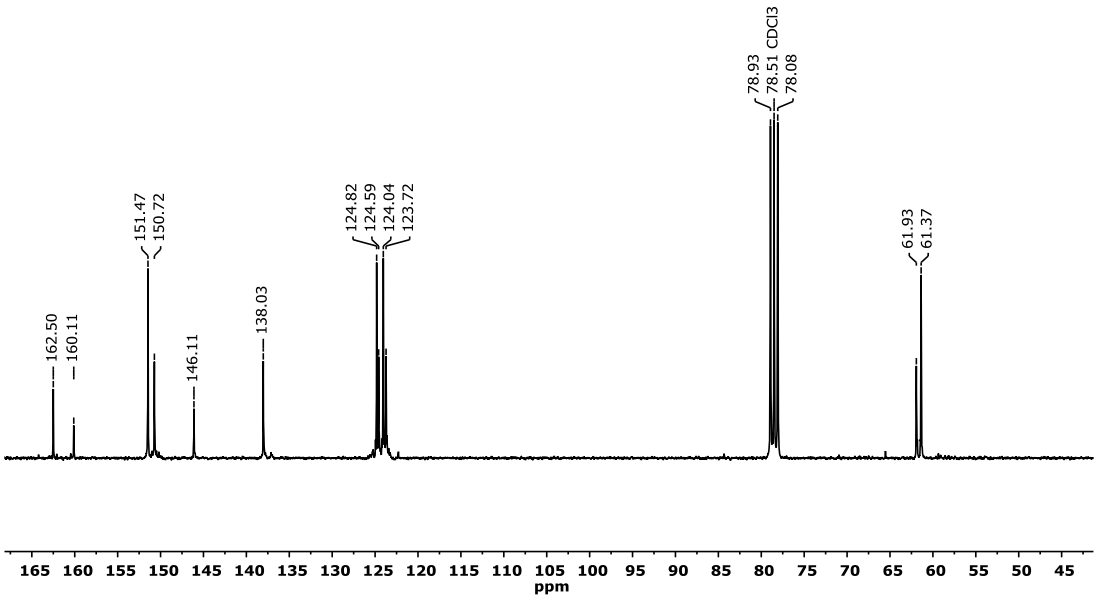

Figure S35: ^{13}C-NMR (75 MHz, $CDCl_3$) of **Cl_2-TPMA 33**

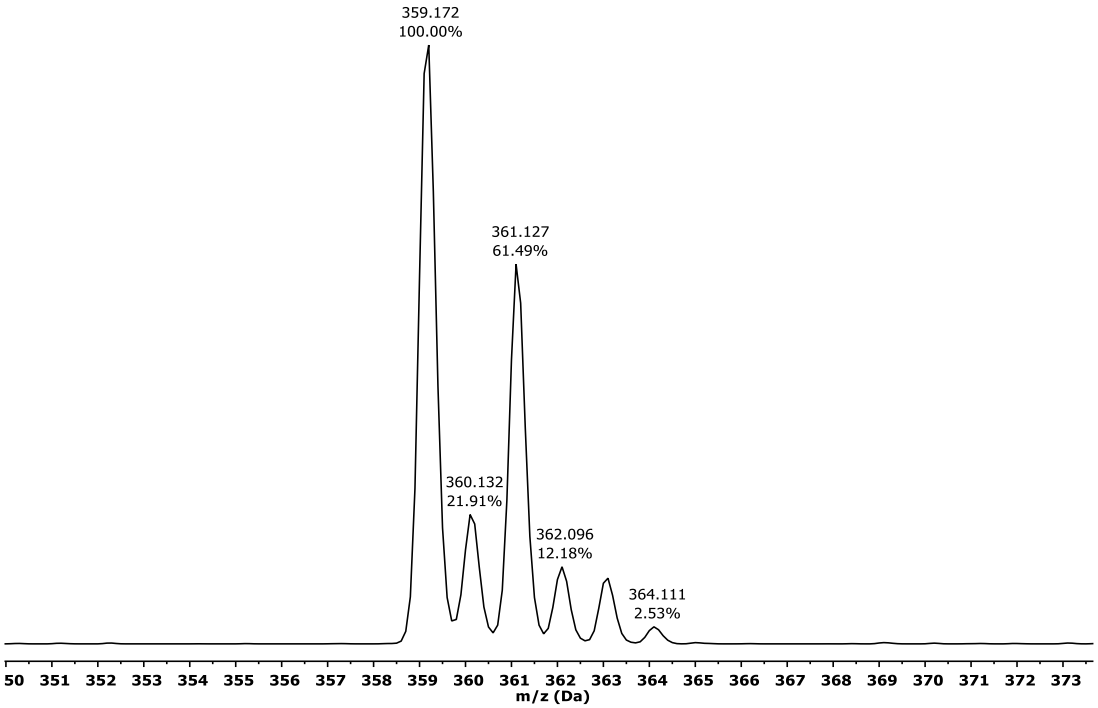

Figure S36: Experimental ESI-MS (ACN/H^+) of **Cl_2-TPMA 33**

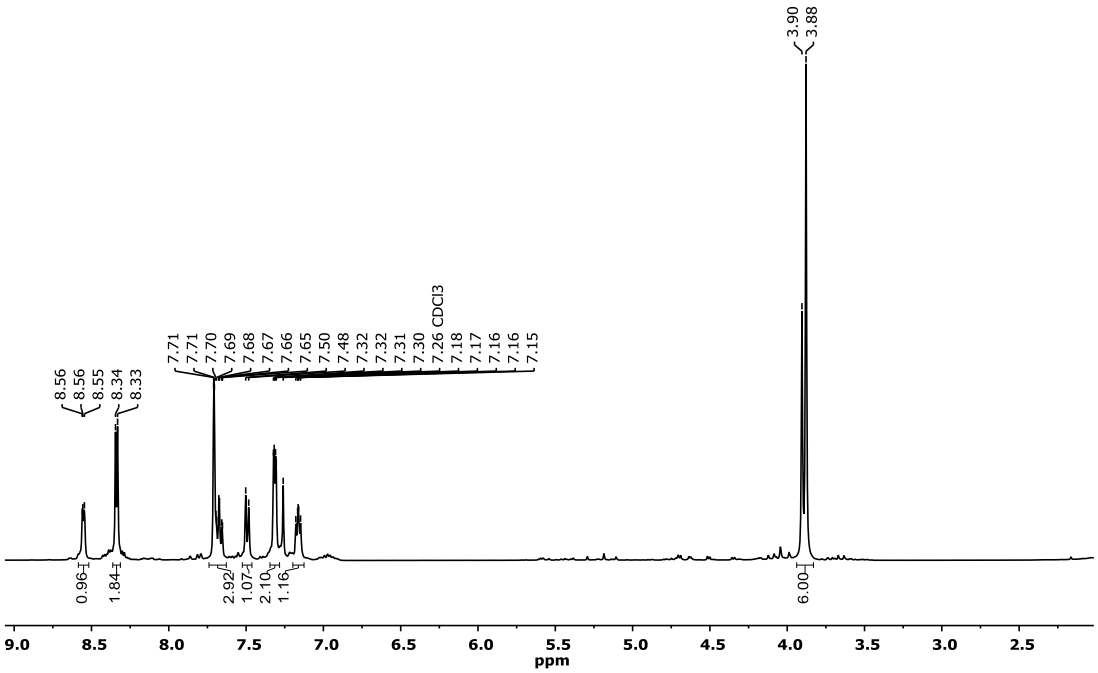

Figure S34: ^{1}H-NMR (400 MHz, $CDCl_3$) of **Br_2-TPMA 36**

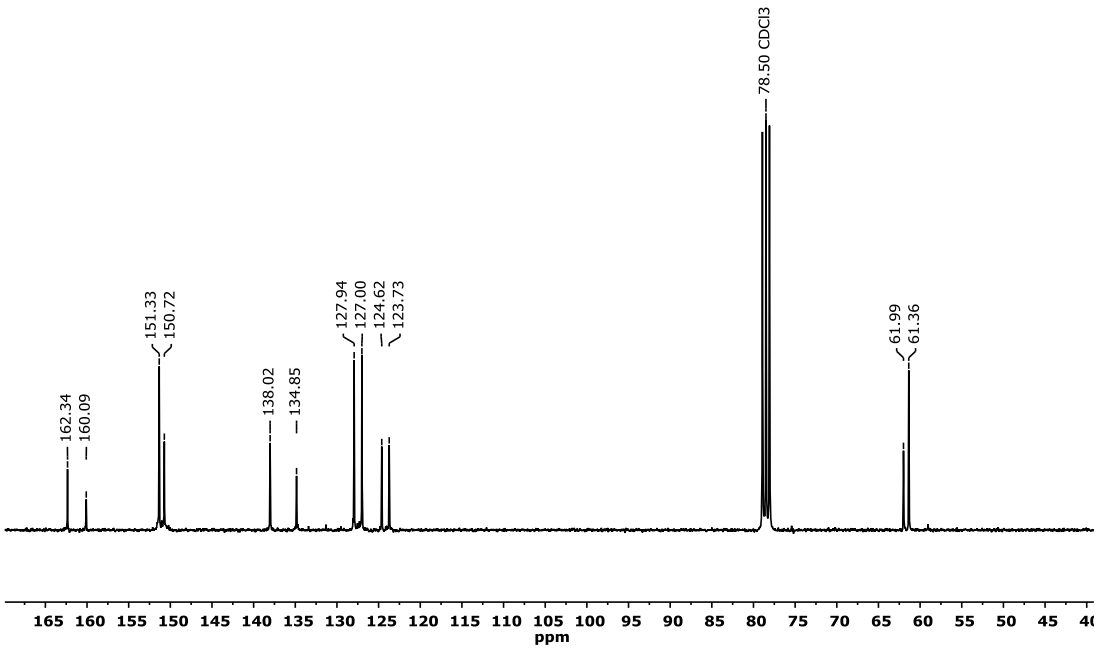

Figure S35: ^{13}C-NMR (75 MHz, $CDCl_3$) of **Br_2-TPMA 36**

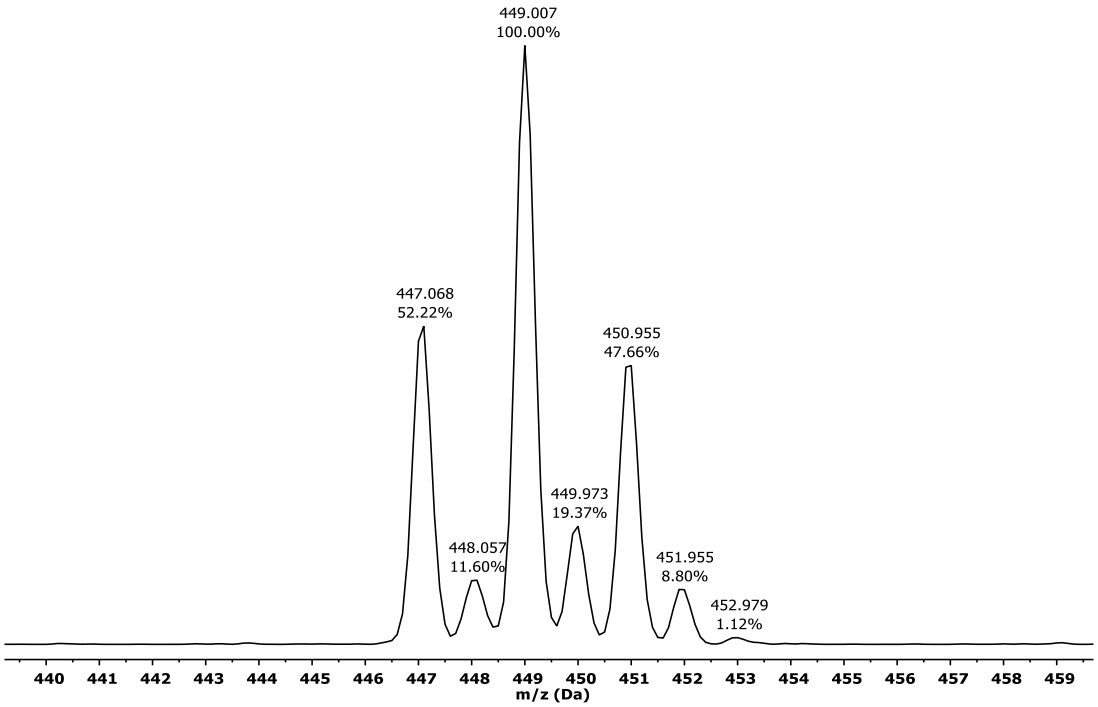

Figure S36: Experimental ESI-MS (ACN/H^+) of **Br_2-TPMA 36**

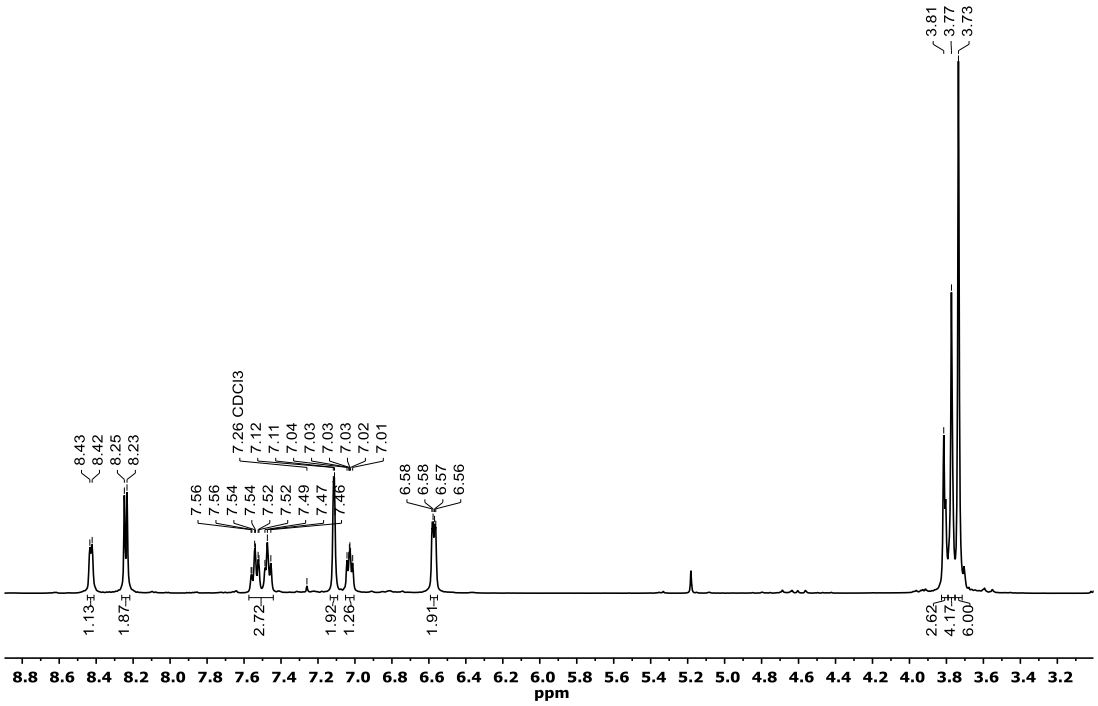

Figure S37: ^{1}H-NMR (400 MHz, $CDCl_3$) of **$(OCH_3)_2$-TPMA 39**

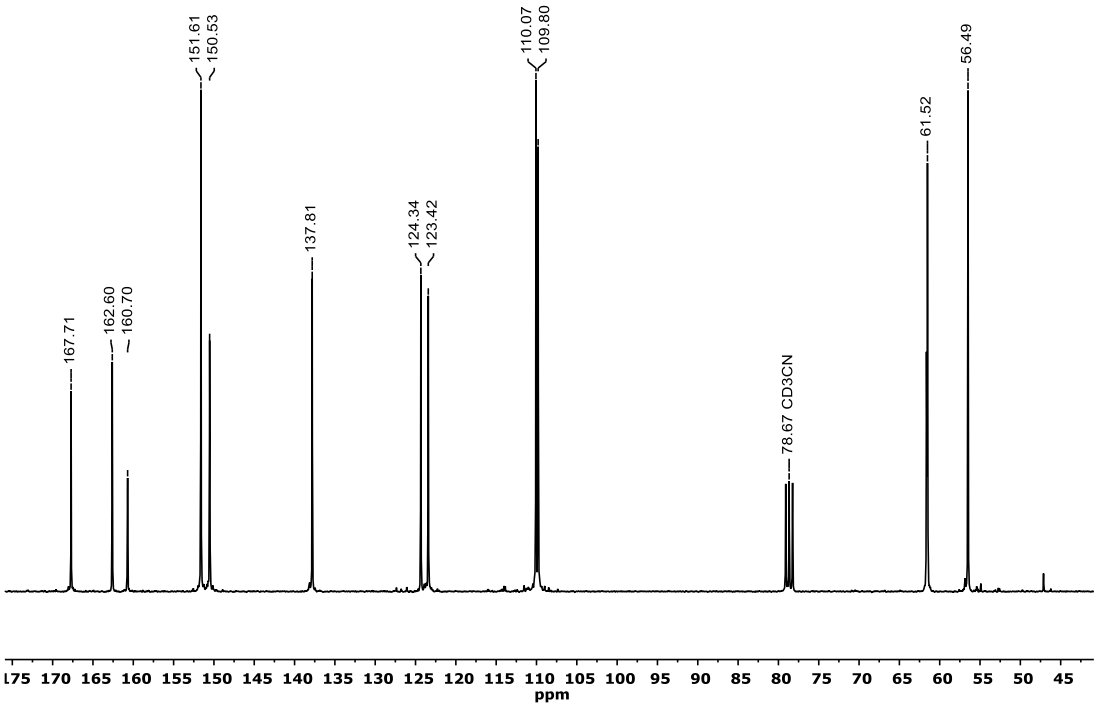

Figure S38: ^{13}C-NMR (75 MHz, $CDCl_3$) of **$(OCH_3)_2$-TPMA 39**

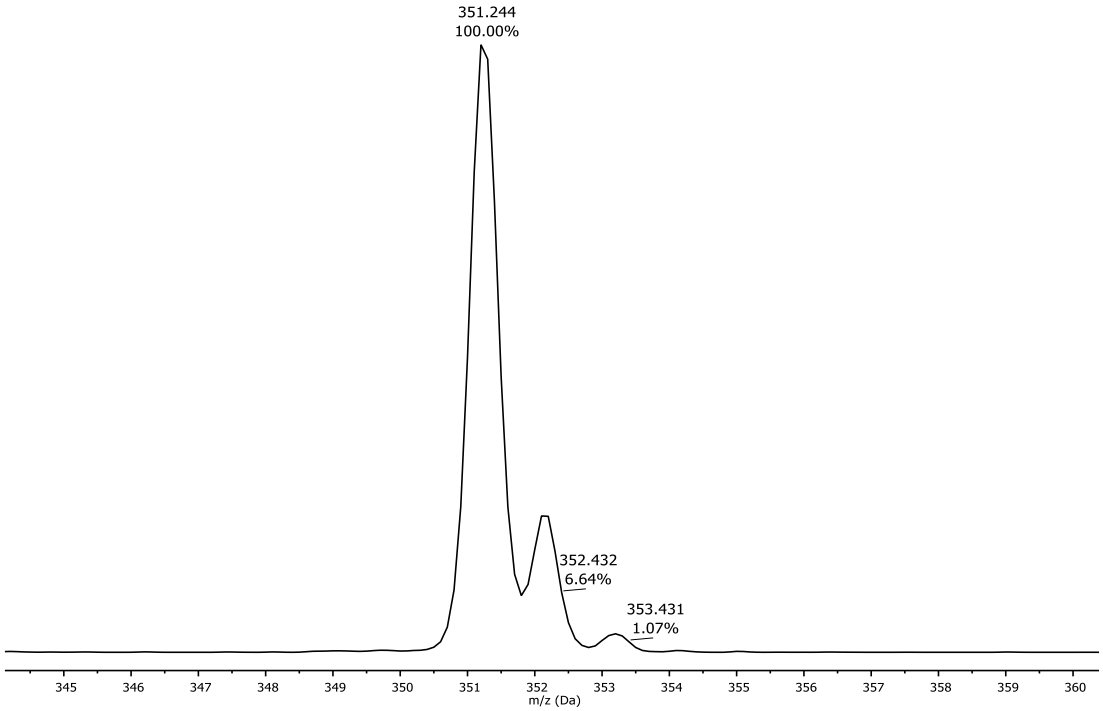

Figure S39: Experimental ESI-MS (ACN/H^+) of **$(OCH_3)_2$-TPMA 39**

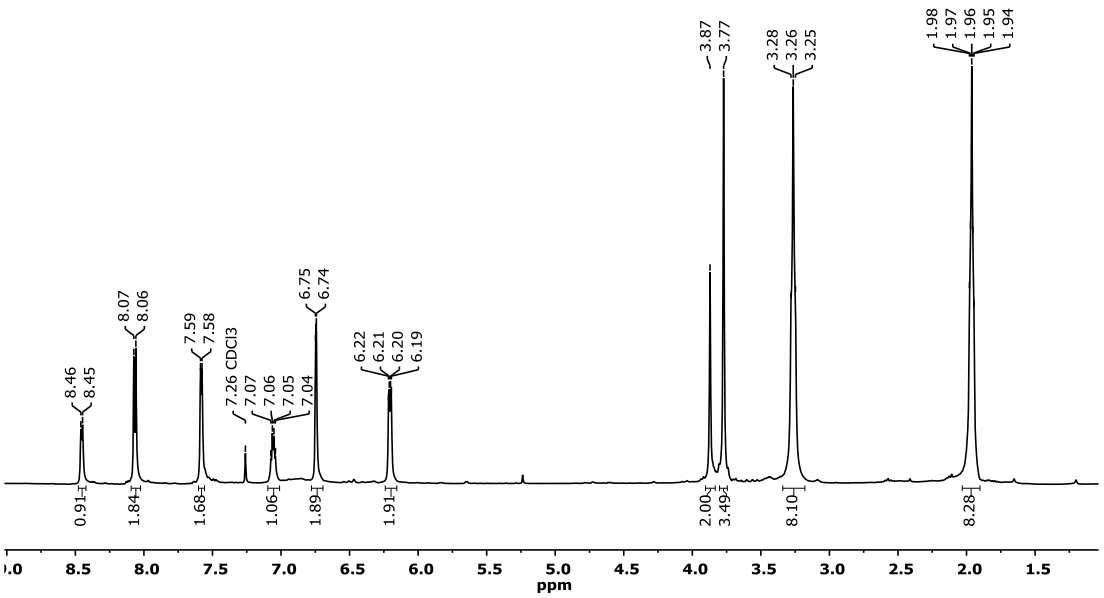

Figure S40: ^{1}H-NMR (400 MHz, $CDCl_3$) of **Pyrr$_2$-TPMA 42**

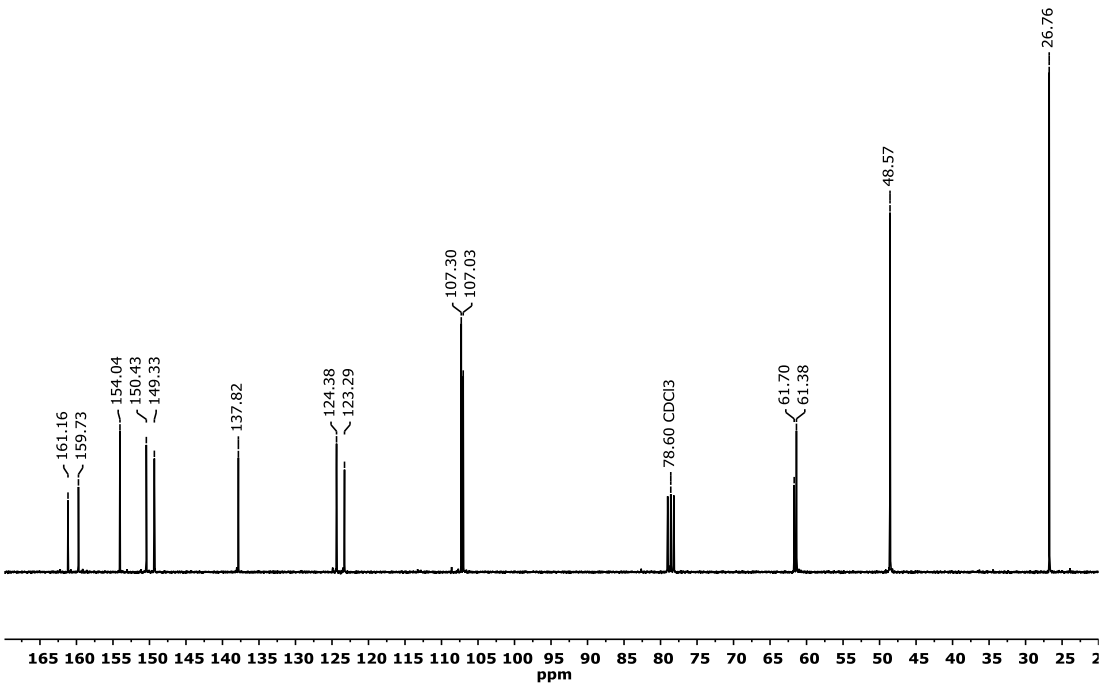

Figure S41: ^{13}C-NMR (75 MHz, $CDCl_3$) of **Pyrr$_2$-TPMA 42**

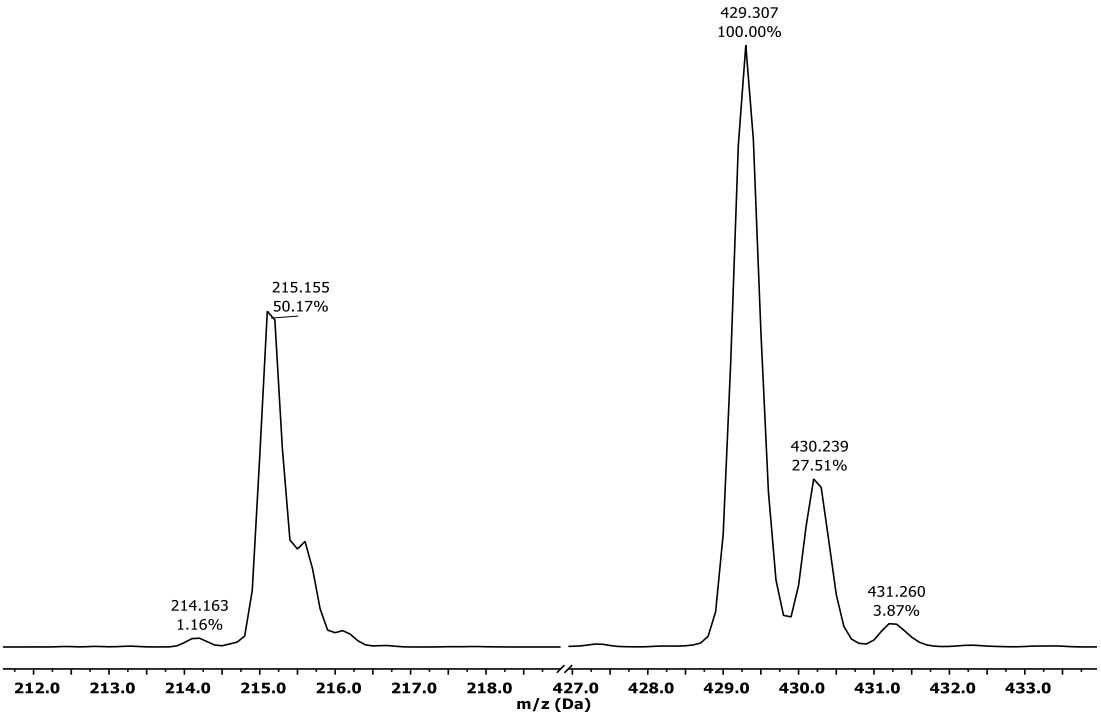

Figure S42: Experimental ESI-MS (ACN/H^+) of **Pyrr$_2$-TPMA 42**

6.2 CHARACTERIZATION OF COBALT (II)-*PARA*-TPMA COMPLEXES

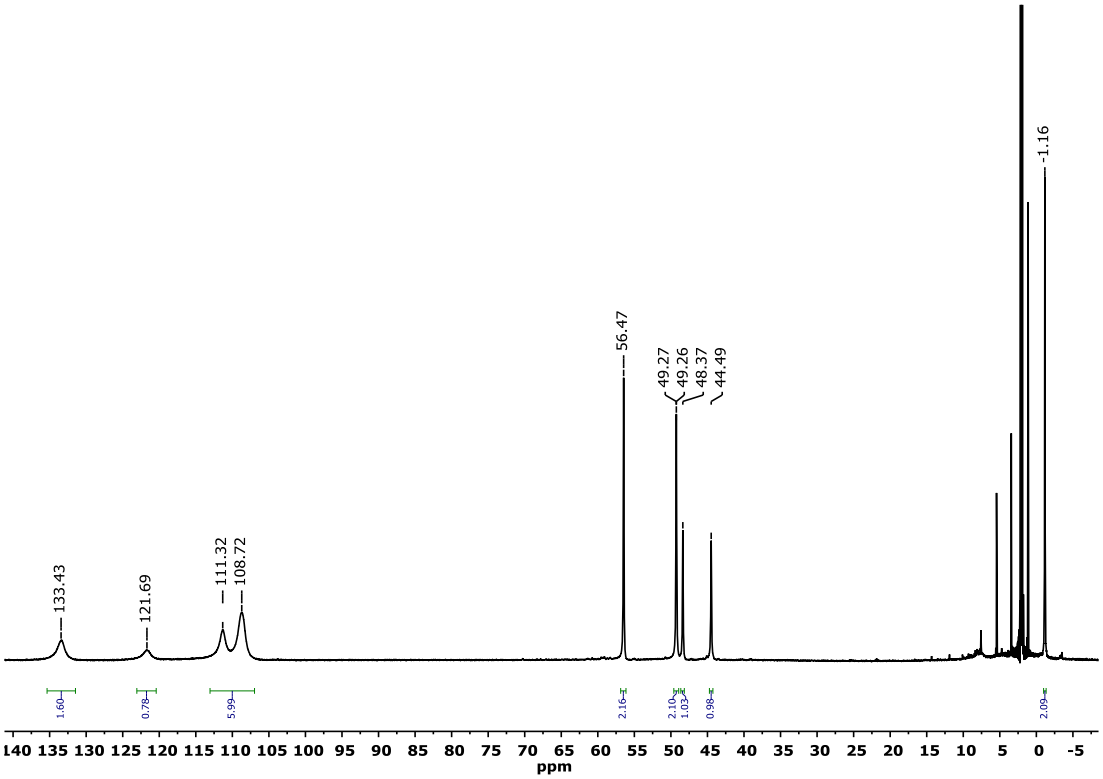

Figure S43: ^{1}H-NMR (400 MHz, CD_3CN) of complex **Co-NO_2-TPMA 29**.

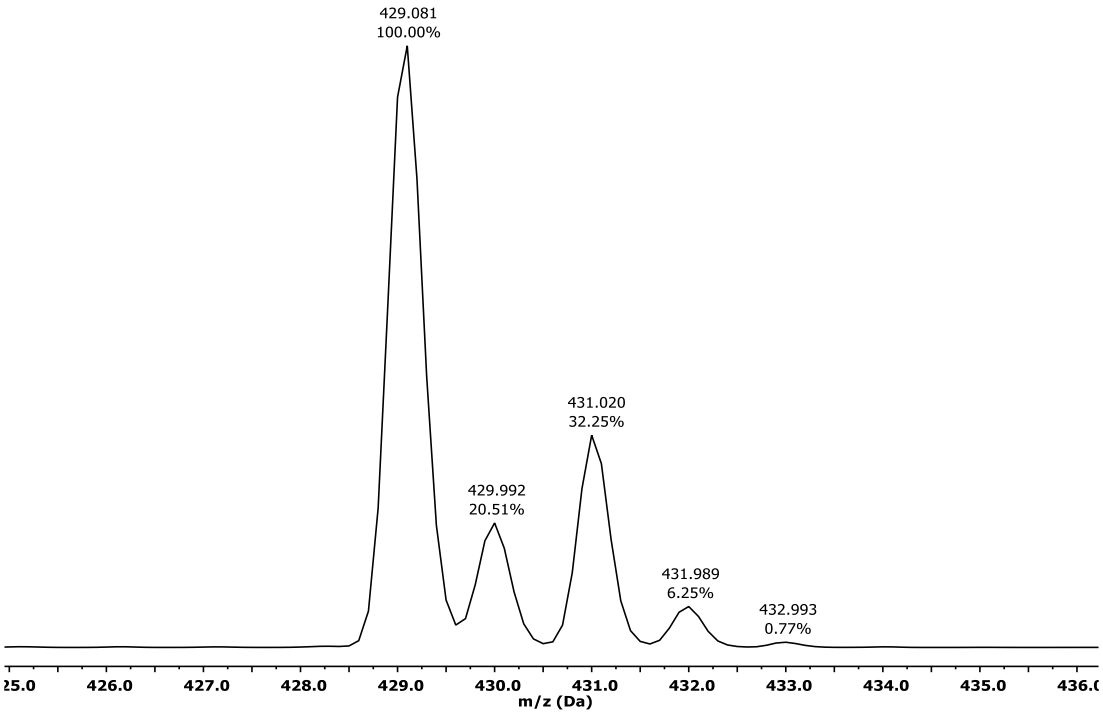

Figure S44: Experimental ESI-MS (ACN/H^+) of complex **Co-NO_2-TPMA 29**.

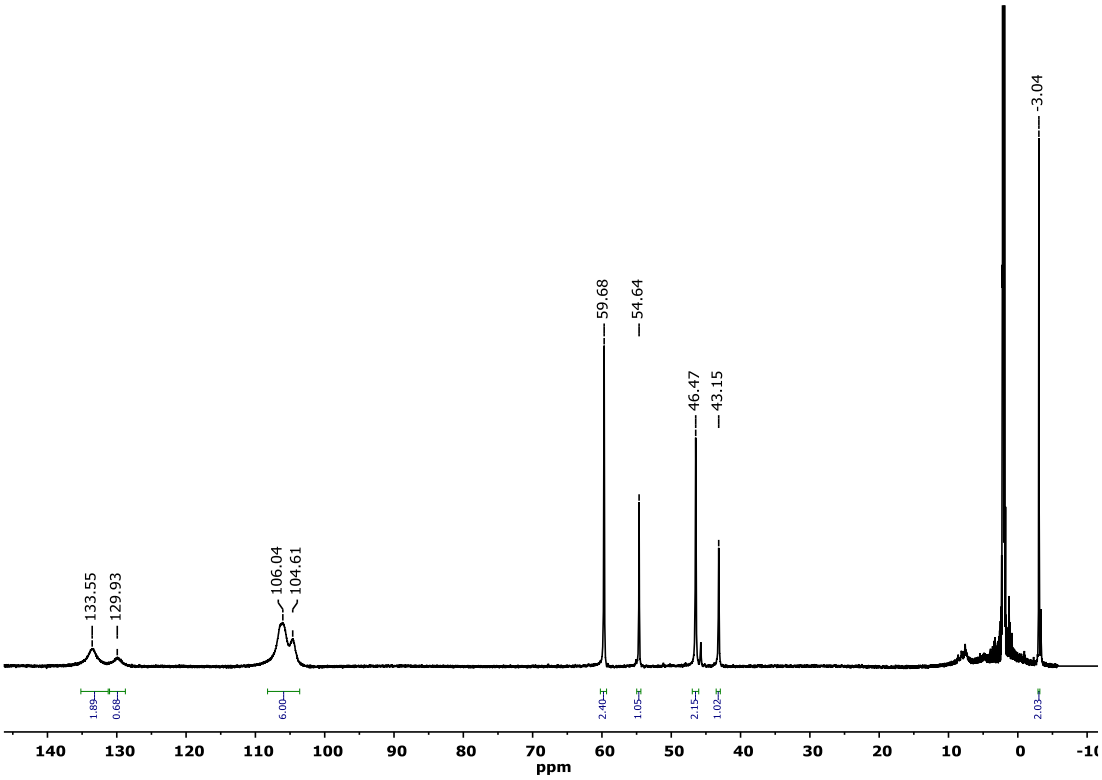

Figure S45: ^{1}H-NMR (400 MHz, CD_3CN) of complex **Co-Cl-TPMA 32**.

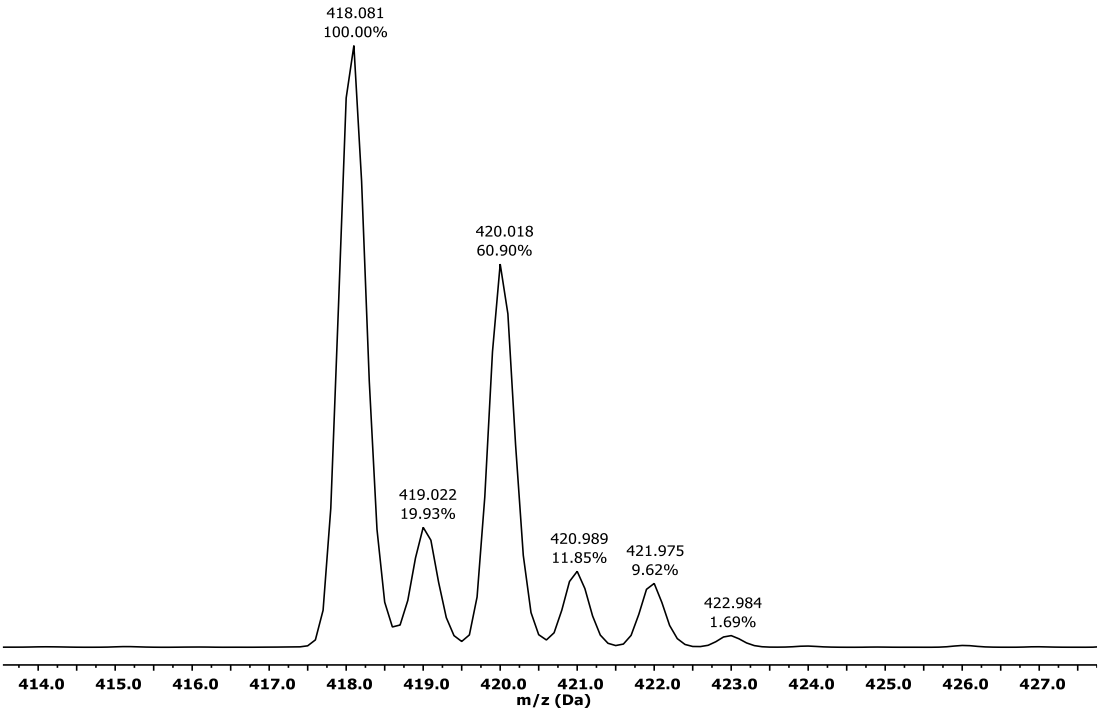

Figure S46: Experimental ESI-MS (ACN/H^+) of complex **Co-Cl-TPMA 32**.

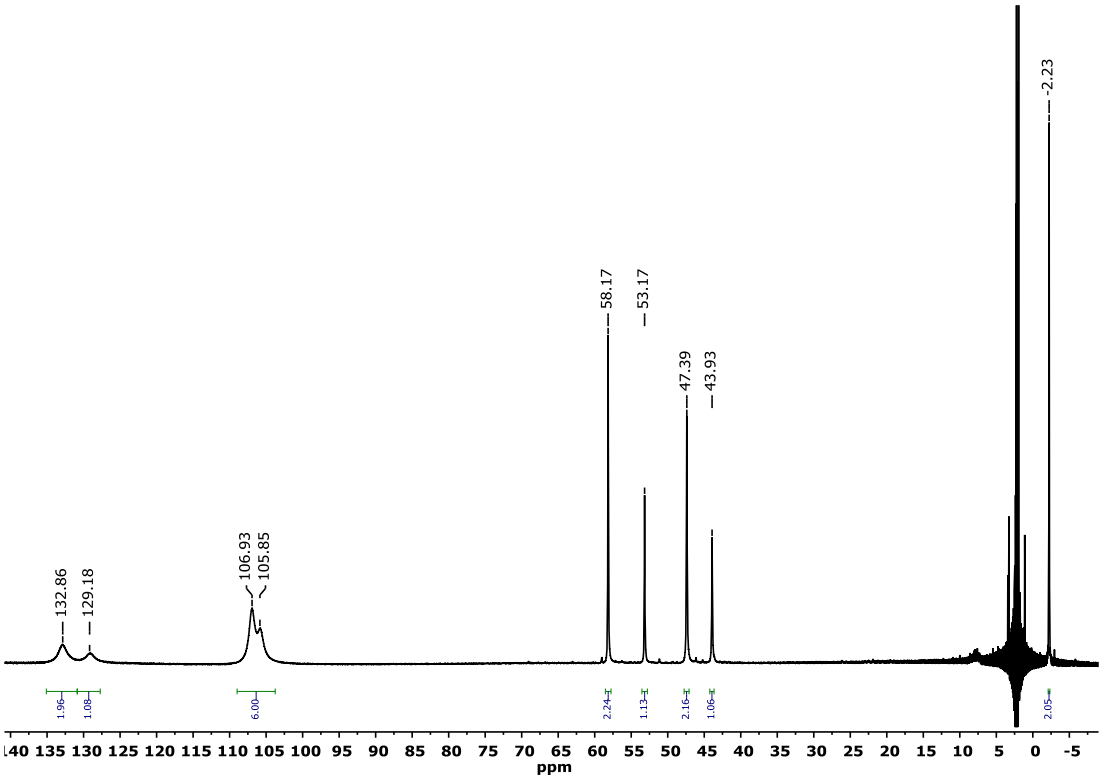

Figure S47: ^{1}H-NMR (400 MHz, CD_3CN) of complex **Co-Br-TPMA 35**

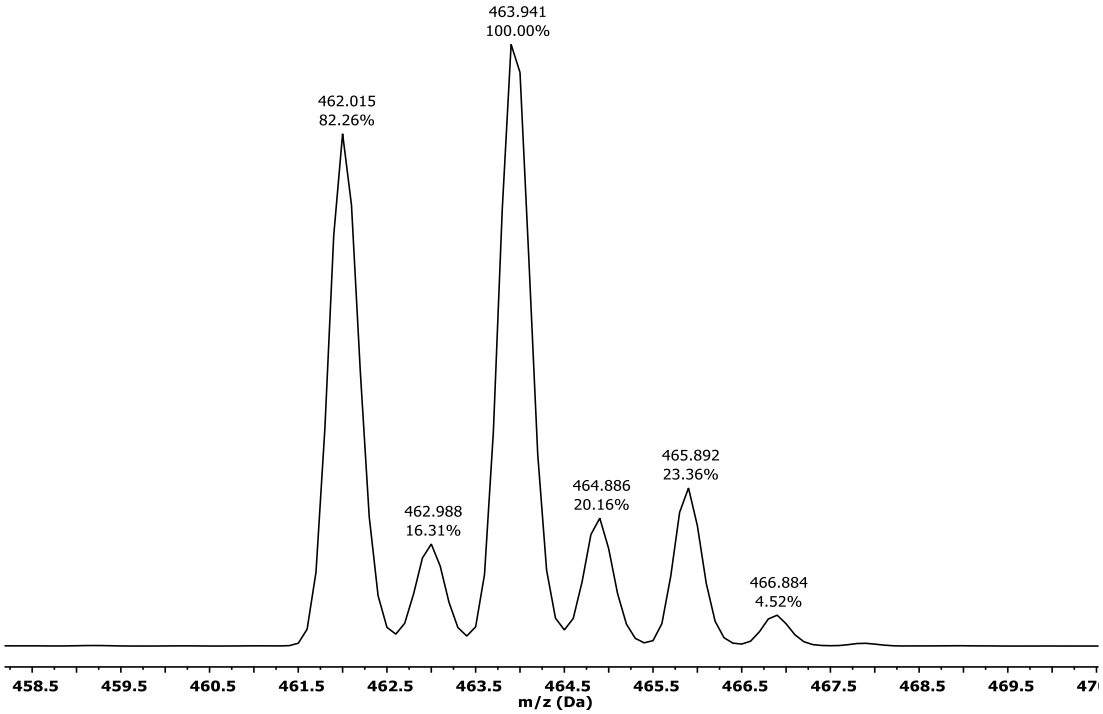

Figure S48: Experimental ESI-MS (ACN/H^+) of complex **Co-Br-TPMA 35**.

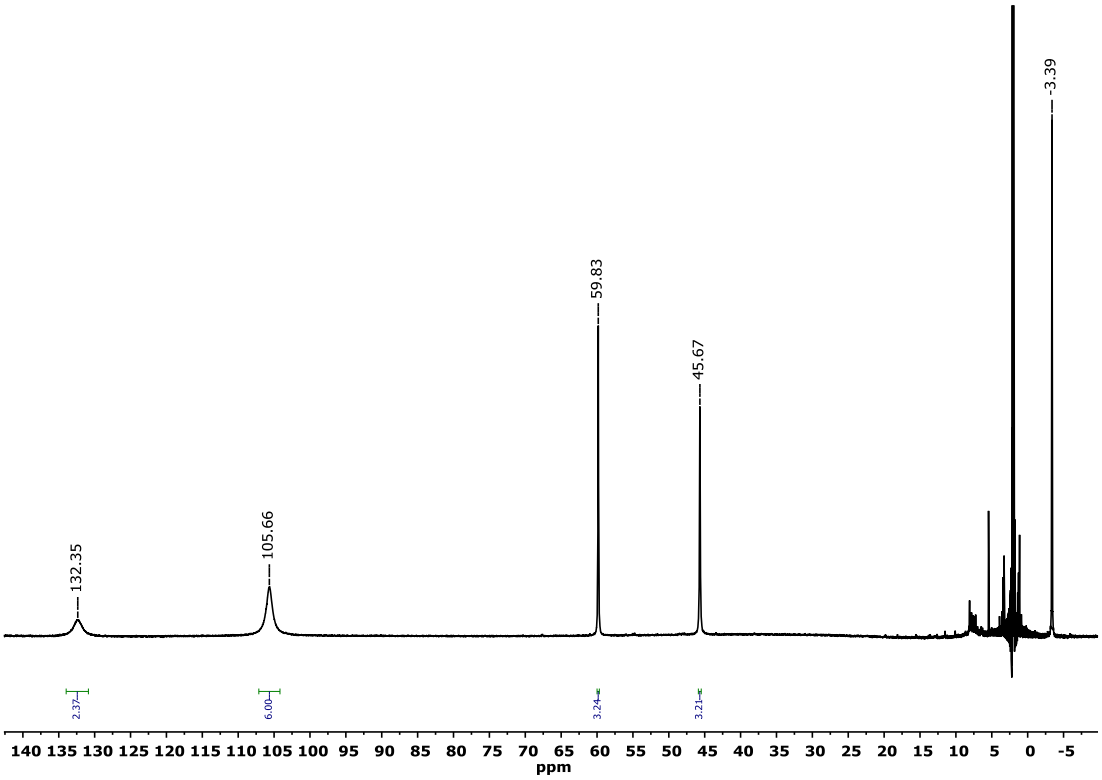

Figure S49: ^{1}H-NMR (400 MHz, CD_3CN) of complex **Co-TPMA**

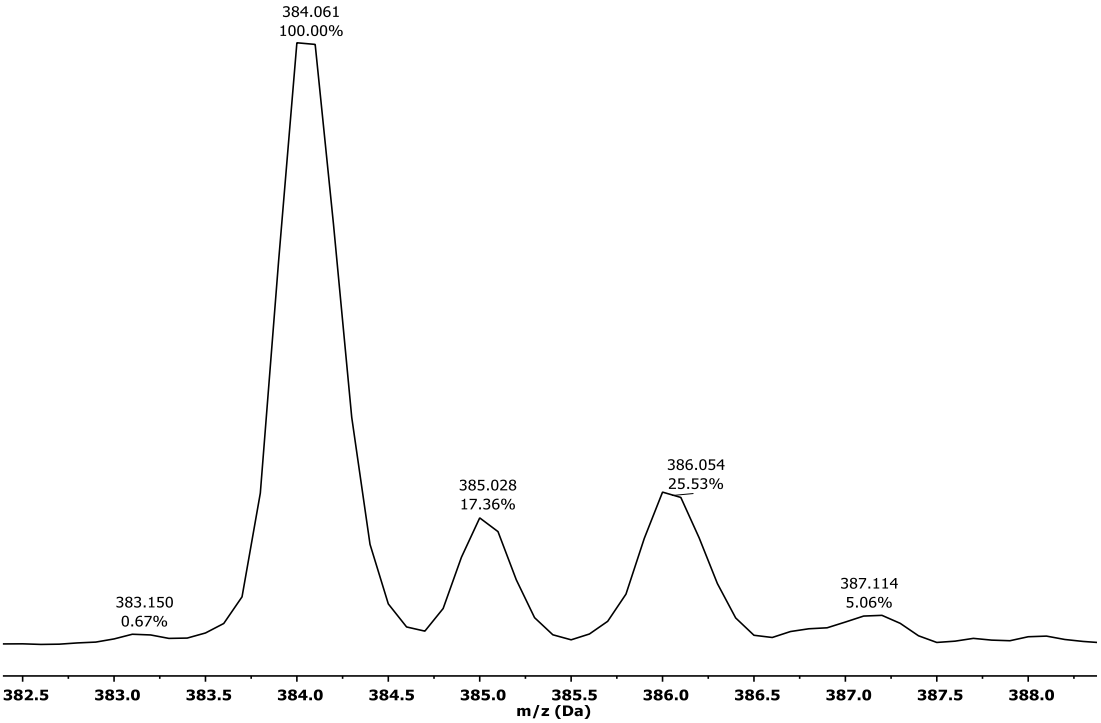

Figure S50: Experimental ESI-MS (ACN/H^+) of complex **Co-TPMA**.

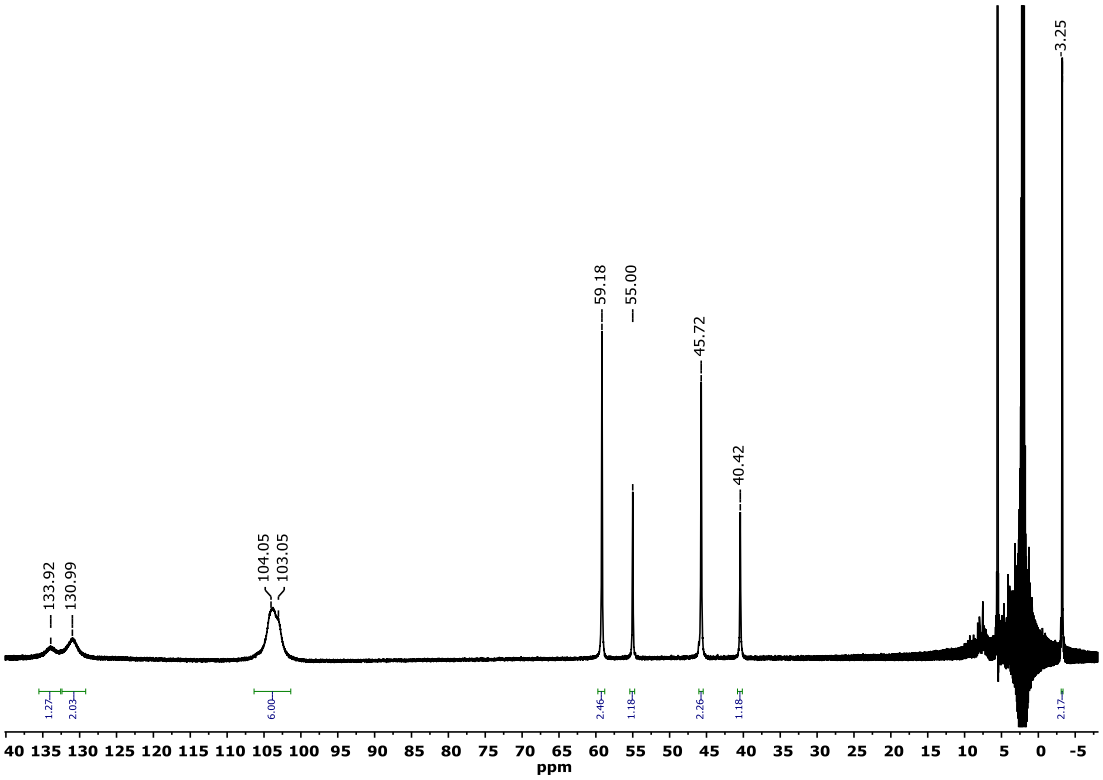

Figure S51: ^{1}H-NMR (400 MHz, CD_3CN) of **Co-OCH$_3$-TPMA 38**

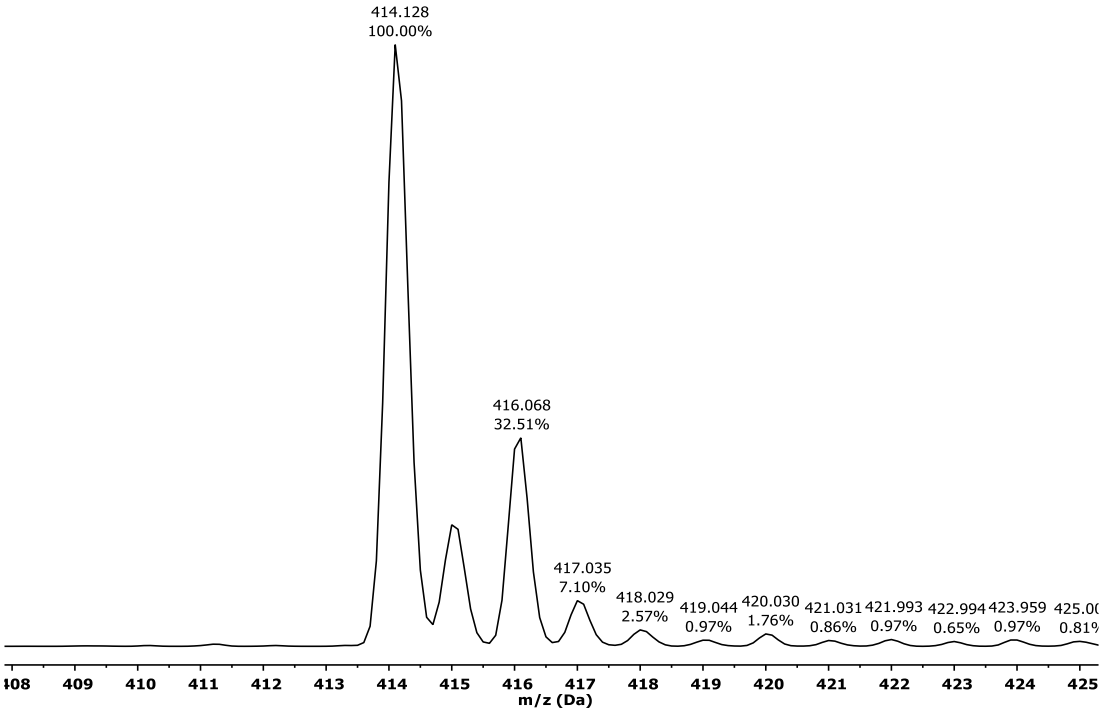

Figure S52: Experimental ESI-MS (ACN/H$^+$) of complex **Co-OCH$_3$-TPMA 38**.

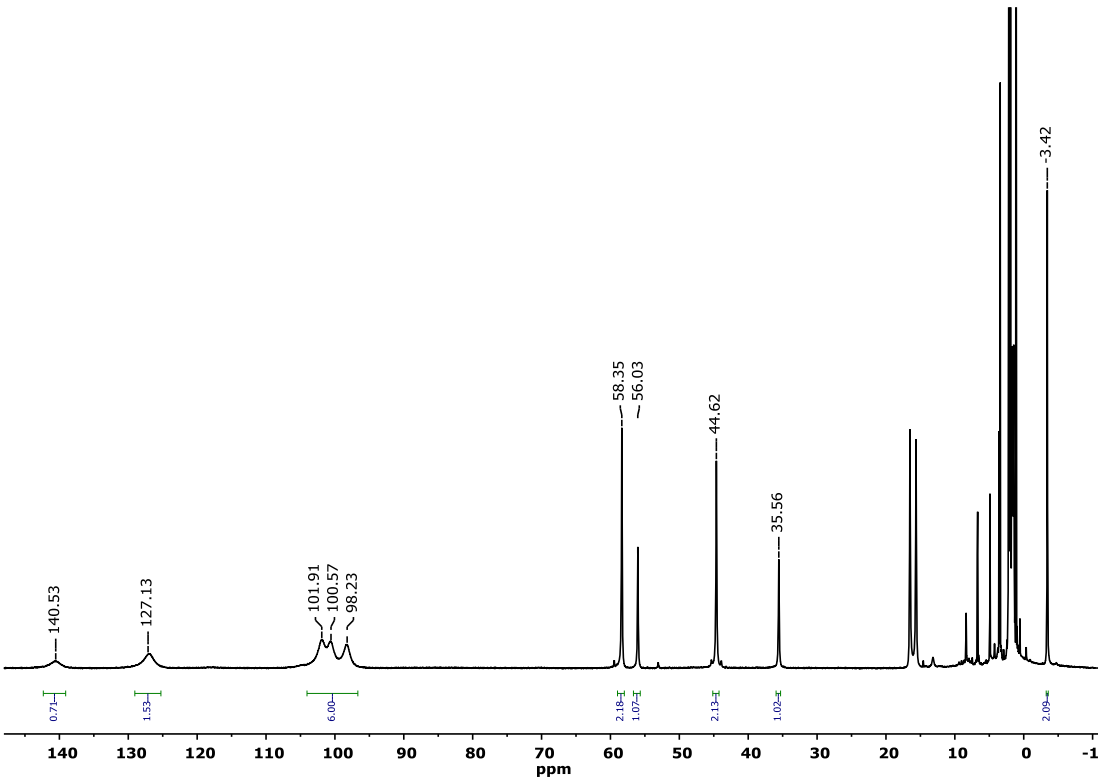

Figure S53: ^{1}H-NMR (400 MHz, CD_3CN) of **Co-Pyrr-TPMA 41.**

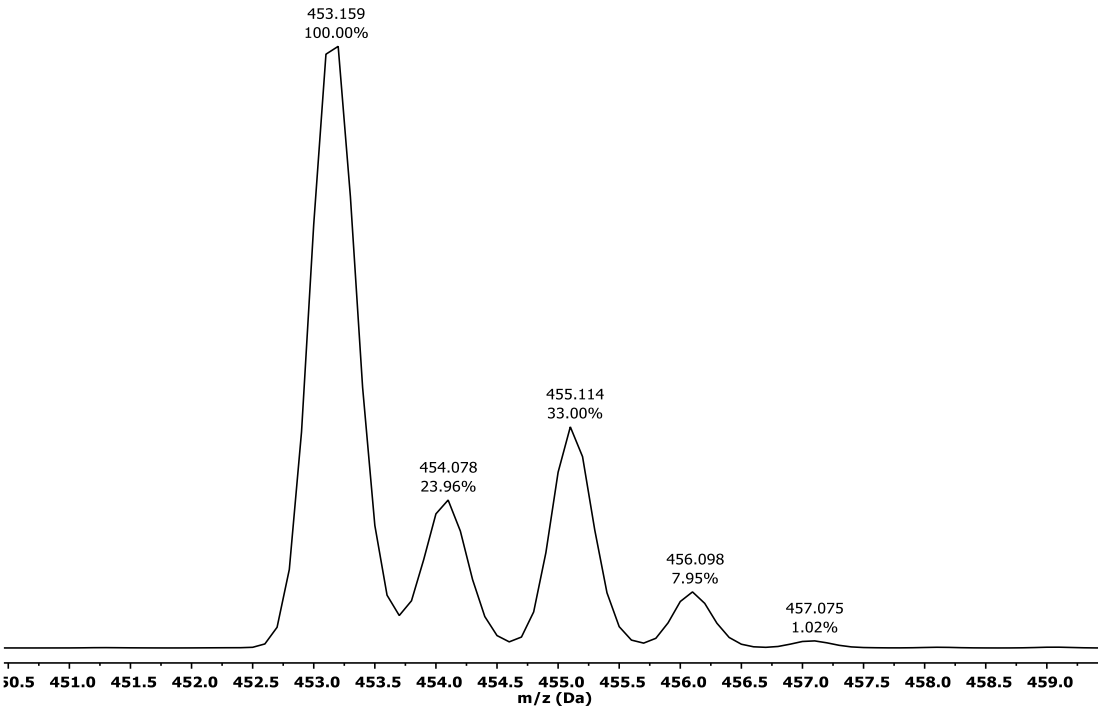

Figure S54: Experimental ESI-MS (ACN/H^+) of complex **Co-Pyrr-TPMA 41.**

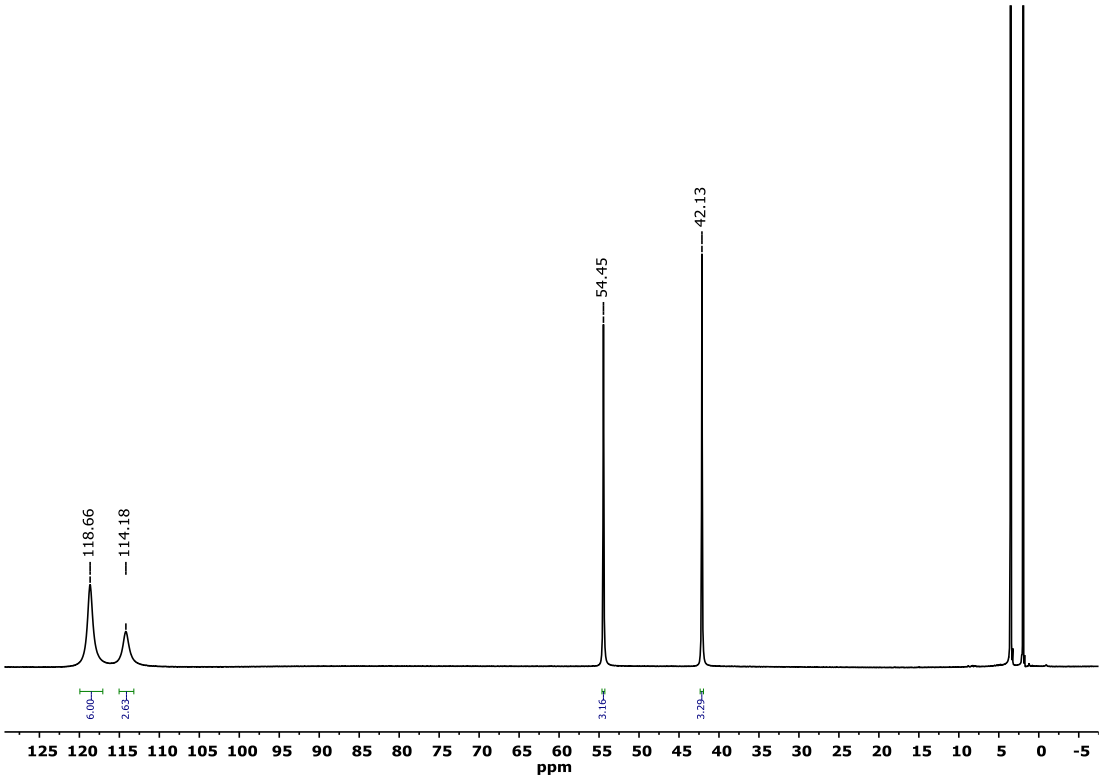

Figure S55: ^{1}H-NMR (400 MHz, CD_3CN) of **Co-$(NO_2)_3$-TPMA 31.**

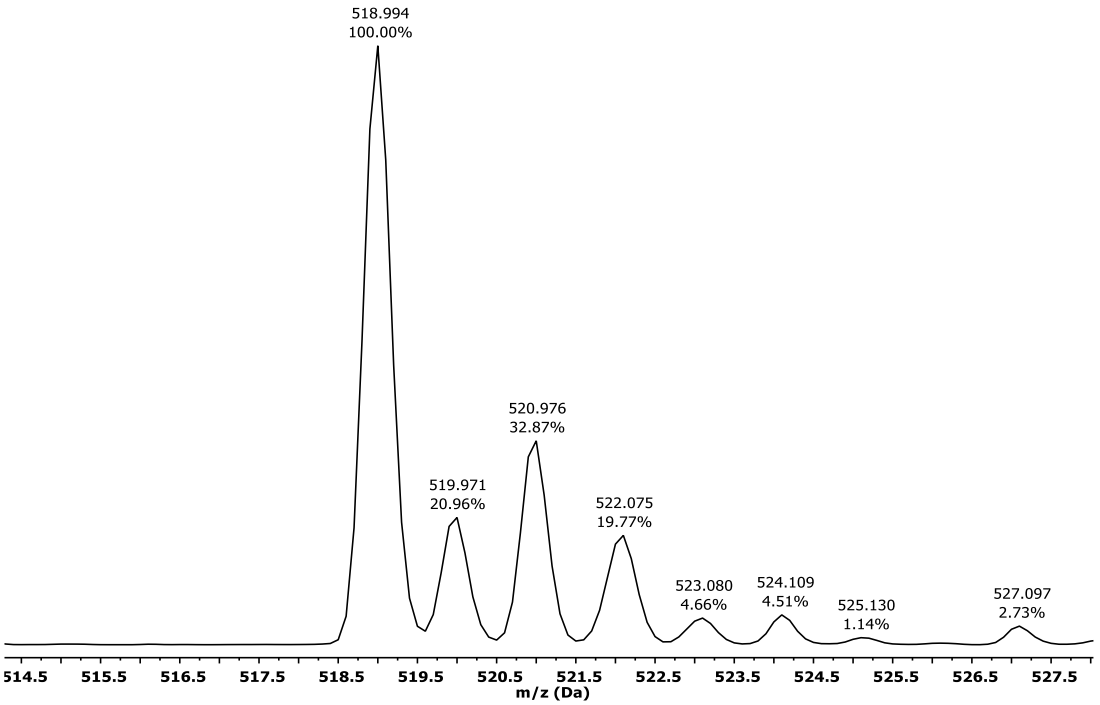

Figure S56: Experimental ESI-MS (ACN/H^+) of complex **Co-$(NO_2)_3$-TPMA 31.**

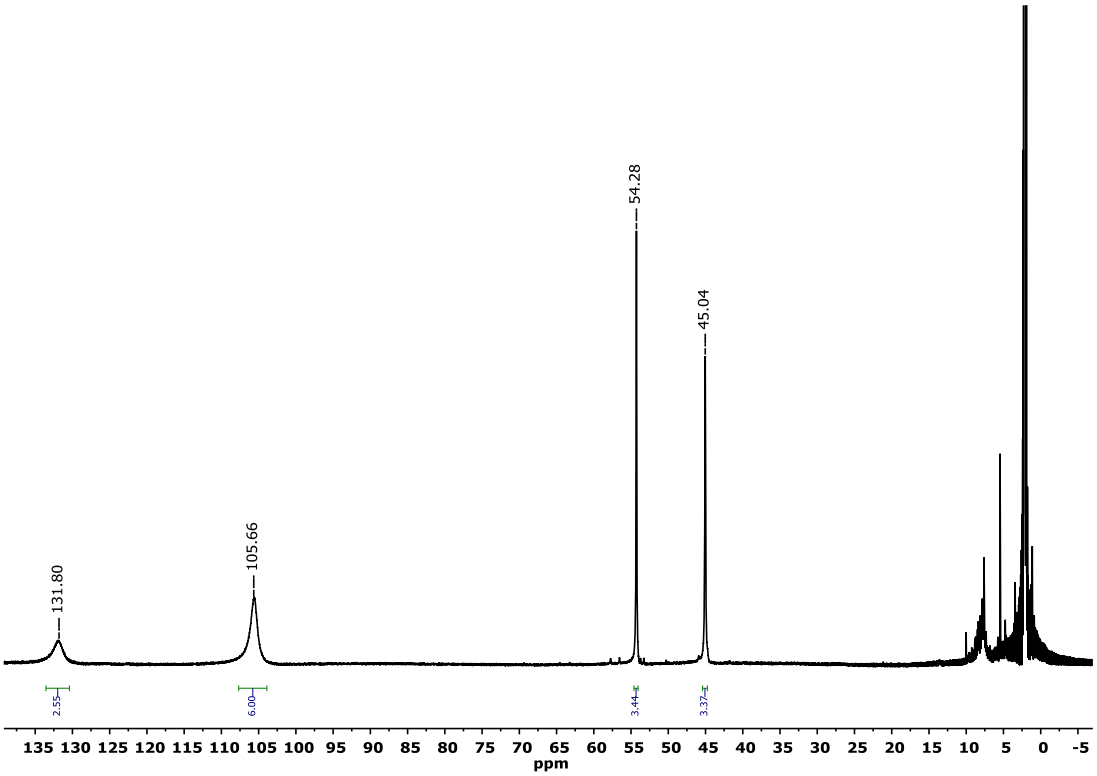

Figure S57: ^{1}H-NMR (400 MHz, CD_3CN) of **Co-Cl_3-TPMA-34.**

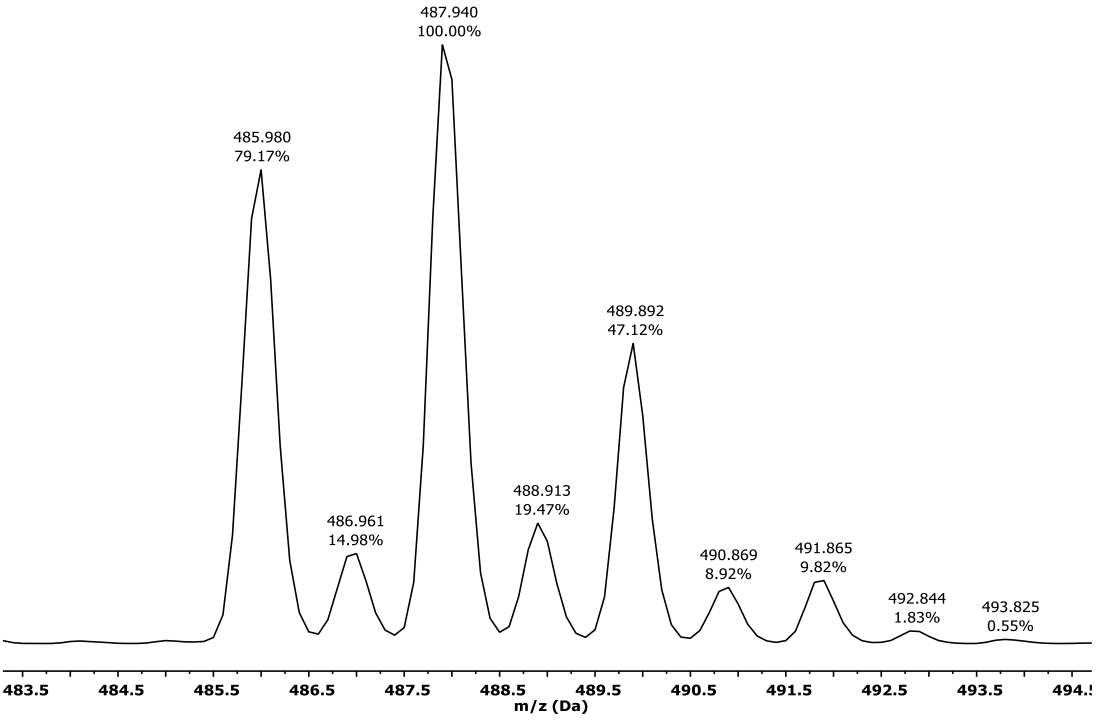

Figure S58: Experimental ESI-MS (ACN/H^+) of complex **Co-Cl_3-TPMA 34.**

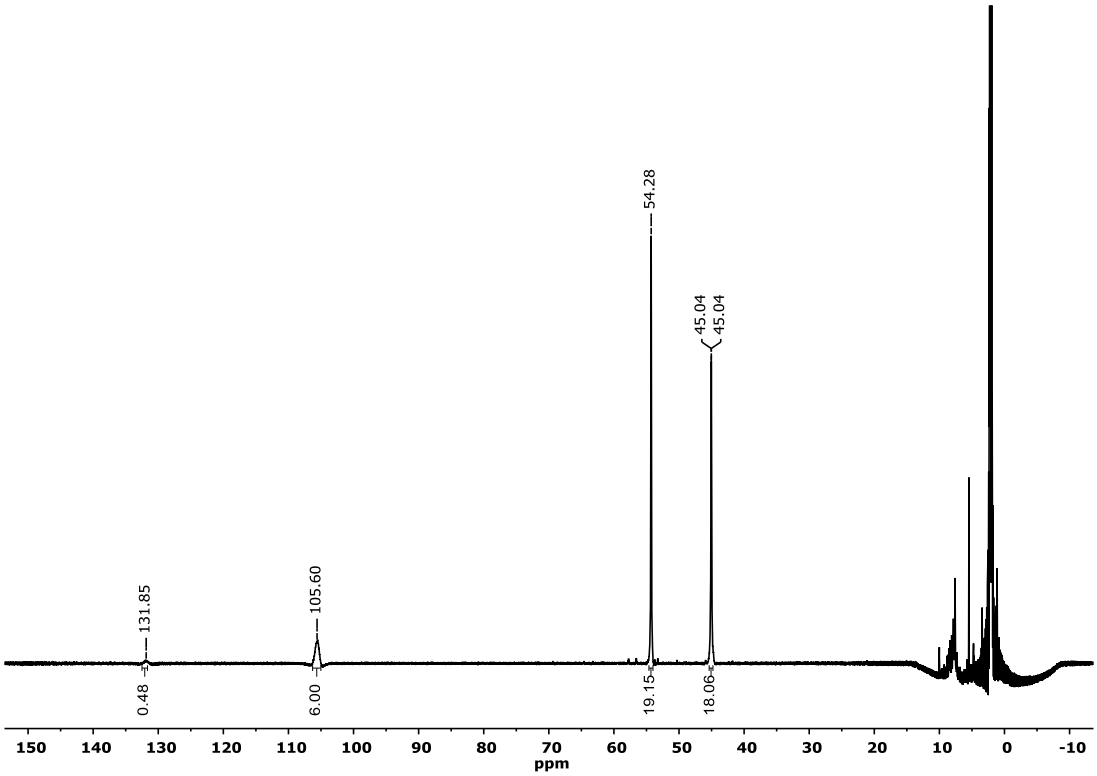

Figure S59: ^{1}H-NMR (400 MHz, CD_3CN) of **Co-Br$_3$-TPMA 37.**

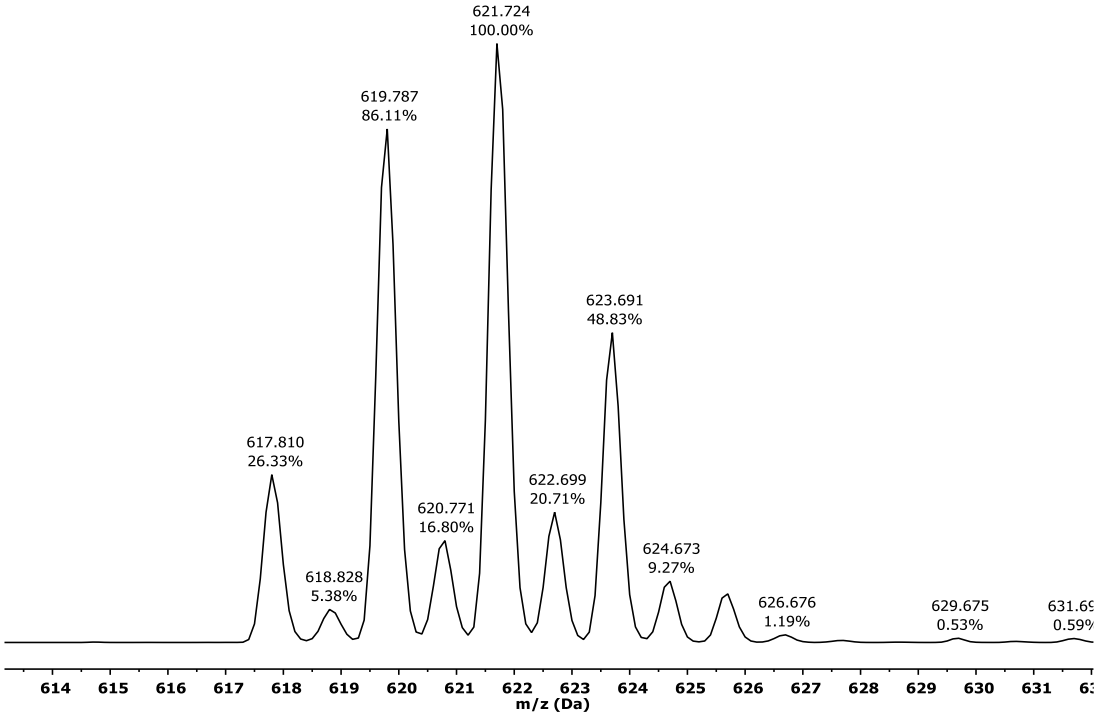

Figure S60: Experimental ESI-MS (ACN/H^+) of complex **Co-Br$_3$-TPMA 37.**

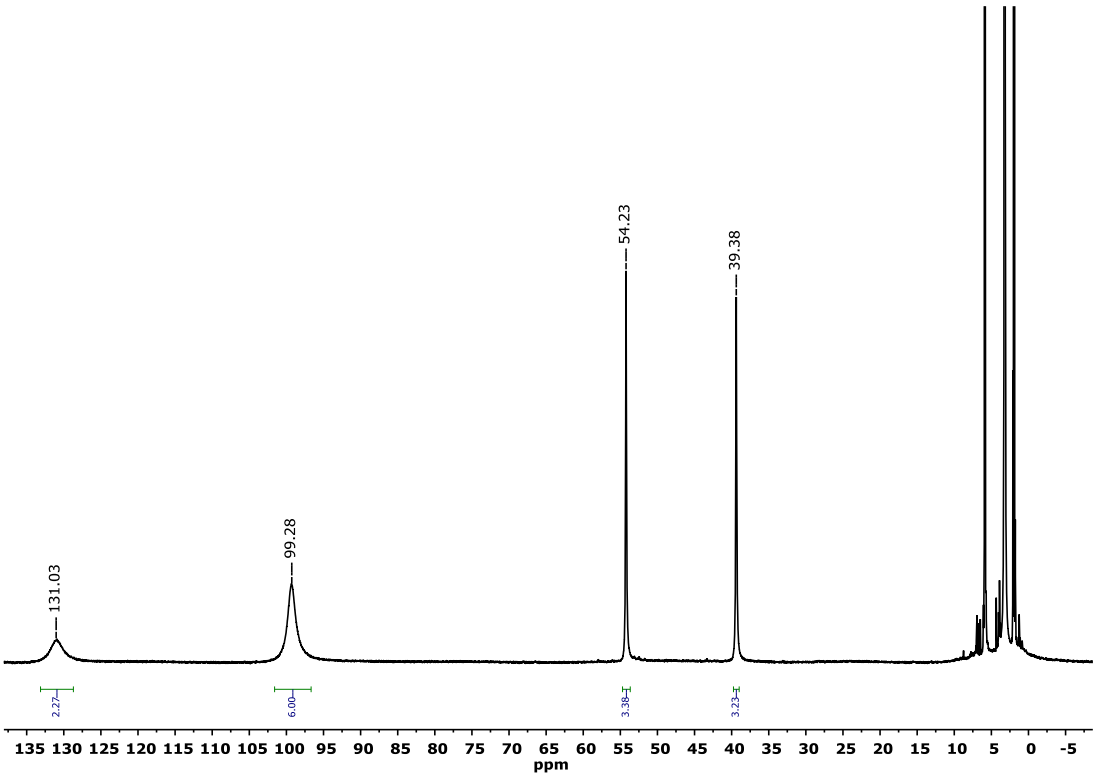

Figure S61: ^{1}H-NMR (400 MHz, CD_3CN) of **Co-$(OCH_3)_3$-TPMA 40.**

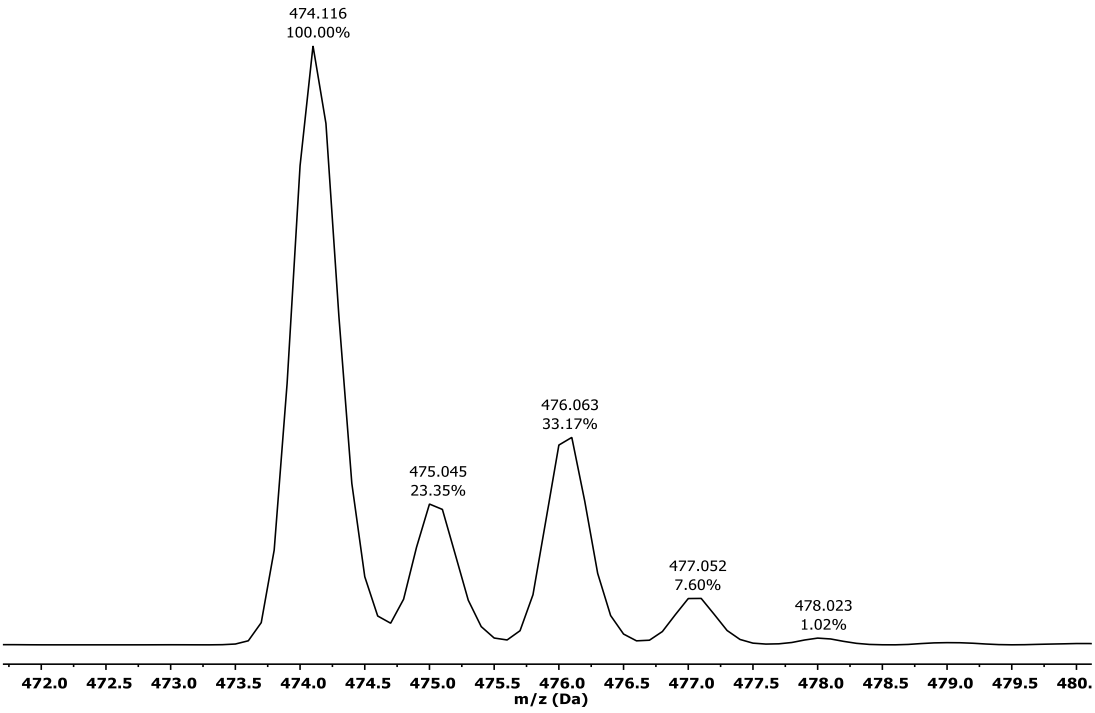

Figure S62: Experimental ESI-MS (ACN/H^+) of complex **Co-$(OCH_3)_3$-TPMA 40.**

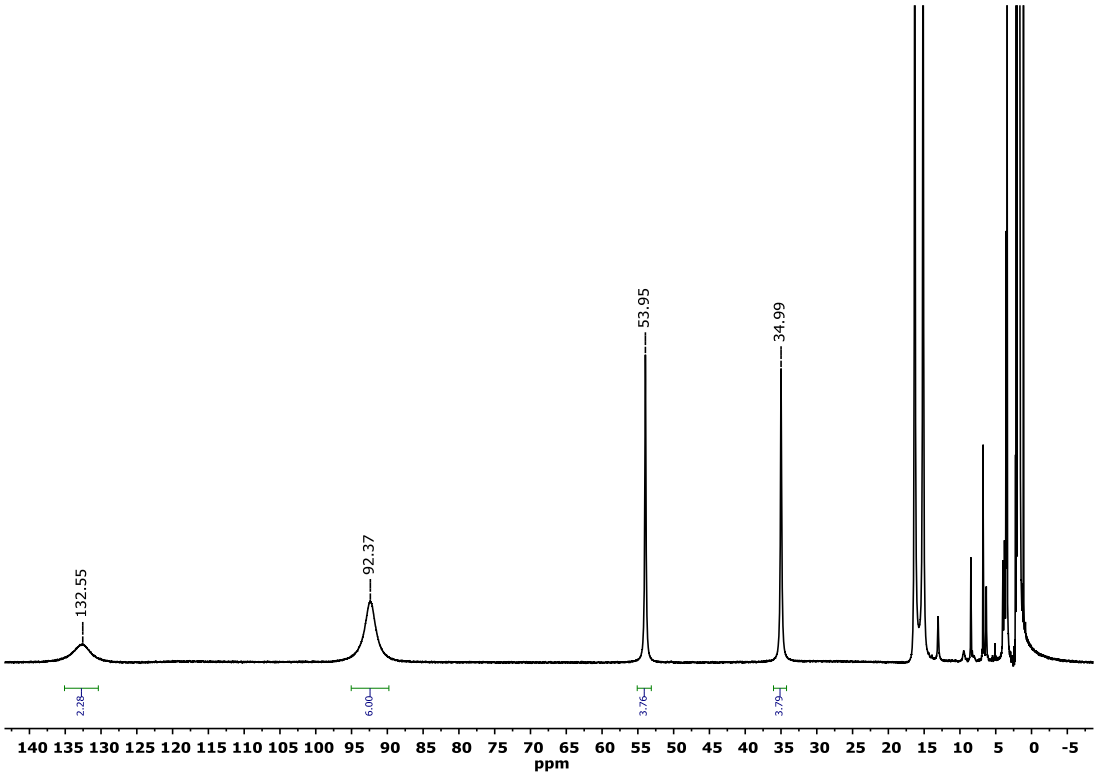

Figure S63: ^{1}H-NMR (400 MHz, CD_3CN) of **Co-Pyrr$_3$-TPMA 43**

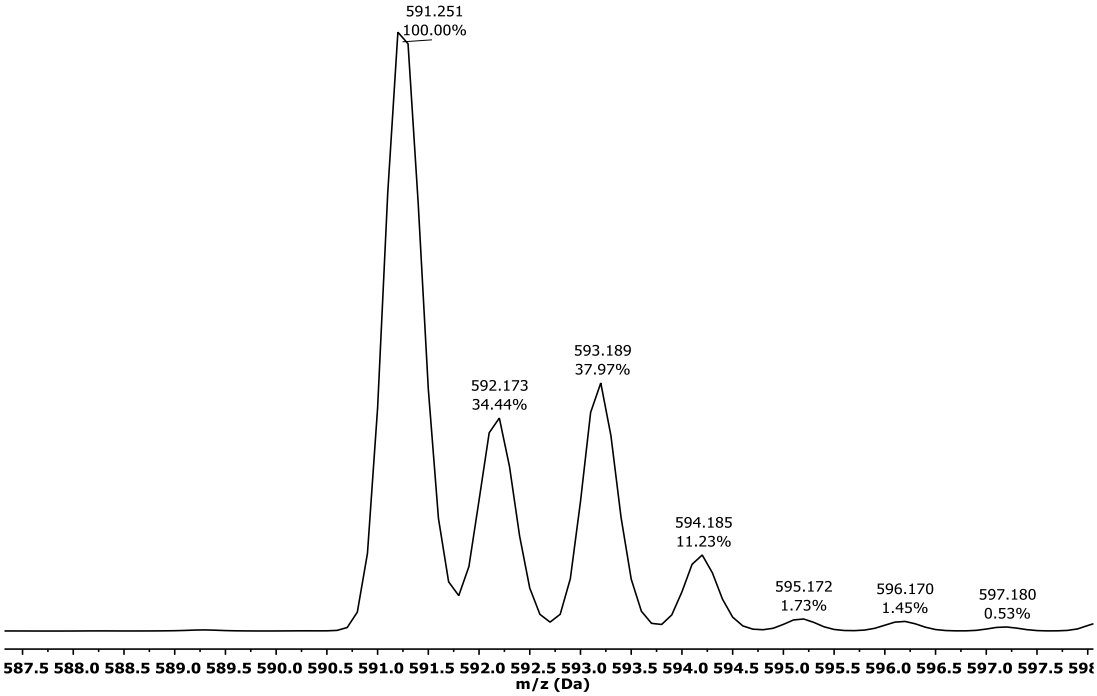

Figure S64: Experimental ESI-MS (ACN/H^+) of complex **Co-Pyrr$_3$-TPMA 43.**

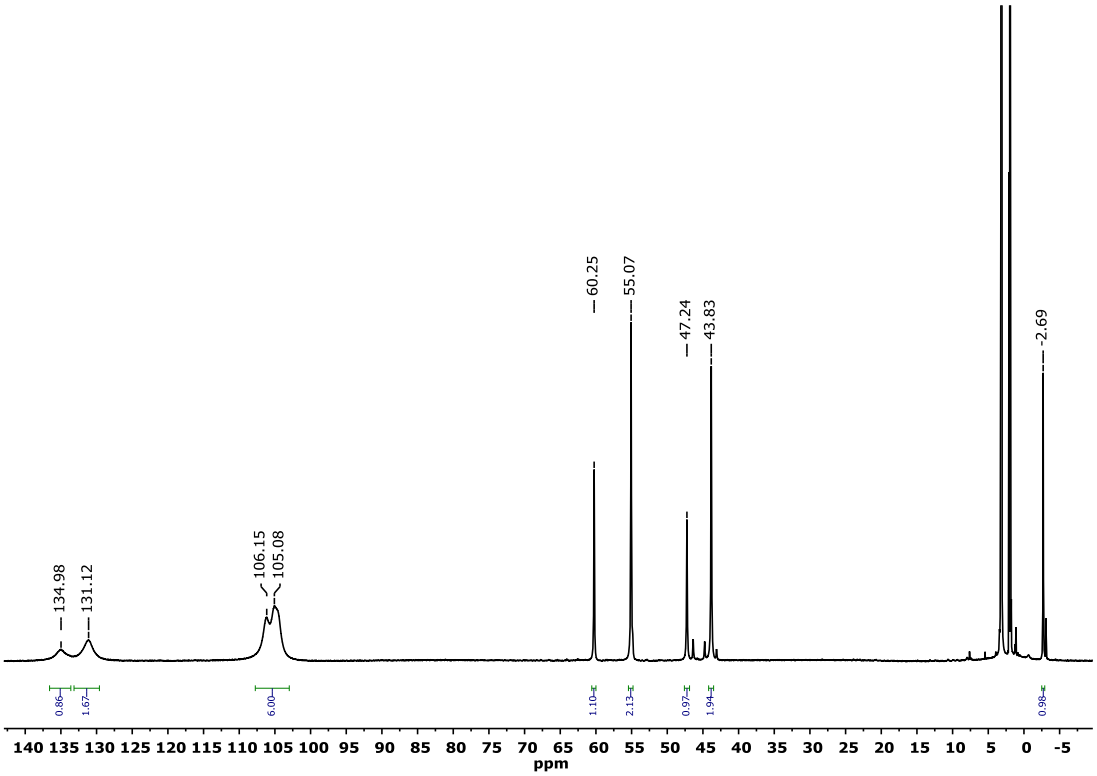

Figure S65: ^{1}H-NMR (400 MHz, CD_3CN) of **Co-Cl_2-TPMA 33.**

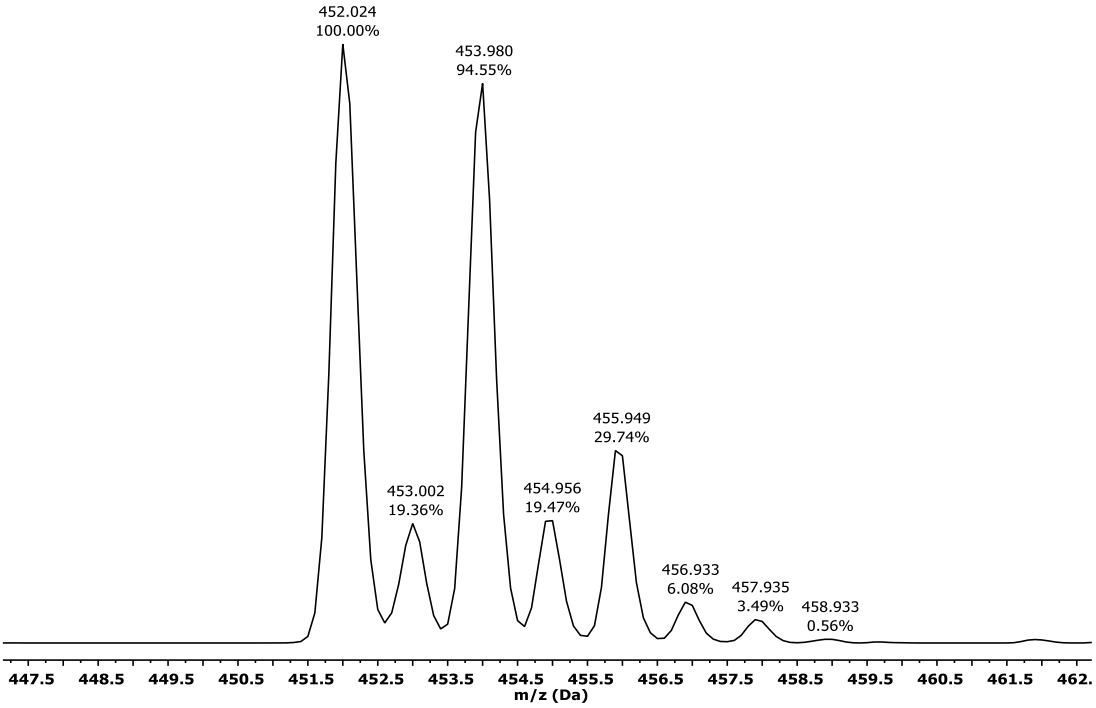

Figure S66: Experimental ESI-MS (ACN/H^+) of complex **Co-Cl_2-TPMA 33.**

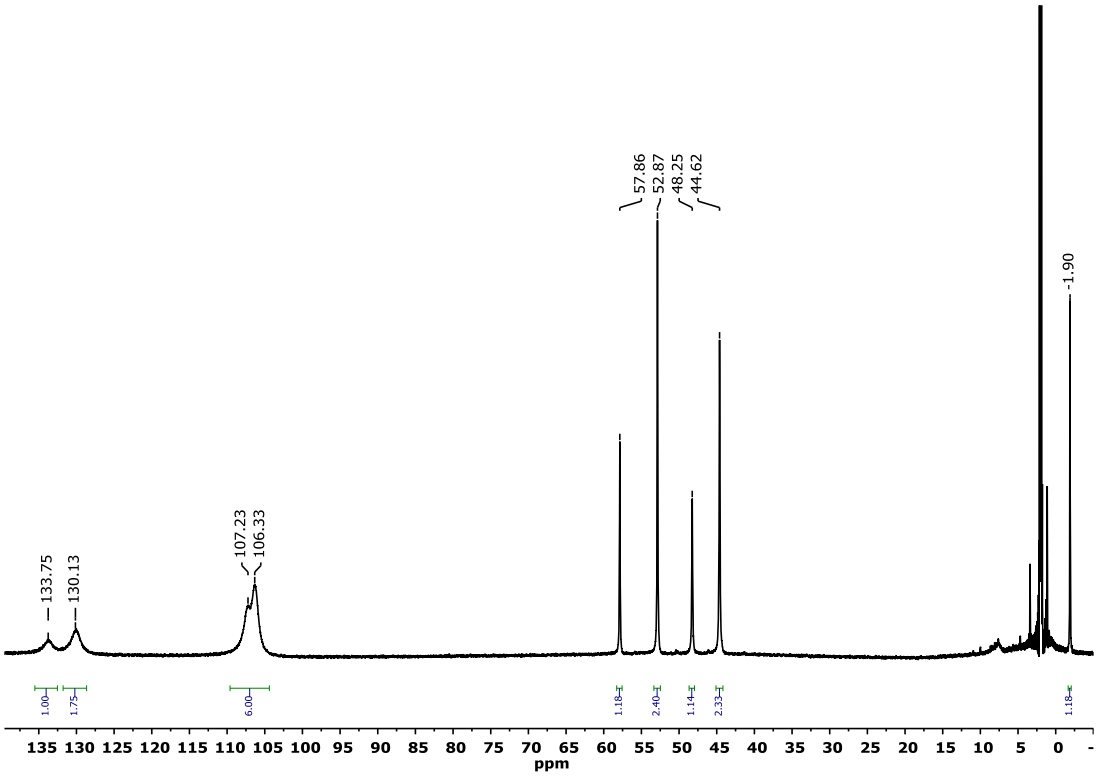

Figure S37: ^{1}H-NMR (400 MHz, CD_3CN) of **Co-Br$_2$-TPMA 36.**

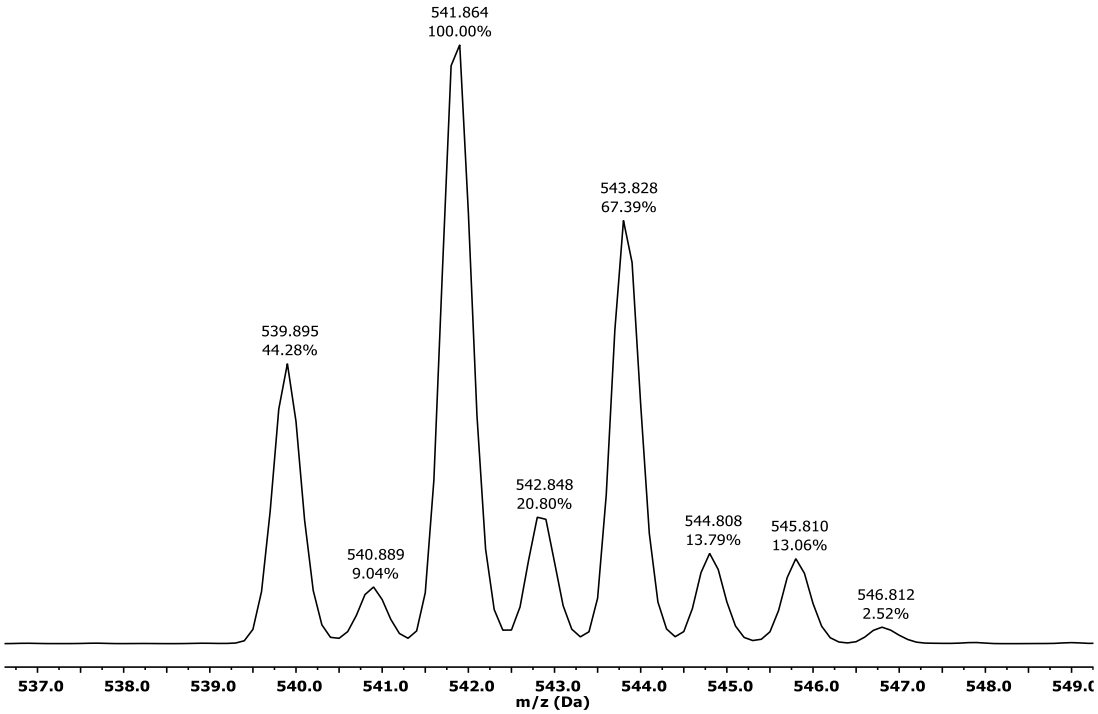

Figure S67: Experimental ESI-MS (ACN/H$^+$) of complex **Co-Br$_2$-TPMA 36.**

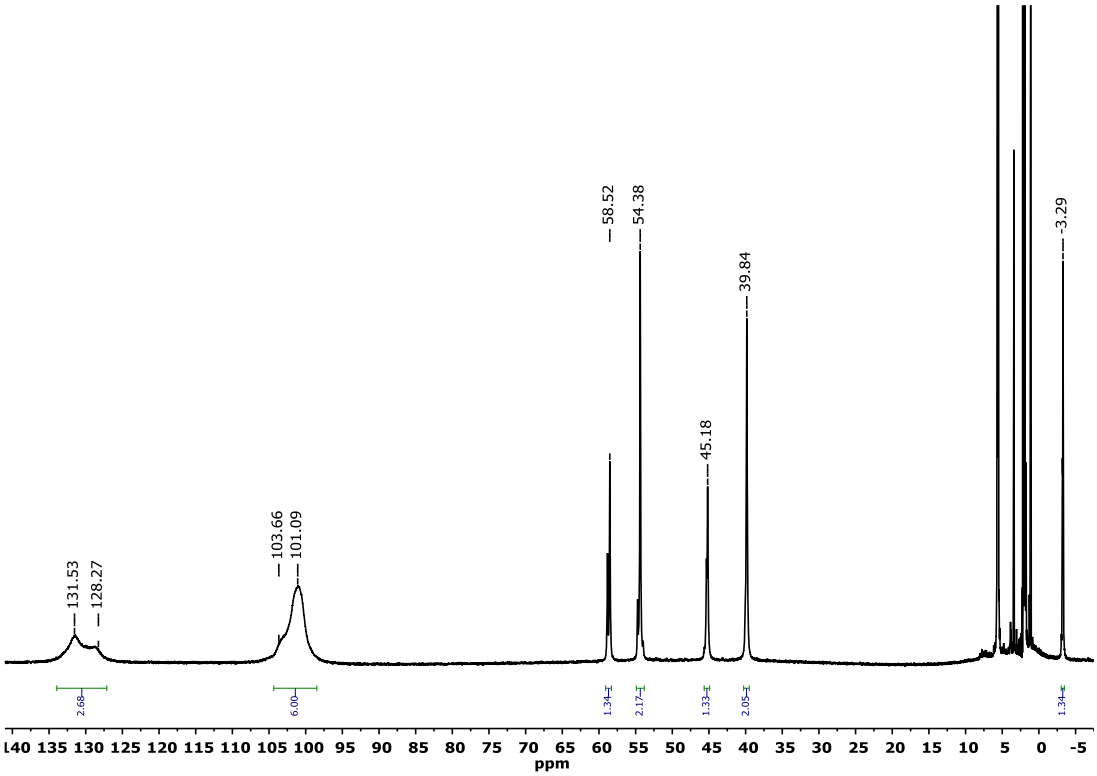

Figure S68: ^{1}H-NMR (400 MHz, CD_3CN) of **Co-$(OCH_3)_2$-TPMA 39.**

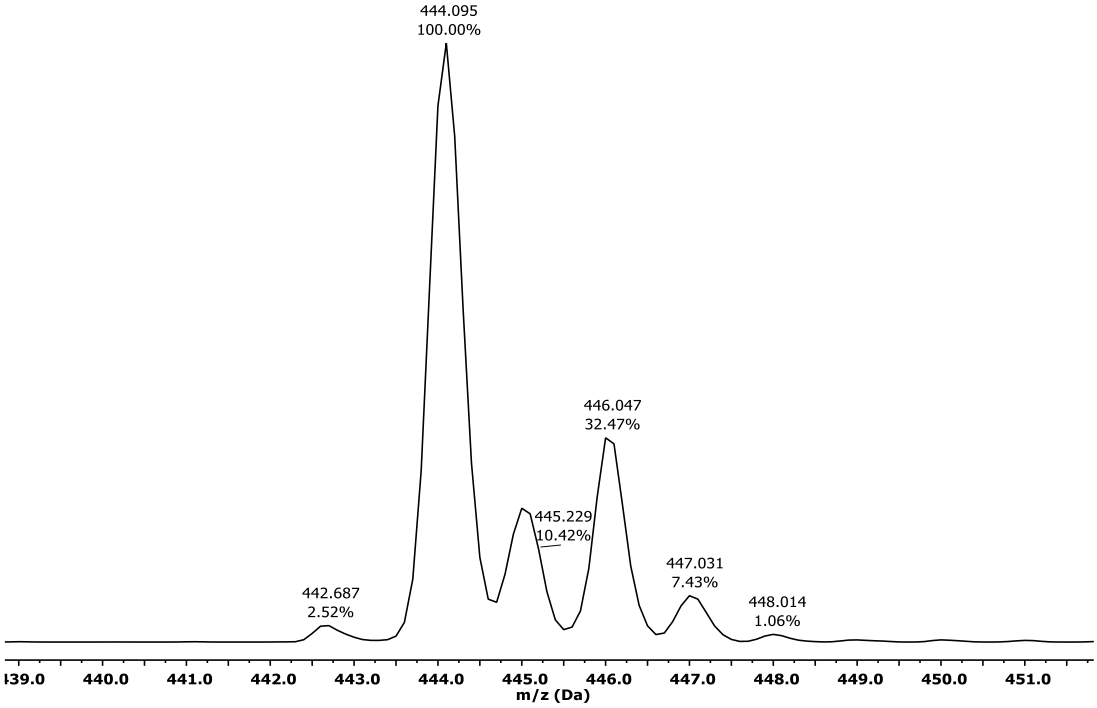

Figure S69: Experimental ESI-MS (ACN/H^+) of complex **Co-$(OCH_3)_2$-TPMA 39.**

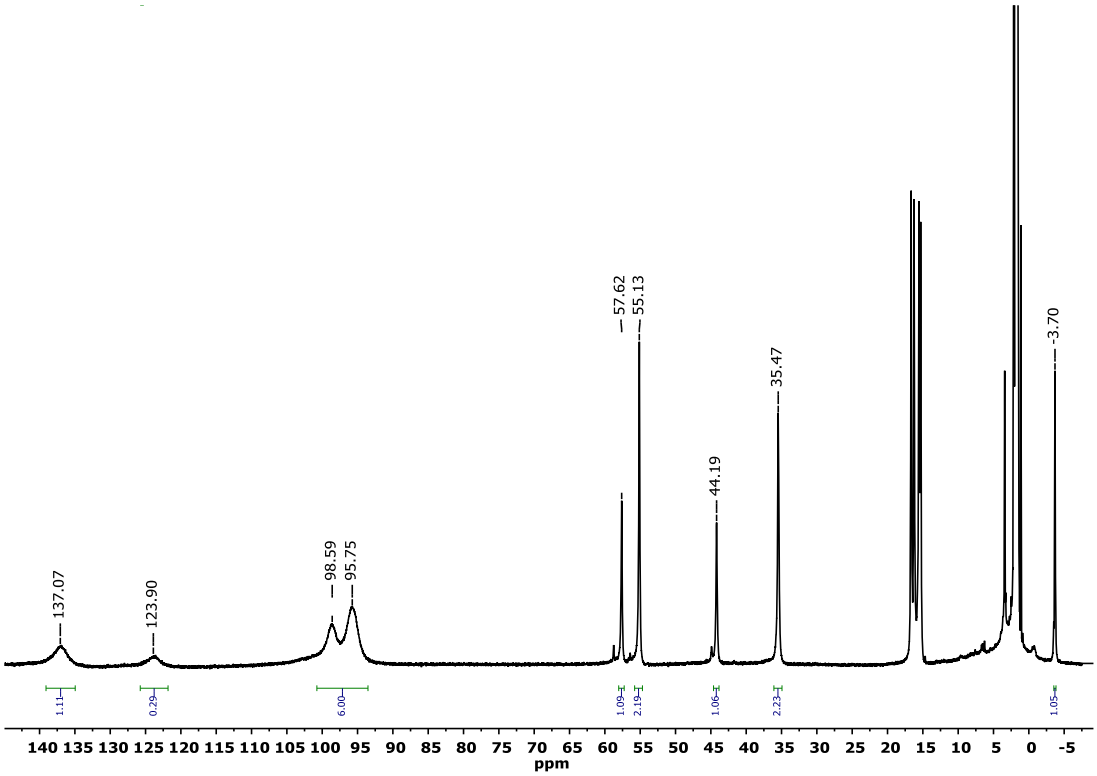

Figure S70: ^{1}H-NMR (400 MHz, CD_3CN) of **Co-Pyrr$_2$-TPMA 42.**

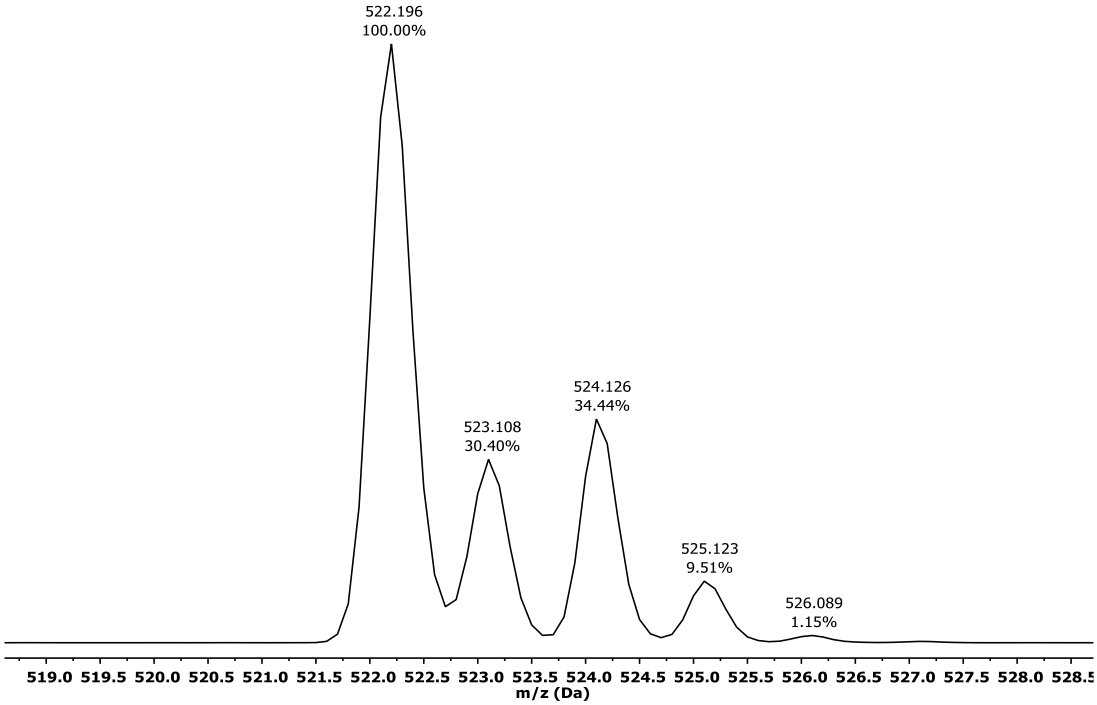

Figure S71: Experimental ESI-MS (ACN/H^+) of complex **Co-Pyrr$_2$-TPMA 42.**

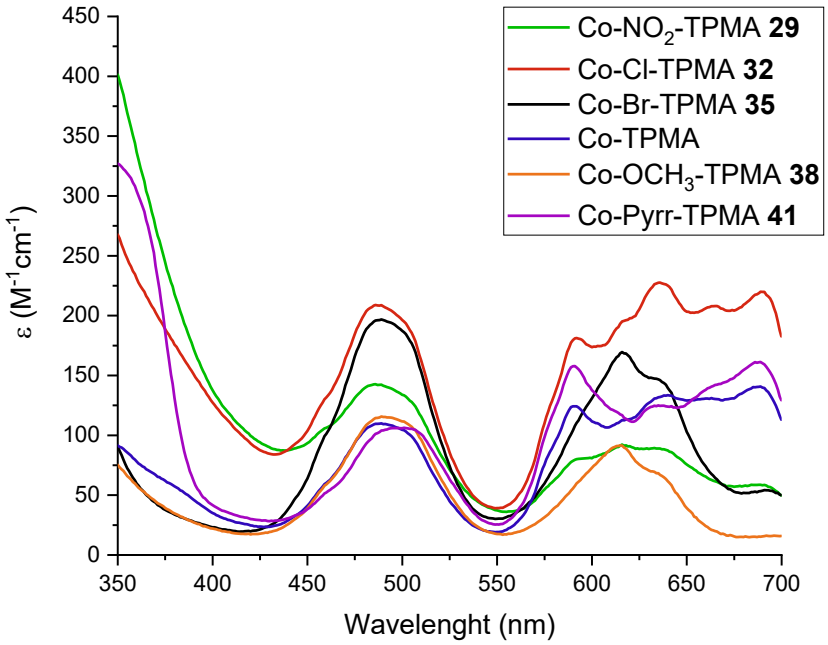

Figure S72: UV-Vis ($1*10^{-3}$ M ACN) spectra of complexes **Co (II)-R-TPMA**

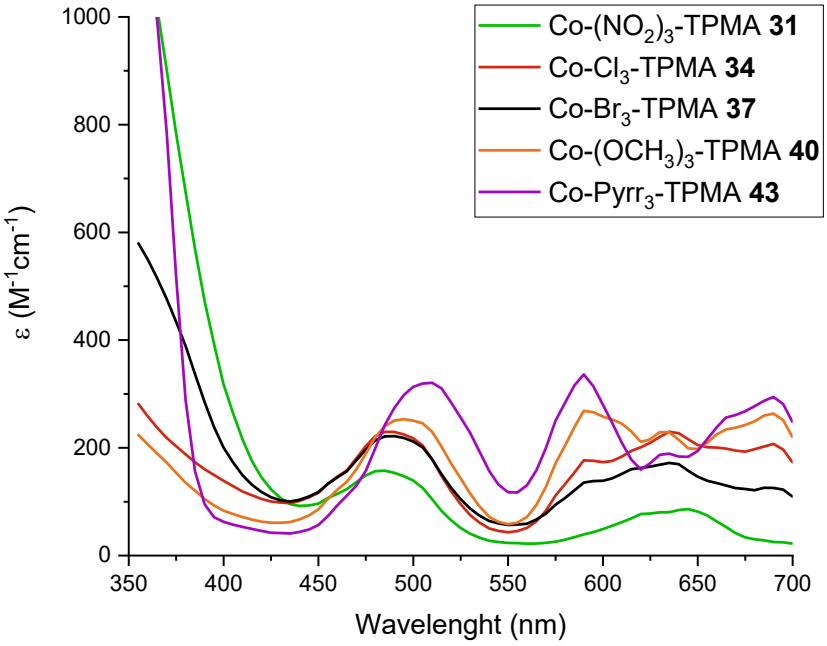

Figure S73: UV-Vis ($1*10^{-3}$ M ACN) spectra of complexes **Co (II)-R_3-TPMA**

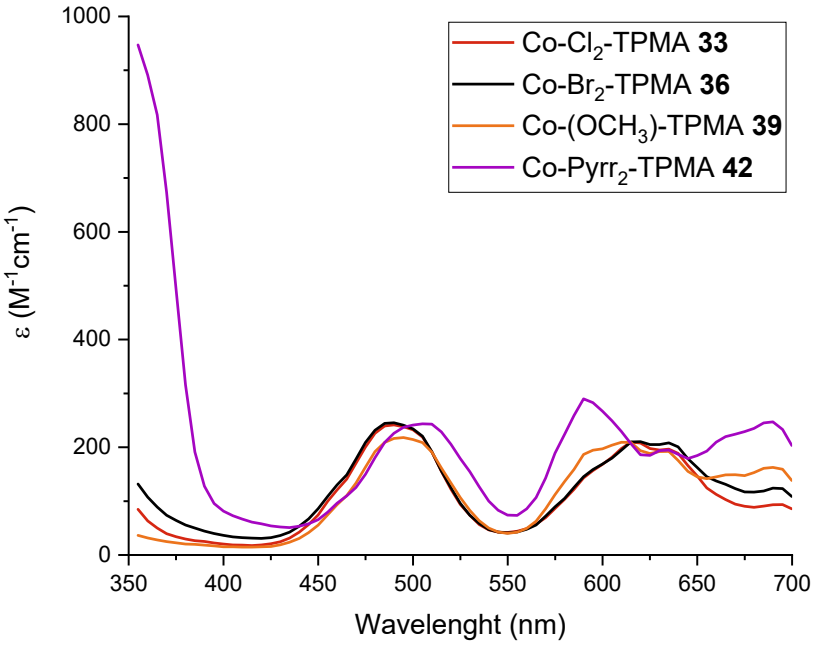

Figure S74: UV-Vis ($1*10^{-3}$ M ACN) spectra of **Co (II)-R_2-TPMA**

7 REFERENCES

(1) T. P. Yoon, E. N. Jacobsen, *Science* **2003**, 299, 1691.

(2) Leenders, S. H. A. M.; Gramage-Doria, R.; de Bruin, B.; Reek, J. N. H. *Chem. Soc. Rev.* **2015**, 433-448.

(3) Bravin, C.; Badetti, E.; Licini, G.; Zonta, C., *Coord. Chem. Rev.,* **2021**. 427, 213558

(4) Blackman, A. G., *Eur. J. Inorg. Chem*. **2008**, 2633–2647.

(5) Anderegg, G.; Wenk, F., *Helv. Chim. Acta* **1967**, 50, 2330–2332.

(6) Anderegg, G.; Hubmann, E.; Podder, N. G.; Wenk, F., *Helv. Chim. Acta* **1977**, *60*, 123–140.

(7) da Mota, M. M.; Rodgers, J.; Nelson, S. M., *J. Chem. Soc. A* **1969**, 2036–2044.

(8) Masaki, M. E.; Paul, D.; Nakamura, R.; Kataoka, Y.; Shinoda, S.; Tsukube, H., *Tetrahedron* **2009**, *65*, 2525–2530.

(9) Hazell, A.; Mcginley, J.; Toftlund, H., *J. Chem. Soc., Dalton Trans* **1999**, 1271-1276

(10) Szajna, E.; Dobrowolski, P.; Fuller, A. L.; Arif, A. M.; Berreau, L. M., *Inorg. Chem.* **2004**, *43*, 3988–3997.

(11) Alain, D.; Hagen, K. S., *Inorg. Chem.*, **1998**, 37, 215-223.

(12) Hui Zhang, Z.; Bu, X. H.; Ang Zhu, Z.; Chen, Y. T., *Polyhedron* **1996**, 2787-2792.

(13) Zahn, S.; Canary, J. W., *J. Am. Chem. Soc.* **2002**, *124*, 9204–9211.

(14) Porras Gutiérrez, A. G.; Zeitouny, J.; Gomila, A.; Douziech, B.; Cosquer, N.; Conan, F.; Reinaud, O.; Hapiot, P.; le Mest, Y.; Lagrost, C.; le Poul, N., *J. Chem. Soc.***2014**, *43*, 6436–6445.

(15) Otter, C. A.; Hartshorn, R. M., *J. Chem. Soc.* **2004**, *4*, 150–156.

(16) Jenkins, H. A.; Klempner, M. J.; Prokopchuk, E. M.; Puddephatt, R. J., *Inorg. Chim. Acta* **2003**, *352*, 72–78.

(17) Natali, M.; Badetti, E.; Deponti, E.; Gamberoni, M.; Scaramuzzo, F. A.; Sartorel, A.; Zonta, C., *Dalton Transactions* **2016**, *45*, 14764–14773.

(18) Benazzi, E.; Begato, F.; Niorettini, A.; Destro, L.; Wurst, K.; Licini, G.; Agnoli, S.; Zonta, C.; Natali, M., *J. Mater. Chem. A* **2021**, *9*, 20032–20039.

(19) Carmo dos Santos, N. A.; Lorandi, F.; Badetti, E.; Wurst, K.; Isse, A. A.; Gennaro, A.; Licini, G.; Zonta, C., *Polymer* **2017**, *128*, 169–176.

(20) Chan, S. L. F.; Lam, T. L.; Yang, C.; Lai, J.; Cao, B.; Zhou, Z.; Zhu, Q., *Polyhedron* **2017**, *125*, 156–163.

(21) Chan, S. L. F.; Lam, T. L.; Yang, C.; Yan, S. C.; Cheng, N. M., *Chem. Comm.* **2015**, *51*, 7799–7801.

(22) Joyce, L. A.; Maynor, M. S.; Dragna, J. M.; da Cruz, G. M.; Lynch, V. M.; Canary, J. W.; Anslyn, E. V., *J. Am. Chem. Soc.* **2011**, *133*, 13746–13752.

(23) You, L.; Pescitelli, G.; Anslyn, E. v.; di Bari, L., *J. Am. Chem. Soc.* **2012**, *134*, 7117–7125.

(24) Energy Agency, I. *Review 2021 Assessing the Effects of Economic Recoveries on Global Energy Demand and CO 2 Emissions in 2021 Global Energy*; **2021**.

(25) Lubitz, W.; Ogata, H.; Rüdiger, O.; Reijerse, E. Hydrogenases., *Chem. Rev.* **2014**, 4081–4148.

(26) Juris, A.; Balzani, V.; Barigelletti, F.; Campagna, S.; Belser, P.; von Zelewsky, A., *Chem. Comm. Rev.*, **1988**, 84-85.

(27) Deponti, E.; Luisa, A.; Natali, M.; Iengo, E.; Scandola, F., *Dalton Trans.* **2014**, *43*, 16345–16353.

(28) Pellegrin, Y.; Odobel, F., *C. R. Chimie*. **2017**, 20, 283–295.

(29) Droghetti, F.; Lucarini, F.; Molinari, A.; Ruggi, A.; Natali, M., *Dalton Trans.* **2022**.

(30) Krishnan, C. V.; Sutin, N., *J. Am. Chem. Soc.* **1981**, 103, 2141-2142.

(31) Krishnan, C. V.; Brunschwig, B. S.; Creutz, C.; Sutin, N., *J. Am. Chem. Soc.* **1985**, 107, 2005-2015.

(32) Bigi, J. P.; Hanna, T. E.; Harman, W. H.; Chang, A.; Chang, C. J., *Chem. Comm.* **2010**, *46*, 958–960.

(33) Tong, L.; Zong, R.; Thummel, R. P., *J. Am. Chem. Soc.* **2014**, *136*, 4881–4884.

(34) Lo, W. K. C.; Castillo, C. E.; Gueret, R.; Fortage, J.; Rebarz, M.; Sliwa, M.; Thomas, F.; McAdam, C. J.; Jameson, G. B.; McMorran, D. A.; Crowley, J. D.; Collomb, M. N.; Blackman, A. G., *Inorg. Chem.* **2016**, *55*, 4564–4581.

(35) Wang, W. H.; Himeda, Y.; Muckerman, J. T.; Manbeck, G. F.; Fujita, E., *Chem. Rev.* **2015**, 12936–12973.

(36) Reda, T.; Plugge, C. M.; Abram, N. J.; Hirst, J., *PNAS* **2008**, 105, 10654-10658.

(37) Qiao, J.; Liu, Y.; Hong, F.; Zhang, J., *Chem. Soc. Rev.* **2014**, 631–675.

(38) Bushuyev, O. S.; de Luna, P.; Dinh, C. T.; Tao, L.; Saur, G.; van de Lagemaat, J.; Kelley, S. O.; Sargent, E. H., *Joule* **2018**, 825–832.

(39) Lacy, D. C.; McCrory, C. C. L.; Peters, J. C., *Inorg. Chem.* **2014**, *53*, 4980–4988.

(40) Elgrishi, N.; Chambers, M. B.; Fontecave, M., *Chem. Sci.* **2015**, *6*, 2522–2531.

(41) Cometto, C.; Chen, L.; Lo, P. K.; Guo, Z.; Lau, K. C.; Anxolabéhère-Mallart, E.; Fave, C.; Lau, T. C.; Robert, M., *ACS Catal.* **2018**, *8*, 3411–3417.

(42) Shimoda, T.; Morishima, T.; Kodama, K.; Hirose, T.; Polyansky, D. E.; Manbeck, G. F.; Muckerman, J. T.; Fujita, E., *Inorg. Chem.* **2018**, *57*, 5486–5498.

(43) Wang, J. W.; Huang, H. H.; Sun, J. K.; Ouyang, T.; Zhong, D. C.; Lu, T. B., *ChemSusChem* **2018**, *11*, 1025–1031.

(44) Gangi, D. A.; Durand, R. R., *J. Am. Chem. Soc.* **1986**.

(45) Koster; Thewissen; Mackor; Beley; Collin; J-p; Sauvage; Petit; Chartier., *J. Am. Chem. Soc.* **1990**, 112, 3420-3426.

(46) Schneider, J.; Jia, H.; Muckerman, J. T.; Fujita, E., *Chem. Soc. Rev.* **2012**, *41*, 2036–2051.

(47) Fernández, S.; Franco, F.; Casadevall, C.; Martin-Diaconescu, V.; Luis, J. M.; Lloret-Fillol, J., *J Am Chem Soc* **2020**, *142*, 120–133.

(48) Shimoda, T.; Morishima, T.; Kodama, K.; Hirose, T.; Polyansky, D. E.; Manbeck, G. F.; Muckerman, J. T.; Fujita, E., *Inorg. Chem.* **2018**, *57*, 5486–5498.

(49) Enciso, A. E.; Lorandi, F.; Mehmood, A.; Fantin, M.; Szczepaniak, G.; Janesko, B. G.; Matyjaszewski, K., *Angew. Chem. Int. Ed.* **2020**, *59*, 14910–14920.

(50) Zaman, N.; Guillot, R.; Sénéchal-David, K.; Boillot, M. L., *Tetrahedron Lett.* **2008**, *49*, 7274–7275.